STUDIES OF THE GROWTH KINETICS AND HABIT MODIFICATION OF SODIUM CHLORATE CRYSTALS

A thesis submitted to the Department of Pure and Applied Chemistry, University of Strathclyde, in accordance with the requirements for the degree of Doctor of Philosophy

by

KRZYSZTOF WOJCIECHOWSKI, MSc

Department of Pure and Applied Chemistry
University of Strathclyde

Instytut Fizyki Politechniki Łódzkiej

J U N E , 1 9 8 9

Pamięci Ojca

poświęcam

Autor

In memory of

my late Father

Author

CONTENTS

ABSTRACT

The thesis describes the results of studies on the morphology, growth kinetics and defect structure of sodium chlorate crystals grown from aqueous solutions at temperatures near the ambient. For the investigation of the growth morphology and habit modification of the crystals as a function of supersaturation and concentration of $Na_2S_2O_6 \cdot 2H_2O$ impurity, experimental data on the morphological importance of different faces were supplemented by examination of the surface topography, the dislocation structure and changes in the lattice parameter of the crystals. The results showed that the habit of the crystals grown from pure solutions is cubic at high supersaturations, while it is cuboid with relatively small {110} and {111} faces at low supersaturations. Optical examination of the as-grown surfaces did not reveal the presence of growth spirals or hillocks, but screw, edge and mixed dislocations were identified by Lang topography at both low and high values of supersaturations (undercooling). Addition of the impurity to the growth solution led to the development of tetrahedral faces with randomly situated hillocks of different sizes at the expense of cubic faces, and to an increase in the lattice parameter of the grown crystals. The influence of the impurity was also studied on the nucleation kinetics of the compound. Effects of applied

supersaturation on the regeneration process at the seed and the dislocation structure at the seed-crystal interface, and of the strain, applied externally on large crystals and inherently present in small crystals of dimensions 50 - 150 μm, on growth rates were investigated by using X-ray diffraction topography. It was found that the strain generated at the newly-grown interface and the numerical density of dislocations formed therefrom increase with the value of the supersaturation used for the refacetting process. It was unequivocally established that the growth rates of crystals decrease with an increase in the strain applied externally on large crystals and inherently present in small crystals.

ACKNOWLEDGEMENTS

I wish to thank the Authorities of both the University of Strathclyde and the Technical University of Łódź for the opportunity given to me to participate in the "Joint PhD Project".

Special thanks are also due to the Authorities of the Department of Pure and Applied Chemistry (University of Strathclyde) and Institute of Physics (Technical University of Łódź) for the collaboration and departmental facilities left at my disposal.

I would like to express my sincere gratitude to my supervisors Professor J. N. Sherwood and Dr K. Roberts from the Department of Pure and Applied Chemistry and Associate Professor Keshra Sangwal from the Pedagogical University of Częstochowa for their guidance, advice, encourage and friendly atmosphere throughout this project.

I would also like to thank all my Colleagues, members of Staff of both Departments, for their encouragement and help. I am particularly grateful to Dr R. Ristic for valuable remarks and helpful discussions.

Finally, I am indebted to my wife for her help and patience at all stages of this project.

Krzysztof Wojciechowski

This work is partly financed under the Research Project CPBP 01.20.3.

CHAPTER 1

INTRODUCTION

The production of single and bulk crystals is necessary for fundamental studies and industrial applications. The growth of high-quality single crystals for modern technology, and industrial crystallization of sugar, fertilizers and table salt are only some of the examples of widely employed crystal growth processes. Typical methods used in crystal growth technology involve crystallization from the vapour phase, from solution and from the melt. Of the different methods, one of the best developed techniques is crystallization from aqueous solution. Using this method high-quality crystals can be obtained with relatively simple and inexpensive equipment.

With increasing interest in the use of single and bulk crystals, the number of research papers in the field of crystal growth has increased rapidly in the past decades. For example, between 1918 and 1968 the number of publications on crystallization has grown exponentially, doubling every five years, whereas the equivalent change for physics as a whole occurred over 10-15 years [1]. However, the number of papers on the technology of crystal growth is enormous in comparison with those on the elementary processes of growth.

Both the growth of large, perfect single crystals and the production of large amounts of crystalline products in the form of small crystals have a lot in common and require better understanding of the fundamentals of crystal growth. Theoretical description of crystal growth processes is a difficult task involving as diverse fields as thermodynamics, hydrodynamics, crystallography, quantum mechanics, etc. In practice, some properties of the crystalline product are usually more important than others and have to be achieved by controlling appropriate parameters of the growth process. In industrial crystallization for example, crystal habit is important in assessing the resulting product purity and storage characteristics. Suppression of the incorporation of mother liquor or other impurities into the crystal is important in the pharmaceutical and electronic industries. Growth kinetics have a dominant influence on crystal habit and impurity incorporation. The habit is determined by the relative rates of growth of different faces, while the incorporation of impurities is influenced by crystal-solution hydrodynamics and impurity adsorption characteristics.

The aim of this work was to establish the effect of growth conditions on the macro- and micromorphology of sodium chlorate crystals grown from aqueous solutions and to assess the correlation of the former with crystal perfection. The experiments were performed for a wide

range of crystal sizes (i. e. the process of crystal growth was monitored for small crystals ranging from 20 to 500 μm and large crystals of sizes up to 2 cm). A variety of experimental techniques, such as optical microscopy, X-ray topography by the Lang method, white X-ray topography using synchrotron radiation source (SRS), X-ray powder diffraction and Laue method using highly intense wiggler line at the SRS, were applied to study the surface morphology, dislocation structure and distribution of strain in the crystals.

CHAPTER 2

PROCESSES OF CRYSTAL GROWTH AND NUCLEATION

Growth of crystals from solutions involves two fundamental stages: first, formation of three-dimensional nuclei, and second, development of these nuclei into crystals with well-defined crystallographic faces. These stages are described below.

2.1. NUCLEATION

One can distinguish two types of nucleation: primary and secondary. The former is defined as a process of the formation of nuclei from the liquid phase only and depending on whether or not impurities are present, one talks about heterogeneous and homogeneous nucleation, respectively. Secondary nucleation is said to take place if there is a crystal present in the liquid phase during nucleation. In this case the presence of the crystal can be a source of new nuclei mechanically stripped from its surface or can lead to a decreased metastable zone-width in comparison with pure solution under the same external conditions.

2.1.1. Homogeneous Nucleation

According to Becker and Döring [2] and Nielsen and Söhnel [3,4], the rate of homogeneous nucleation

$$J = K \exp(-\Delta G^*/k\,T), \qquad (2.1)$$

where K is the kinetic factor, ΔG^* is the Gibbs free energy for the formation of a critically-sized nucleus and k is the Boltzmann constant. The Gibbs free energy is given by

$$\Delta G^* = \beta\,\gamma^3\,\Omega^2 / [kT\,\ln(S)]^2, \qquad (2.2)$$

where the shape factor $\beta = 16\,\pi/3$ for a spherical nucleus, γ is the surface free energy, Ω is the molecular volume and $S = c/c_o$ (c and c_o are, respectively, the concentration of supersaturated and saturated solutions at temperature T) is the supersaturation ratio. The radius, r^*, of a critically-sized stable nucleus is given by

$$r^* = \frac{2\,\gamma\,\Omega}{k\,T\,\ln S}\,. \qquad (2.3)$$

For a given volume of the solution, the rate of ucleation, J, is inversely proportional to the induction period τ [3,5-7]. Thus from eqs (2.1) and (2.2), one obtains

$$\ln \tau = A + \beta\,\frac{\gamma^3\,\Omega^2}{k^3}\;\frac{i}{T^3\,(\ln S)^2}\,, \qquad (2.4)$$

where A is a constant. The linear dependence of $\ln \tau$ on $T^3\,(\ln S)^{-2}$ gives the slope

$$m = \beta\,\gamma^3\,\Omega^2/k^3, \qquad (2.5)$$

from which γ may be calculated.

2.1.2. Heterogeneous Nucleation

The presence of impurities in a nucleating solution may affect the nucleation rate through the kinetic factor K or through the thermodynamic parameter ΔG^*, the Gibbs free energy for the formation of a critical nucleus (see eq. 2.1).

An impurity decreases the nucleation rate and disturbs the nucleation process which becomes more or less irregular [25]. The former effect is frequently observed, whereas the latter one seems to depend on the nature and size of the impurity. Since the nucleation rate decreases in the presence of an impurity, the effect of the kinetic factor should be less important than that of the surface free energy. It is theoretically possible to get a high nucleation rate in the presence of impurities but it has never been observed experimentally. The inhibition of nucleation by the active impurities is associated with two factors. First, adsorption preferentially takes place at the growth sites of the nucleating clusters. Therefore, only a few impurity molecules can inhibit their growth, while the surface free energy is still unchanged. Second, some impurities, like long-chain compounds and surfactants, are able to form a compact adsorption layer which can drastically decrease the exchange kinetics of the solute molecules between the bulk and the cluster surface. This can occur without a noticeable change in the value of the surface

free energy.

2.1.3. Secondary Nucleation

The occurrence of secondary nucleation depends on the presence of existing crystals in the solution and may be defined, after Botsaris [8], as nucleation taking place only because of the prior presence of crystals of the material being crystallized. Secondary nucleation phenomena are of vital importance in industrial crystallization processes and a number of reviews have been published [8-10], where it has been demonstrated that secondary nucleation can take place by several different mechanisms.

Initial breeding occurs when dry crystals are first introduced into a solution and small crystalline fragments present on their surfaces are washed off by the solution and form new nuclei. For industrial crystallization this mechanism is important when crystallizers are seeded with fresh material.

Needle breeding arises at high supersaturations where dendrites may develop or needles grow from an existing crystal. In stirred solutions these crystals easily break and may produce secondary nuclei of visible size. This mechanism is not of much importance in industrial crystallization since the supersaturation levels for this type of growth are far above the normal operating levels.

One of the most important mechanisms of secondary nucleation is contact nucleation, sometimes referred to

as collision breeding or collision nucleation. Contacts between the growing crystal and walls of the container, the stirrer or other crystals result in the formation of contact nuclei. Under certain conditions fluid shear forces are sufficient to produce secondary nuclei by the detachment of submicroscopic fragments from an existing surface of the crystal.

2.2. CRYSTAL GROWTH

2.2.1. Growth from Pure Solutions

The process of the development of stable nuclei into large crystals involves the transport of growth units from solution to the crystal-solution interface and then their integration into surface sites. We can divide this process into several steps, such as transport of growth units (which are generally solvated entities) to the crystal surface, partial desolvation of the growth units at the interface and surface diffusion of the adsorbed growth units to the preferred sites (i.e. kinks at steps) on the surface. Depending on the rate-determining step we can distinguish between surface- and volume-diffusion controlled processes.

2.2.1.1. Types of Surfaces and Their Relation to Crystal Morphology

Surfaces of a crystal can be classified as smooth and rough on an atomic scale. Smooth surfaces are

characterized by a low density of kinks present either in the edges of "islands" of growth units (two-dimensional nuclei) or in surface "steps" of molecular height generated by screw dislocation outcrops. On the other hand, rough surfaces have a preponderance of potential kink sites and neither surface diffusion nor fine details of surface topography are important for the development of a face. Atomically smooth surfaces grow by a layer displacement mechanism while rough surfaces develop by a continuous growth mechanism.

The equilibrium habit of a crystal is determined by the total Gibbs free energy defined as

$$G_{total} = G_{solid} + G_{fluid} + G_{surface}. \qquad (2.5)$$

For a given temperature and pressure the only variable in this equation is $G_{surface}$. The crystal will thus change its shape to minimize $G_{surface}$. Since, in general, a crystal is bounded by n faces each of area A_n, it is convenient to write

$$G_{surface} = \sum_{k=1}^{n} \gamma_k A_k = \text{minimum} \qquad (2.6)$$

as the equilibrium criterion. Here γ_k is the surface tension of the k-th face and is related to the work required to form new surface. For a crystal having n faces with surface tensions γ_1, γ_2, ..., γ_n, the habit consistent with eq. 2.5 is that for which

$$\gamma_1/h_1 = \gamma_2/h_2 = \ldots \gamma_n/h_n = \text{constant}, \qquad (2.7)$$

where h_1, h_2,..., h_n are the lengths of normals to the faces which intersect at some central point in the crystal.

Typical growth experiments, and particularly industrial crystallization processes, usually operate far from equilibrium. Therefore, although the question of equilibrium habit is interesting, growth habit is of greater practical importance. Growth habit is more closely related to kinetic factors than to thermodynamic concepts. The problem then is how to predict growth habit knowing the crystal structure. The following two important features must be taken into account while predicting the growth habit.

The faces which appear on a growing crystal are the slowest growing crystallographic planes. The problem of predicting habit, therefore, reduces to predicting the relative growth rates of different crystal planes in a given structure. The slower the growth rate, the larger the surface area of that face and the higher the morphological importance.

Hartman and Perdok [11,12] made a simplifying hypothesis that growth rate is proportional to the attachment energy E_{att}. This energy is different for different crystallographic planes and is equal to the energy released per molecule when a new layer is deposited on the given face. According to this assumption, the larger the value of E_{att} the higher the

growth rate.

In order to simplify concepts and calculations, Hartman and Perdok introduced the idea of periodic bond chains (PBCs). There are three types of faces which can be distinguished. An F (flat) face is one whose slice contains at least two PBCs, an S (stepped) face contains one PBC while a K (kinked) face has no PBC. A PBC is an uninterrupted chain of strong chemical bonds within a slice. On the atomic scale, an F face is smooth while S and K faces are rough. In general, fast growing S and K faces tend to disappear leaving the crystal bounded by slow growing F faces which grow by the layer displacement mechanism.

One of the results of computer simulation studies [13] is the development of the concept of surface roughening temperature. From the viewpoint of growth kinetics, this is a temperature, T_R, above and below which continuous growth and layer growth mechanism occur, respectively. It can be expressed with the aid of α, which is a factor characterizing the bond strength of the surface divided by the temperature i.e.

$$\alpha = \zeta \frac{L}{kT}, \qquad (2.8)$$

where ζ, the crystallographic anisotropy factor as defined by Jackson [14], is the ratio of the energy of growth units within the slice, E_{sl}, to the total crystallization energy, E_{cr}, defined with reference to

vacuum, and L is the latent heat of melting.

There are limitations of the PBC method. The bonds forming the PBCs are bonds in the first coordination sphere (called strong bonds) and the classification does not say anything about the crystallization temperature. Therefore, if α is smaller than a critical value (if crystallization temperature is above the roughening temperature), the face will develop according to the linear continuous growth mechanism and a strict crystallographic orientation is probably not maintained. This occurs when E_{el} is small or T is high. K faces grow according to this mechanism because E_{el} is low and the face is above its roughening temperature at all temperatures used in practice for crystal growth. Thus at $T > T_R$ an F face behaves as a K face. In general, an F face need not grow by the layer growth mechanism if α is lower than the critical value and the bonds within a surface show a high degree of anisotropy.

2.2.1.2. Crystal Growth Kinetics

We consider an atomically smooth surface of a crystal assuming that the rate-determining step is the surface diffusion of growth units. Because the surface is flat, the formation of a two-dimensional nucleus can only ensure the lateral spreading of a new layer across the surface. According to Ohara and Reid [15], we may distinguish three different cases of the development of a crystal by two-dimensional nucleation. In the mononuclear

model, after the formation of a critically-sized nucleus the lateral spreading of new layers is infinitely rapid. In the polynuclear model, it is assumed that the velocity of the lateral spreading of new layers is zero and growth takes place by the generation of critically-sized nuclei. In the Birth-and-Spread (B+S) model the nuclei grow and spread at finite velocities.

The mononuclear model predicts that the linear growth rate, R, of a face depends on the area of a growing surface, while according to the polynuclear model R has a maximum at some supersaturation. Such growth rate behaviour has not been observed experimentally and, therefore, the applicability of these two models remains unproved for crystal growth from solutions.

According to all two-dimensional nucleation theories, a supersaturation of 25-50% is required to achieve a measurable growth rate [16]. For the low supersaturation region the surface diffusion theory was developed by Burton, Cabrera and Frank (BCF) [17]. According to this theory, a screw dislocation emerging on a crystal surface serves as a permanent source of steps and eliminates the need for two-dimensional nucleation. The BCF equation describes the functional dependence of the growth rate, R, on relative supersaturation, $\sigma = S-1 = (c-c_o)/c_o$. At low supersaturations this equation leads to a parabolic dependence while at high supersaturations to a linear dependence.

Finally, it should be emphasized that although the predicted dependences of R on σ are different for the BCF and B+S models, it is very difficult to establish conclusively the actual mechanism of growth only on the basis of the experimental data on the dependence of R on σ [18-20]. In order to arrive at the correct growth mechanism of a crystal, studies on growth kinetics have to be complemented by additional studies on surface micromorphology by optical microscopy and/or on characterization of growth defects.

2.2.2. Growth in the Presence of Impurities

It is well known that the presence of impurities in a growth solution often causes the appearance of faces which are not observed from pure solutions [21]. This phenomenon is attributed to differences in adsorption processes on different crystal faces, which lead to changes in relative growth rates of these faces.

Several attempts have been made to describe the mechanism of action of impurities on growth kinetics and habit [21-25]. Adsorption of impurities occurs at kinks, steps or on the surfaces between the steps. The impurity molecules are either adsorbed randomly at isolated sites or link to each other forming a two-dimensional adsorption layer on the given surface. Adsorption at kinks would effectively reduce their number and, therefore, reduce the layer velocity. An increase in the interkink distance would reduce the importance of surface

diffusion in the growth process. As reported by Bennema [26], this would lead to a dependence of the rate of advance of steps on the density of kinks and result in the polygonisation of growth layers. Adsorption of impurities at a step, considered first by Cabrera and Vermilyea [22], predicts that there is a reduction in the rate of advance of step and that a step section can move only if the mean distance between the strongly adsorbed impurity particles is greater than the diameter of the critical two-dimensional nucleus at the given supersaturation. If the distance between two impurity particles is small, the step will be stopped and will squeeze between them. Its curvature will increase and its velocity will decrease. This phenomenon leads to a sharp decrease in the growth rate.

Some impurities may be immobile on a crystal surface whereas others may move easily. In the former case, the exchange rate of the impurity molecules is lower than the exchange rate of the growth units. Therefore, adsorption influences the kinetic parameters involved in nucleation and growth. Conversely, a higher exchange rate of the impurity molecules than that of the growth units leads to a changes in the thermodynamic parameter, i.e. surface and edge free energies.

Chernov [27] distinguishes between two effects of adsorbed impurities. If the impurity entities are relatively small and mobile, their main effect will be to

reduce the effective number of kinks. Relatively large and immobile impurities, such as organic dye molecules, act as obstacles for the movement of surface steps. Mullin et al. [28] considered that the mechanism of physical blocking of growth sites on a crystal surface is an oversimplification, and that impurity particles in the vicinity of the surface will retard growth by their interaction with the solvent even if they are not adsorbed on the crystal surface. The presence of impurities may reduce the effective supersaturation by 'dilation', retard diffusion and hinder aggregation of growth units.

Hartman [12] proposed that certain impurities will cause S or K faces to become flat due to the formation of a two-dimensional adsorption layer over the face. In this case lateral growth is possible only at steps and the growth process is thus similar to that of a normal F face. The epitaxial layer of impurities effectively imposes its own PBCs on the face.

From the foregoing it is obvious that it is difficult to describe the role of impurities in crystal habit modification. It is still more difficult to demonstrate conclusively the mechanism of impurity absorption.

CHAPTER 3

SURVEY OF THE LITERATURE ON SODIUM CHLORATE

The literature on the crystallization of sodium chlorate deals with studies both on nucleation and growth processes. The main attention in nucleation studies has been paid to secondary nucleation processes. By using a variety of experimental techniques various aspects of growth processes have been investigated. These latter studies deal with growth kinetics, visualization of profiles of solute concentration and its gradients around growing crystals by different optical methods, observation of surface features by optical microscopy, determination of crystallographic structure and the nature and number of lattice defects of crystals by chemical etching, topographic and diffraction techniques, and simulation experiments on growth. The published experimental results on nucleation, growth and morphology of sodium chlorate are presented in the following sections.

3.1. NUCLEATION

There has been considerable interest in studies of the secondary nucleation of sodium chlorate rather than its primary nucleation. This is due to the fact that

nucleation, which occurs in suspensions of crystals encountered in industrial crystallizers, appears to involve secondary nucleation. Therefore, sodium chlorate has been studied for the better understanding of its production process as a bulk chemical. Moreover, because of its wide metastable zone-width and relatively simple structure sodium chlorate is a good choice as a model substance.

Lal et al. [29] performed a series of experiments involving the sliding of a seed crystal along the bottom of a crystallizer. The crystal-glass contact produced nuclei which were counted when they grew sufficiently to be visible. The resulting functional dependence of the number of crystals on supersaturation was an S-shaped curve. This is consistent with the survival theory proposed by Strickland-Constable [30]. According to this theory, particles produced by sliding (coming from the crystal surface by the microattrition process) are in the range of the critical nucleus size. Particles of dimensions smaller than the critical size redissolve, while those which are larger than it survive. The higher the supersaturation, the larger the number of the finally surviving particles. Because the theory implicitly assumes that the number of the fragments generated is not affected by supersaturation, the percentage of the total number of fragments which survive depends only on supersaturation.

Botsaris and Sutwala [31] repeated sliding experiments for sodium chlorate and found good agreement between their results and those of Strickland-Constable. However, experiments at high supersaturation led to nuclei counts higher than the theoretically predicted maximum. Using dummy seeds made of glass it was found that at supercooling greater than 7 K nuclei are produced. This observation reveals that they cannot be considered as secondary nuclei. This effect was attributed to shock or heterogeneous nucleation on the glass surface. Thus a type of induced nucleation takes place in addition to secondary nucleation, which leads to the generation of nuclei by primary nucleation. This effect becomes appreciable only at high supersaturations.

A series of experimental runs was made by the same authors [31] at 1, 5, 10 and 100 ppm of borax impurity. The maximum numbers of the surviving nuclei at constant supersaturation were found to decrease with increasing impurity concentrations. This observation can be explained on the basis of the survival theory. That a larger critical size of the nucleus is required at higher impurity content is consistent with the observation of primary nucleation in the presence of impurity reported in Subsec. 5.2.1. Another important conclusion derived from the experimental results was that, in the presence of impurity, the attained plateau on the graph of the number of surviving nuclei on supersaturation was smaller

than that from pure solutions. This implies that in impure solutions there are a number of particles produced during sliding, which will never be able to survive no matter how high the supersaturation, because they are rendered inactive by the impurities.

Denk and Botsaris [32] continued experiments on the secondary nucleation of sodium chlorate using the two enantiomorphic forms as an indicator of the source (mother solution or fragments of seed crystal) of secondary nuclei. It was found that in pure stagnant solutions secondary nucleation took place above a certain supersaturation level and 60 % of the crystals were of the same enantiomorphic type as the seed. For higher supersaturations only crystals of the type of the seed were observed and then at still higher supersaturations spontaneous nucleation began to take place. For impure stagnant solutions the dependence was similar but the supersaturation required for spontaneous nucleation was higher than that for pure solution. In the case of stirred solutions the results for low stirring rates (25 rpm) were similar to those for stagnant solutions, but for high stirring rates (300 rpm), when secondary nucleation occurred, only crystals with the structure of the seed were obtained regardless of the supersaturation employed. The most intriguing observation was that 60 % of the crystals of the enantiomorphic type of the seed were generated at low supersaturations. In order to

explain this phenomenon, two cooperating mechanisms were assumed. The first yields only crystals with the seed structure and produces 20 % of the crystals, while the second produces an equal number of the left- and right-handed crystals giving the remaining 80 % of the population. The former mechanism probably involves a kind of growth and detachment of surface irregularities but the latter mechanism is not obvious. However, it was hypothesized that this kind of secondary nucleation might be the result of an ordering of the solvent water molecules near the crystal-solution interface as shown by Drost-Hansen [33]. If the kind of ordering proposed by Drost-Hansen were to occur, the solubility of the crystallizing species in the ordered water region could be less than the solubility in the bulk solution, and the local supersaturation in the ordered water region could be much higher than the bulk supersaturation and could become high enough for spontaneous nucleation.

3.2. KINETICS AND MECHANISM OF GROWTH FROM PURE SOLUTION

The first results concerning the growth of sodium chlorate crystals were reported in 1903 by Miers [34]. By measuring the angle of total internal reflection at a growing crystal face and by determining the refractive index of the solution and hence its composition, he showed that the solution at a growing surface is

appreciably supersaturated.

Bunn [35] and Berg [36] developed the method of observation of concentration profiles during the growth of small crystals. Their experimental set-up consisted of a small cell. Crystals were placed in a supersaturated solution in a very thin wedge-shaped space between two half-silvered glass plates. They established surfaces of equal concentration in the vicinity of the crystals and simultaneously observed whether or not growth occurred on a given face. They concluded that supersaturation is higher at the corners of faces than at the centre and, consequently, more solute arrives at the centre of the given face than at the edges. Since the faces remain flat, the excess must be dissipated by surface migration. Thus despite nonuniform concentration along a particular face, the latter remains smooth on an atomic level. Layers spread from the centres of the crystal faces where supersaturation is the lowest. Therefore, the magnitude of supersaturation does not control the inception of layers. There was a lack of correlation between the rate of growth and the supersaturation at a given face in their experiments.

Follenius [37] used a similar technique. By calculating the growth rate from the concentration gradient in the vicinity of a given face, she obtained an R-σ curve. It is worthwhile to mention that for supersaturations below 2×10^{-2}, no measurable growth rate

was observed. However, this observation can be attributed to a poor accuracy in measuring very low R and σ values. The dependence of R on σ was linear in the supersaturation range $2 \times 10^{-2} - 10^{-1}$.

Humpreys-Owen [38] studied the rate of advance of individual faces and compared them with the predictions of Nernst's diffusion theory of dissolution. He found that faces sometimes grow according to this mechanism, but sometimes a smaller growth rate was observed. In some cases complete stoppage of growth took place.

Another approach to growth rate measurements was applied by Bennema [39]. The growth rate of sodium chlorate was estimated by weighing the growing crystal. The crystal was suspended in a crystallizer filled with solution and the required supersaturation was attained by cooling the external water jacket to the appropriate temperature. The temperature control was ± 0.005 K. The saturation temperature was estimated experimentally by suspending the seed crystal from a balance and observing the change in its mass. When the crystal stopped growing or dissolving, it was assumed that the saturation point was achieved. Growth rates were measured within a supersaturation range of $3 \times 10^{-5} - 1.5 \times 10^{-3}$ and the BCF theory was applied for interpretation. A change from parabolic to linear dependence of R on σ was observed for supersaturation equal to 6×10^{-4}. However, such an approach gives only the average of growth rates of the

six faces of cubic sodium chlorate crystals and cannot distinguish between the growth rates of different faces of the growing crystal.

Hosoya et al. [40] studied normal growth rates of {100} faces of $NaClO_3$ crystals using a specially designed cell for in-situ observation. The supersaturations used in the experiments lay in the range 2.8×10^{-2} - 5.2×10^{-2}. The experimental apparatus consisted of a vessel for the preparation of saturated solution, a cell to be used on the microscope stage and temperature control units with an accuracy of ± 0.01 K. The cell had a double construction with upper and lower chambers. Two external water baths, "hot" - thermostated at temperature above and "cold" - kept below the saturation point of the solution, were used. The temperature of the cell was controlled by regulating the flow of thermostated water running in the lower chamber. A small seed was placed at the centre of the bottom face of the upper chamber of the cell while the cell was maintained above the saturation temperature by switching water flow through the hot bath. Then the saturated solution was poured into the upper chamber, followed by sealing the chamber with molten paraffin. After a partial dissolution of the seed crystal, the temperature of the cell was decreased by exchanging water circulation to the cold bath; this resulted in the crystal recovering its polygonal form. It was observed that in all experiments the {100}, {110} and

{111} type surfaces showed somewhat depressed centres. This feature is due to the fact that growth takes place more preferentially along the edges of the faces rather than in their central areas. This work revealed that the cubic morphology was the stable growth form in the supersaturation range used in the experiments. From kinetic measurements, it was found that B+S model of two-dimensional nucleation fits sufficiently well. The transition from BCF to two-dimensional mechanism was observed at a supersaturation of about $2 \times 10^{-2} - 3 \times 10^{-2}$.

It should be pointed out that during the above experiments the supersaturation decreases gradually and the growth conditions are not stable for long term measurements. Moreover, in the absence of solution flow through the cell, it might be expected that the growth process is governed at least partly by volume diffusion.

Takeuchi and his coworkers [41] investigated the growth rate and size distribution of $NaClO_3$ crystals. A flow system was used (solution velocity 5 to 25 cm/s) to measure, under the microscope, the linear growth rate of {100} faces parallel and normal to the direction of flow. Because the growth rates for these faces were different, the average growth rate was measured in a stirred glass cell placed in water bath. A speed of 200 rev/min was used to ensure the absence of volume-diffusion transport to the crystal. The growth rates were determined by a weighing technique. The third experimental method applied

was crystallization from a cone-type fluidized-bed crystallizer. A known amount of seeds with known size distribution was introduced to the top of the column containing supersaturated solution and the fluidization of seeds initiated. After a given time the seed slurry was discharged from the crystallizer and rapidly filtered, and the seeds were dried, weighed and subjected to screen analysis. Thus overall mass growth rate was determined. In all three experiments the linear growth rate was found to be first-order with respect to supersaturation. The surface incorporation coefficient was found to follow the Arrhenius relationship, with an activation energy of 67.9 kJ/mol. The average growth rate, $\bar{R}$ of the crystals in a fluidized-bed crystallizer was dependent on size, L, as $\bar{R} = 0.96 \times L^{0.95}$ for $\Delta C = 0.65$ wt % and the size range 0.34 - 0.90 mm.

An interesting experiment on the temperature dependence of growth rates was reported by Sipyagin [42] and Chernov et al. [43]. The supersaturation of the solution was controlled by means of supercooling because the solubility of $NaClO_3$ is a linear function of temperature. The growth rates were measured in a flow cell attached to the microscope stage. At a constant supersaturation there was a general tendency for the growth rate to increase with temperature. However, it was found that there are two regions of anomalous variation. First, in the temperature interval from 274.15 to

286.15 K there are oscillations, and second, at 310.15 and 313.15 K there are two peaks with a depression at 311.65 K between them. This phenomenon was attributed to changes in the structure of the water and the solution at the face boundary. It is very likely that traces of dissolved gases are deposited as bubbles at the growth front at certain temperatures and influence the process, as reported by Wojciechowski and Karniewicz [44].

Mussard and Goldsztaub [45] measured growth rates of sodium chlorate crystals in a small cell under a microscope. They observed that {100} faces of the same crystal do not grow at the same rate and that the ratio of the growth rates of the fast-growing faces to slow-growing faces decreases with increasing supersaturation. As indicated by the observation of interference fringes around the growing crystal, the supersaturation at the fast growing faces was much higher than at the "blocked" faces. When the supersaturation was increased, "deblocking" of certain slow growing faces occurred and the supersaturation at such faces decreased to the same value as at the fast-growing faces. In order to explain these observations, these authors assumed that the growth of the fast-growing faces at low supersaturation was governed by the presence of screw dislocations, while the growth of the slow-growing faces at high supersaturation was due to the two-dimensional nucleation mechanism. The deblocking of growth was

simultaneously caused by a generation of dislocations with screw component parallel to the growth direction. To verify these hypotheses the crystals were subjected to investigations by the Lang topography technique. It was found that dislocations with a screw component were indeed created before the deblocking was observed. However, there were, in general, groups (also called fans or bundles) of dislocations of different (screw and edge) character because there was a lack of total extinction in every reflection presented by the authors. Therefore, the question of the possible effect of edge dislocations on growth remained unsolved.

Kito and Kato [46] studied the dislocation structure of sodium chlorate crystals grown on the bottom of small vessels by the solvent evaporation technique (the growth rate being about 2 mm/day). X-ray diffraction topographs were taken by the standard Lang method. The as-grown crystals always contained bundles of dislocations originating from the spontaneous nucleus, running perpendicularly to the growing surface and lying close to the lower surface of the crystal (i. e. the side lying on the bottom of the container used). Some of the observed configurations of dislocations suggested a post-growth movement of dislocations, originally lying in different growth sectors, due to a redistribution of crystal stress during growth. Therefore, some of the dislocations combined. Sometimes, dislocations originated

from a tiny dot which could be an image of strain associated with an impurity or inclusion. Except for the types of dislocations described above, the crystals were nearly perfect within different growth sectors and Pendelösung fringes were clearly observed in all cases. Additionally, a set of fringes with opposite extinction rules was observed leading to the conclusion that the growth sectors were mutually misoriented with an angle of the order of 10^{-6} rad. This means that the crystals were likely to be appreciably strained during the early stages of growth and the distortion was preserved during growth.

Matsunaka et al. [47] measured the normal growth rates of {100} faces of $NaClO_3$ crystals under well-controlled supersaturations ranging from 2.9×10^{-2} to 6.3×10^{-2}. The experimental procedure was as follows: in-situ observation of the growth process, measurement of the normal growth rate and X-ray topographic investigation of the selected crystals. The construction of the growth cell for the in-situ observation was similar to that reported by Hosoya and Kitamura [40]. Seed crystals of the {100} form ranging in size from 0.2 to 0.8 mm were slightly dissolved in the cell before an experiment. Altogether 14 crystals were grown at various supersaturations and 7 representative crystals were selected for X-ray topography by the Lang method. Starting from a rounded seed, the crystal showed at first both {100} and {110} faces but the latter faces

disappeared soon and the morphology of the crystal, bounded by {100} faces, was stabilized. The recovery process of the crystals observed by Matsunaka et al. [47] was similar to that reported by Hosoya and Kitamura [40]. All the crystals investigated by Matsunaka et al. [47] by X-ray topography showed bundles of dislocations running almost perpendicularly to the growth surfaces and originated at the central portion of the interface between the seed and the newly-grown crystal. Two different types of dislocations were observed: straight and curved. All the crystals investigated showed straight dislocations, whereas in crystals grown under low supersaturations curved dislocations were mainly observed. Based on the extinction criteria for Lang topography, it was found that the curved dislocations were of the pure screw type and the straight ones were mostly dislocations with an edge component. On the basis of the results of Bennema [39] and Hosoya and Kitamura [40], these authors concluded that the crystals with the curved dislocations were grown by the BCF spiral growth mechanism while those with the straight dislocations were grown by the two-dimensional nucleation mechanism. It was also concluded that the straight dislocations were formed as a result of the mismatch between growth layers spreading inward from the edges and did not play the role of active growth centres, whereas the curved dislocations appeared when spiral growth started to operate and played

the role of active growth centres.

An interesting holographic interferometric technique for in-situ measurements of the concentration gradients was reported by Bedarida et al [48]. The experimental set-up consisted of an argon-ion laser, an optical system to obtain the splitting of the incident beam into a beam illuminating the object (cell filled with solution with crystal in it) and a reference beam. In such a system holographic interferometric measurements in real time were possible. The most outstanding conclusion of this work was that convective movements are always present even in very small volumes and, therefore, theoretical calculations of growth on the basis of diffusion alone are deceptive. The multidirectional holographic interferometry, presented by Bedarida et al. [49], which is a sort of optical tomography, gives a concentration field at different levels in the solution.

These two holographic techniques are very promising experimental tools for the investigation of solute transport processes in crystal growth. However, they should be supplemented by in-situ surface topographic observations and X-ray topography to get correlation between the observed concentration profiles, the active surface sites and the dislocations content of a crystal. In the above papers there is a lack of interpretation of the observed patterns in relation to the growth conditions. Moreover, the absence of growth conditions

for the presented examples of visualization of concentration profiles around the growing crystals does not enable one to obtain more information about growth processes.

3.3. KINETICS OF GROWTH IN THE PRESENCE OF IMPURITIES

Despite the fact that the first papers concerning impurity effect on habit modification of sodium chlorate were published by Buckley in nineteen thirties [52,53], there are very few papers dealing with the kinetics of growth in the presence of impurities.

The effect of sulphate ions on the growth of {100} and {111} faces of sodium chlorate has been investigated by Bliznakov and Kirkova [50, 51]. It was found that the linear rate of growth, R, decreases in the presence of impurity on both type of faces in comparison with growth from pure solution. However, due to a stronger passivation of {111} faces by the sulphate ions, the relative rate of growth, R_{111}/R_{100}, decreases gradually with increasing impurity content, resulting in a change of morphology of the crystal from cubic to tetrahedral one. Direct adsorption measurements were performed using radioactive sulphur. The adsorbed quantity of Na_2SO_4 was measured radiometrically using the intensity of S^{35} radiation. It is worthwhile to mention that preliminary experiments showed that sulphate ions are completely

removed by washing the freshly obtained crystals. Therefore, one should expect that the impurity acts by surface adsorption rather than incorporation into the growing crystal. From the experimental data on the surface coverage by the impurity, heats of adsorption of sulphate ions were estimated. It was found that the values of heat of adsorption on the {111} and {100} faces were 16.7 and 9.2 kJ/mol, respectively, whereas on the active centres of growth on the same faces were 58.2 and 19.7 kJ/mol, respectively. These results confirm that the crystal faces grow through active centres whose adsorption potentials for some faces are considerably higher than the adsorption potentials on the rest of the surface. The difference between the adsorption characteristics of the {100} and {111} faces may be explained by the difference in the structure of the corresponding lattice planes. The cubic planes have a chequer board-like arrangement of sodium and chlorate ions, while the tetrahedral planes are composed of alternating layers of identical ions. This difference determines the presence of greater fields of force around the tetrahedral faces, which explains the predominant adsorption of sulphate ions on these faces.

3.4. CRYSTAL MORPHOLOGY

The first systematic studies of the effect of

additives on crystal habit modification were performed by Buckley [52]. He investigated the action of RO_4^{2-}-type ions, and of thiosulphate, pyroborate and dithionate ions, and found that the change in the morphology of sodium chlorate to simple tetrahedra occurs at different levels of impurity content. Thus for sulphate ions the ratio of ClO_3^- to SO_4^{2-} ions was 7 to 1, for thiosulphate 20 to 1, for pyroborate 60 to 1, and for dithionate 1000 to 1. The very strong effect of dithionate ions in changing the habit of the crystals was explained by the same author [53] in terms of the surface retardation of growth. In Buckley's view, the size and disposition of forces in the O_3 portion of the impurity ion are the main consideration in deciding whether the latter will get entangled and obstruct lateral growth.

Bunn [54] pointed out the role of external conditions of growth on the formation of crystals of particular morphology. When crystals grow rapidly in well stirred, highly supersaturated solutions there is a plentiful supply of solute round each growing crystal, external conditions are fairly uniform and the structure of the growing crystal is the controlling factor for morphology. Therefore, the crystal is bounded by the few slowly growing faces with the highest reticular density. On the other hand, crystals of many minerals, for instance, grow under low supersaturation, with a limited supply of solution in which the supersaturation can vary because of

stagnant conditions, local convection currents, the proximity of other crystals, local temperature fluctuations, etc. This situation can lead to highly faceted crystals with many faces not normally observed under well controlled and stable growth conditions. For sodium chlorate crystals grown at low supersaturations, the theoretical morphology should be cubic with, additionally, four {111} type faces and twelve {110} type faces.

This general conclusion seems to be contrary to Kern's observations on the dependence of the morphology of sodium chlorate on supersaturation. According to Kern [55], at low supersaturations the morphology is purely cubic whereas at higher supersaturations the tetrahedral faces tend to appear. However, he did not mention anything about the effect of growth rates on morphology.

Aoki [56] analysed the morphology of sodium chlorate crystals by using the method of Linkage of Coordination Polyhedra developed by him. His analysis supported Kern's observations. According to Aoki, the ion distribution in solution at high supersaturation is similar to that of the molten salt, and thus cations are expected to concentrate to form the coordination polyhedra such as those in the crystal. In such a situation the cations represent nearest neighbour positions with respect to the anions of the coordination polyhedra. After the cations become bonded with the anions of the coordination

polyhedra, anions in solution will soon concentrate at the nearest neighbour position to these and will continue the bonding to expand the coordination polyhedra. Consequently, the crystals will grow along the direction of linkage of coordination polyhedra. Thus in the case of growth from slightly supersaturated solutions the strong bonds between atoms may have a dominant effect upon the crystal habit, whilst during growth from highly supersaturated solution the clustering of ions has the dominating influence.

The above experimental results are contradictory to those reported by Simon [57]. He found that at very high supersaturations the only growth form is cube and at decreasing supersaturation additional faces can appear. However, he reported that the appearance of additional {110}, {120} and {111} faces is not the result of the effect of supersaturation itself but is strongly dependent on the direction of the flow of solution.

It seems that the problem of prediction of macromorphology of the crystals has been directed to two different aspects: first, the equilibrium morphology predicted on the basis of crystallographic structure of the crystal, and second, the growth morphology dependent mostly on various growth factors. Some authors confuse these two concepts and speculate about equilibrium morphology on the basis of the observed growth morphology. This misconception leads to misleading

conclusions on macromorphology.

Gonzales et al. [58] showed that growth morphology of sodium chlorate changes depending on the height of the crystal suspended in a cylinder with supersaturated solution. For pure sodium chlorate solution without agitation, the higher the crystal the more developed {110} faces were observed, whereas in agitated solution the morphology was purely cubic independent of the height. It seems that the forced transport of solution to the growing crystal is the reason for the disappearance of the faster growing {110} faces, while in stagnant solutions the convective and diffusive transport is insufficient to vanish the high index faces. Alternatively this observation can be explained in terms of the stratification of the solution due to gravity [7].

A relationship between growth morphology and strain content may be deduced from the results of Offerman and Ulrich [59]. They found that hurt and unhurt crystals grow at different rate which decreases with decreasing size. Thus, depending of total strain built-in to particular growth sectors, the morphology can be related to the change of relative growth rates of different types of faces. The dependence of growth rates on the total incorporated strain in $NaClO_3$ and $NaNO_3$ crystals was reported by Ristić et al. [60, 61], while Bhat et al. [62] observed a relation between growth rate and dislocation content in potash alum crystals. The results

concerning sodium chlorate crystals are presented in chapters 6 and 7 of this thesis.

CHAPTER 4

EXPERIMENTAL TECHNIQUES

For the investigation of the growth mechanism and defect structure of $NaClO_3$ crystals grown from aqueous solutions without and with $Na_2S_2O_6 \cdot 2H_2O$ impurity, a number of experimental techniques were used. The commonly used techniques were optical microscopy, Lang topography and synchrotron topography. These techniques are described in the present chapter.

4.1. OPTICAL MICROSCOPY

Optical microscopy was employed for the observation of as-grown surfaces and for the optical assessment of crystal quality. The observations of crystal surfaces were made by using optical reflection microscopy. This highly sensitive method has been applied to the investigation of growth steps and all kinds of microtopography of surfaces. The fact that crystal growth is a surface process implies that a detailed examination of crystal surfaces in relation to growth conditions is the obvious means for testing the applicabilities and limitations of different crystal growth models. However, the surface morphology is, to a large extent, determined by the internal defect structure of the crystal. For the

rapid assessment of the quality of seeds to be used for growth experiments, the samples were examined by optical transmission microscopy. However, in order to characterize as-grown dislocations in the crystals and to complement the results of their surface microtopography, diffraction topography was found to be essential.

4.2. X-RAY TOPOGRAPHY

X-ray topography is a defect imaging technique which depends on the scattering of X-rays from the strain associated with the defects. Two theories, namely, the kinematical and the dynamical theories, have been developed to describe the image formation. The former assumes that the amplitudes of the diffracted waves are small compared to those of the incident beam and there is no interaction between the incident primary and the diffracted waves. This approach is justified only for good quality, very thin crystals or highly defective, thick crystals. In the case of thick, nearly perfect crystals one must take into account all interactions between the incident and the diffracted waves. These phenomena are described by the dynamical theory.

The contrast in an X-ray topograph depends on the diffraction and absorption properties of a crystal. The angular range of reflection of a perfect crystal is typically 1 to 10 seconds of arc. The angular divergence

of the incident beam of characteristic radiation in Lang topography is 2 to 3 minutes of arc. A similar divergence takes place in synchrotron white radiation topography where, out of the continuous spectrum, a number of lattice planes select the proper wavelengths to be reflected according to Bragg's law. It is obvious that only a small fraction of the incident beam is diffracted by a perfect crystal. However, if the crystal contains defects, the resulting distortion of the lattice planes allows diffraction of a much larger proportion of the incident beam. The increased diffracted intensity produces an image, known as direct or kinematical image, of the strain field of the defects.

Generally speaking, in the case of thin crystals with $\mu t < 1$ (where $\mu = \frac{n}{V} \sum_i \mu_i^a$ is the linear absorption coefficient of the crystal, n is the number of molecules per unit cell, μ_i^a is the atomic absorption coefficient of atomic species i, V is the unit cell volume and t is the crystal thickness), the direct image is strongly contrasted. In the case of thick crystals ($\mu t > 1$) where the topographic image formation must be considered in terms of the dynamical theory, taking into account the interaction between primary and diffracted wave fields. In this work, for all cases examined, $\mu t < 1$. All topography results were therefore interpreted in terms of the theory for thin crystals.

4.2.1. Parameters for X-ray topography

The design of an X-ray topographic experiment involves the selection of four major conditions: X-ray reflection, sample slice plane, wavelength of radiation and sample thickness. these conditions are generally interdependent.

4.2.1.1. Selection of X-ray Reflection

One of the most important parameters for the purpose of selection of X-ray reflection is the half-width of the intensity peak of diffracted X-rays obtained by rocking the crystal around the particular Bragg angle, given by

$$\Delta\theta_{hkl} = \frac{2\, d_{hkl}\, \lambda\, |F|\, R_e}{\pi\, V\, \cos\theta_B}, \qquad (4.1)$$

where λ is the characteristic X-ray wavelength, d_{hkl} is the interplanar spacing for the (hkl) set of planes, C is the Lorentz polarization factor equal to unity for the symmetrical reflection, $|F|$ is the structure factor, V is the unit cell volume, R_e is the classical radius of an electron and θ_B is the Bragg angle for a particular reflection. This parameter is important in defining the spatial resolution and the strain sensitivity of an X-ray reflection. These factors are related by the empirical rule :

Spatial resolution x Strain sensitivity = constant. (4.2)

It is obvious that in order to get precise information about dislocation content and their

orientation in a sample, a strong reflection having large rocking-curve width giving high spatial resolution is required. On the other hand, a weak reflection with narrow rocking curve width gives high strain sensitivity which can be applied to get information about lattice distortion caused by clusters of points defects or impurities.

A second important parameter is the extinction distance, ξ, of an X-ray reflection given by

$$\xi^{-1} = \frac{\lambda |F| R_e}{\pi V \cos\theta_B}, \qquad (4.3)$$

and is related to rocking curve width $\Delta\theta$ by

$$\Delta\theta = 2 d \xi^{-1}. \qquad (4.4)$$

Extinction distance is important for two reasons. Firstly, a dislocation image cannot be observed if the sample thickness is less than 0.3ξ and, secondly, dislocation images are most strongly contrasted at thicknesses corresponding to 0.88ξ.

Another important requirement is that the condition $\bar{g}\cdot\bar{b} = 0$ should be satisfied by at least one reflection for each of the probable Burgers vectors. Sometimes it leads to a selection of reflections with lower spatial resolution. However, it is rather straightforward to establish whether or not the dislocation contrast will disappear even using a reflection at inferior resolution.

4.2.1.2. Selection of Slice Plane

The chosen slice plane should be cut perpendicularly to the growth faces and through the seed (central part) of the crystal because growth dislocations are generated at the seed interface and generally lie approximately normal to the growth face. In order to avoid geometrical distortion of images, the Bragg angles used should not be greater than 20 degrees. Highly asymmetrical reflections should be excluded to avoid a decrease in the rocking-curve width and, consequently, spatial resolution. The chosen slice plane must also allow the maximum number of reflections to be used.

4.2.1.3. Selection of X-ray Wavelength and Sample Thickness

The choice of these two conditions is limited by four factors: rocking-curve width, μt value, extinction distance and defect density. From eq. 4.1 it can be seen that the rocking-curve width and, consequently, the spatial resolution is greater for long wavelength radiations such as copper Kα. On the other hand, soft radiation is strongly absorbed and it would be necessary to use very thin samples, particularly for inorganic crystals. Hence, the lower limit of the sample thickness (the thickness less then 0.3ξ) could be exceeded and no diffraction contrast would occur. Generally, low values of μt are preferred to obtain strongly contrasted direct images and minimized dynamical images (usually being

diffuse). Under these constraints Ag or Mo Kα radiation is used for the examination of inorganic crystals and Cu Kα radiation for organic materials. The upper limit of μt factor is governed by sample perfection. Unless the defect density is low, superimposition of defects may prevent resolution of individual defects.

4.2.2. Lang Topography

Several X-ray topographic techniques have been devised for imaging defects in crystals. These have been described in several reviews [63-67]. The most versatile and widely used method is transmission Lang topography. The experimental equipment for this technique is shown in figure 4.1. A narrow, collimated beam of monochromatic X-rays intersects the crystal C which is oriented to allow diffraction from a chosen set of planes. The slit S allows only the diffracted beam to pass through the photographic film or plate F. The diffracted peak is located and monitored using a detector D set at twice the Bragg angle to the incident beam. The crystal and the film are simultaneously traversed back and forth through the narrow X-ray beam thus producing an image of the entire crystal.

In Lang topography the spatial resolution differs in the horizontal and vertical direction. Therefore, they will be considered separately.

The diffracting planes are vertical in this technique and thus there is essentially no diffraction in

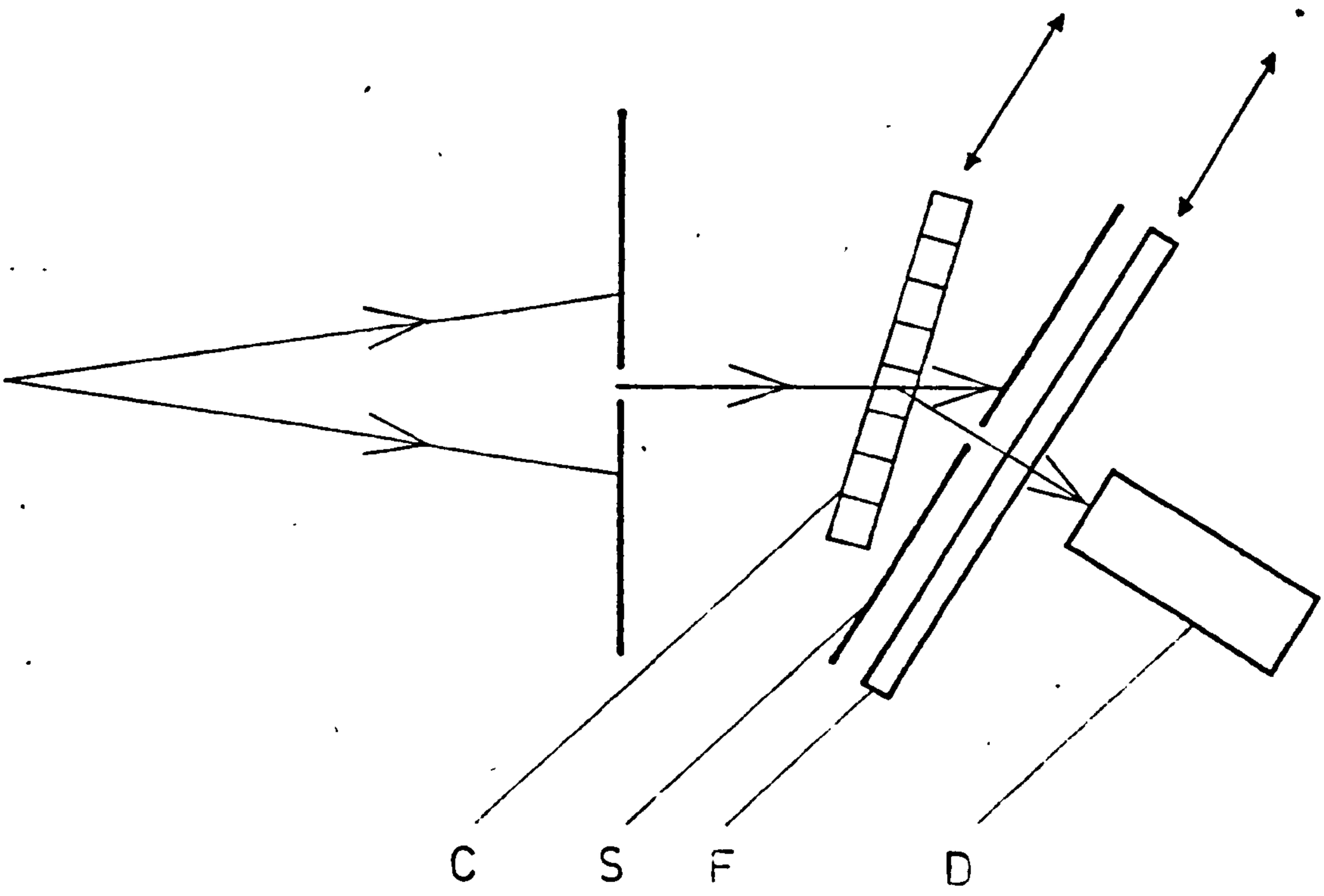

Figure 4.1. The experimental set-up for Lang topography: (C) crystal slice, (S) stop slits for primary beam, (F) film in cassette and (D) photomultiplier.

the vertical plane. The vertical resolution, v, on the plate is given by

$$v = \frac{H\,f}{L}, \qquad (4.5)$$

where H is the source height, L is the source-specimen distance and f is the specimen-plate distance. As it is practically impossible to reduce f below 1 cm and when one substitutes typical values for H = 100 μm and L = 1 m, a resolution on the order of a few microns is obtained.

The divergence of the diffracted beam in the horizontal direction is very small and is not a limiting factor in resolution. There are four other factors to be considered: vibrations, fundamental width of an X-ray line, simultaneous diffraction of both Kα lines and the fundamental width of a dislocation image.

It is very important to ensure that the specimen and the plate do not move relative to each other. Therefore, the camera should be mounted on a heavy table separately from the X-ray generator.

The spectral width of the characteristic X-ray lines, although small, can lead to a loss of resolution for large Bragg angles. Generally, this contribution is small as large Bragg angles are rarely used. Closely related to the previous consideration is the problem of diffraction of more than one line. The angular separation of $K\alpha_1$ and $K\alpha_2$ lines is between 10^{-4} and 10^{-3} rad. The maximum

permissible beam divergence is that which just allows the resolution of $K\alpha_1$ and $K\alpha_2$ peaks in the rocking curve.

Equation 4.4 shows that the rocking-curve width is inversely proportional to the extinction distance, which in turn, determines the strength of reflection. The extinction distance is inversely proportional to the scattering factor and, hence, there is a relatively weak scattering of X-rays by atoms, that leads to the narrow reflecting range. For X-rays this is typically 10^{-5} rad compared with 10^{-2} rad for 100 keV electrons. Misorientation around a dislocation line varies roughly as r^{-1}. The narrower the reflection range the farther will the crystal appear "misoriented" from the dislocation core. Roughly, one may expect dislocation images in X-ray topographs to be two or three orders of magnitude wider than those in transmission electron micrographs, as is observed. It can be seen from eq. 4.1 that, for maximum spatial resolution, strong low-order reflections should be used.

4.2.2.1. Sample Preparation

The principal requirement of any sample preparation technique is that it should produce specimens of desired shape and flatness without the generation of new defects. Samples of sodium chlorate were prepared in the form of thin slices cut from as-grown crystals by means of solvent saw using habit faces as the reference for orientation. Dissolution at the point of contact of the

saw with the crystal cuts the latter with minimal damage. Excess solvent was periodically removed from the cut with soft tissue paper to prevent dissolution of the surrounding crystal. The solvent selected for the slicing of sodium chlorate was a one-to-one mixture of ethanol and water. The slices prepared in this way were generally fairly flat, though small ridges on the surface of the cut frequently occurred. These were avoided by cutting the slices slightly thicker than required and then polishing them in the same solvent to the final thickness. In order to obtain direct images on the topographs, 0.7 to 1 mm thick slices were used.

4.2.2.2. Sample Mounting

X-ray topography is a strain sensitive method. Therefore, it is very important to handle the sample with care. Mounting of the sample should be strain free because even a slightly bent slice gives rise to dark areas on the topograph. The best way of fixing the slice is to put it in between two pieces of Mylar foil fixed in two rings or use soft wax to place the sample at its corner to the ring. Fast epoxy resins should be excluded because they introduce strain into the sample.

4.2.2.3. Procedure for Recording Lang Topographs

The experimental procedure for recording Lang topographs has been described by Lang [63] and Tanner [64]. The following paragraphs outline the procedure used in a step by step manner.

(1) The mounted sample was clamped onto the goniometer head in such a way that the desired diffracting planes were vertical. Orientation to within ± 1° was achieved using an adjustable set square with known habit face as a reference. The slice plane was normal to the X-ray beam.

(2) The crystal was centred in the X-ray beam with the aid of a fluorescent screen.

(3) The detector was set at an angle of 2θ to the incident beam.

(4) The crystal was rotated about its vertical axis to an appropriate angle. In the case of a symmetrical reflection this was the Bragg angle.

(5) The crystal was then rotated slowly until a peak was observed on the ratemeter. Once the peak had been found, the crystal was finely rotated to give maximum diffracted intensity on the $K\alpha_1$ peak.

(6) The traverse width limits were set by scanning the crystal through the beam and noting where the diffracted intensity dropped to background level.

(7) The diffracted beam slit was then moved into a position perpendicular to the diffracted beam and as close to the crystal as possible. The slit was adjusted to allow only the diffracted beam to pass.

(8) A test exposure was taken using fast Agfa M3 X-ray film. The film was placed in a light-proof cassette and positioned parallel to and as close as possible to the diffracted beam slit. This provided a check that the

topograph had been aligned properly and gave an estimate of exposure time.

(9) If the test exposure was satisfactory, then a high resolution Agfa D4 X-ray film was inserted and the topograph recorded.

4.2.2.4. Photographic Enlargement

All recorded topographs were enlarged using photomicrographic equipment with camera and then printed on Ilford paper in order to obtain the proper contrast. It should be mentioned that all of the stages of photographic processing are critical and a great care must be applied not to lose the initial resolution of the topograph.

4.2.3. Synchrotron Radiation - Its Application to X-ray Topography

Synchrotron radiation has several important, unique properties including high intensity, broad spectral range and natural collimation. In addition, synchrotron radiation produced by storage rings offers small source-spot size and stability. Any of these properties would make synchrotron radiation an important experimental tool.

Conventional X-ray sources emit unpolarized divergent, quasi-monochromatic radiation. The conversion of electron power to characteristic X-radiation is less

than 0.1% efficient. In contrast, accelerated electrons in a storage ring or in a synchrotron emit linearly polarized "white radiation" as a near plane wave with almost 100% efficiency. Unlike conventional X-ray diffraction topography with characteristic radiation, the whole source contributes to the intensity diffracted by each point in the sample. The spatial resolution is therefore determined by the projected size of the source so that, for a crystal distance L from the source and distance f from the film, the vertical resolution is $v = \frac{H f}{L}$ (where H is the source height) and the horizontal resolution is $h = \frac{W f}{L}$ (where W is the projected width of the source). For white topography station at Synchrotron Radiation Source at Daresbury the source height is 0.4-1.9 mm, the source width is 13-7.8 mm, the distance from the source to the crystal is 80 m and the typical specimen-to-film distance is 5 cm. Therefore, the vertical resolution is 8-5 μm and the horizontal resolution is 0.3 to 1.2 μm [68]. These resolutions are comparable to those obtained by classical Lang topography. Another advantage of white beam topography is crystal assessment with greater range than Lang topography (poor crystals can be studied). The intensity of diffracted beam is several orders of magnitude higher than for Lang topography. Therefore, the exposure times are typically 10-20 minutes while they are 20-40 hours using conventional X-ray generator.

4.2.3.1. Procedure for Recording White Radiation Topographs

The principles of sample preparation and sample mounting for white radiation topography remain the same as for the conventional Lang topography. This section outlines the procedure for recording synchrotron topographs underlining differences with Lang topography.

(1) The mounted sample was clamped onto the goniometer head in such a way that the slice plane was normal to the X-ray beam.

(2) The crystal was centred in the synchrotron X-ray beam using X-ray sensitive "green" paper.

(3) The pinhole Laue photograph was obtained and compared with computer simulation of the pattern corresponding to the given orientation of the sample. The crystal was gently rotated along the horizontal and vertical axes and Laue patterns were monitored to get the matching pattern for the required setting of the sample. This procedure ensured the exact orientation of the sample.

(4) The crystal was set at the appropriate Bragg angle θ by a computerized motor system and the film cassette was set at 2θ angle.

(5) Fast Agfa M3 X-ray film was used for a test exposure.

(6) If a test exposure was satisfactory, then a high resolution Agfa D2 or D4 X-ray film was used.

In order to record simultaneously the whole set of topographs the Laue configuration was set, i. e. after

recording the pinhole Laue pattern the film cassette was moved 20-25 cm from the crystal and the beam size was increased to "light up" the whole crystal. In such a way a set of nonoverlapping images from different sets of lanes was recorded. In spite of the geometrical distortion of such topograph it is a useful tool for fast preliminary assessment of sample quality.

The procedure for photographic enlargement of synchrotron topographs is the same as for Lang topography.

CHAPTER 5

GROWTH, MORPHOLOGY AND CHARACTERIZATION OF PURE AND DOPED $NaClO_3$ CRYSTALS

The survey of the published literature on the nucleation and growth of sodium chlorate, presented in chapter 3, indicates the following:

(1) There is an absence of studies of the effect of impurities on the homogeneous nucleation of this compound.

(2) The reported results on the effect of supersaturation on the growth habit of the crystal are conflicting. Moreover, there is a lack of investigations dealing with simultaneous observation of habit and surface micromorphology to deduce the growth mechanism of the crystal.

(3) The mechanism of habit modification of the crystal by ionic impurities is poorly understood.

The present chapter presents the results of our investigation of the influence of supersaturation and impurity on the nucleation characteristics and growth morphology of sodium chlorate. For the investigation sodium dithionate was selected as an impurity because of its well known profound influence in changing the growth habit of the crystals. In order to elucidate the mechanism of adsorption of the impurity in changing the

growth morphology of the crystals, the micromorphology of the surfaces of the crystals, their defect distribution and the variation of their lattice parameter were investigated.

5.1. NUCLEATION OF SODIUM CHLORATE IN THE PRESENCE OF SODIUM DITHIONATE

In order to investigate the nucleation process of $NaClO_3$ in the presence of $Na_2S_2O_6 \cdot 2H_2O$ impurity and to estimate nucleation parameters such as surface free energy, activation energy for nucleation and radius of critically-sized nucleus, homogeneous nucleation experiments were performed from pure solutions and those containing known amounts of sodium dithionate. The experimental set-up, presented in figure 5.1, is based on the principle of scattering of light by particles of sizes of the order of wavelength of light or smaller. As soon as nucleation initiates in the solution, a decrease in the intensity of the transmitted light takes place. Thus the high sensitivity of the technique, which is obviously a turbidimetry technique, ensures a reliable estimation of surface free energy for pure and doped crystals.

The experimental set-up, figure 5.1, consists of a double-walled glass cell (1) filled with solution and sealed for the whole series of experiments at a known

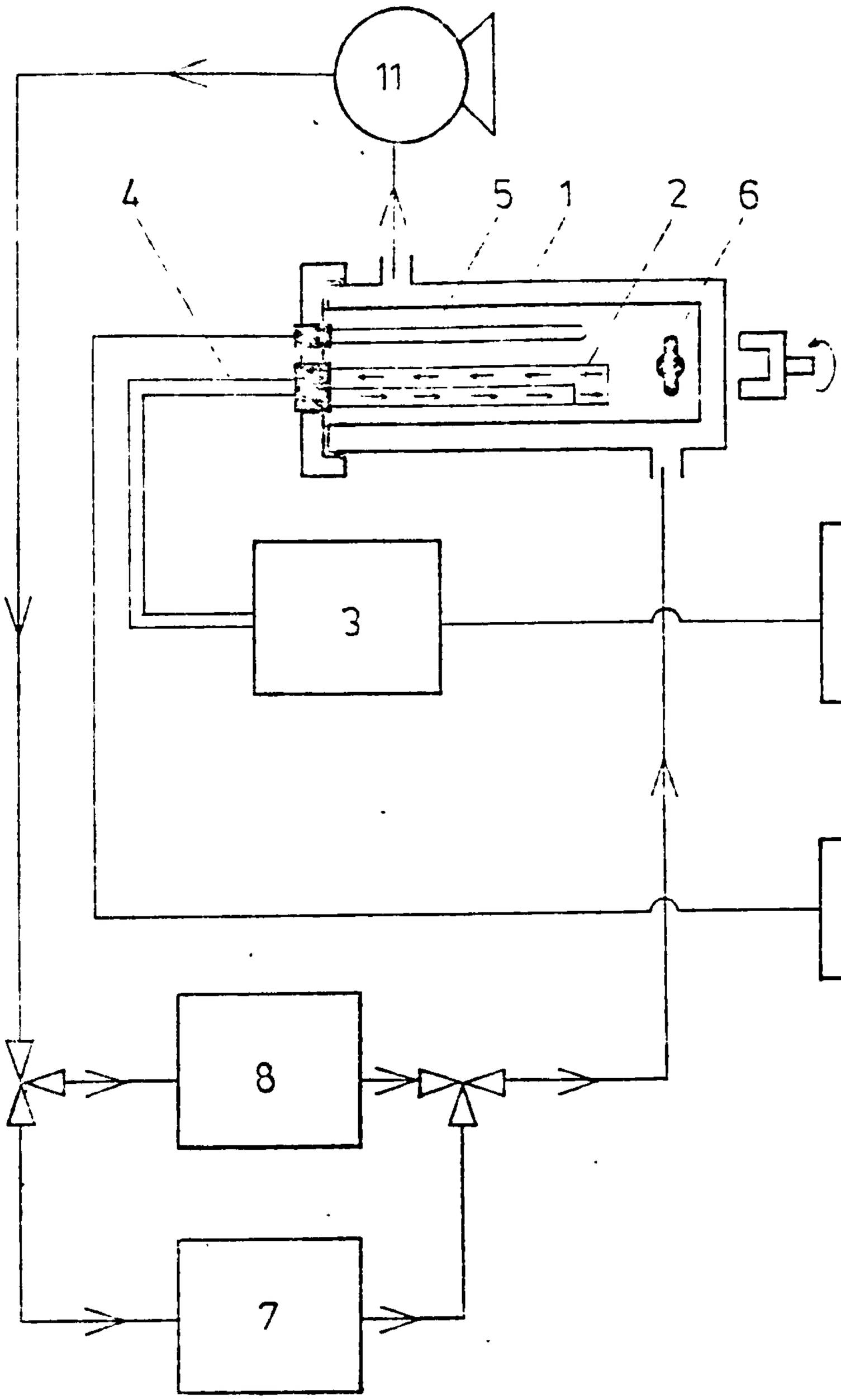

Figure 5.1. Experimental device for the measurement of induction period for nucleation:
(1) double-walled glass cell, (2) light probe, (3) colorimeter, (4) optical fibre, (5) platinum resistance thermometer, (6) magnetic stirrer, (7, 8) water tanks, (9) digital display, (10) chart recorder and (11) magnetic pump.

value of impurity concentration. The cell is fitted with a light probe (2) connected with a colorimeter (3) by an optical fibre (4). Temperature in the cell is monitored by a platinum resistance thermometer (5). Temperature control of the measurement cell is maintained by water circulating through the double walls from a water tank kept at the desired constant temperature.

At the beginning of the experiment, the solution was kept above the saturation temperature, T_s = 303 K, and efficient stirring by a small magnetic stirrer (6) enabled the dissolution of all small crystallites formed during the previous measurement. The desired supercooling, $\Delta T = T_s - T_{exp}$, was obtained by switching the water circulation from the hot (7) to the cold tank (8) kept at preset temperatures T_h and T_{exp}, respectively, such that $T_h > T_s > T_{exp}$. The induction period for nucleation, i.e. the time required to observe the first nuclei (in this case, to observe a decrease in the intensity of the light transmitted through the cell) was noted for different values of supercooling, ΔT, which was fixed between 10 and 20 K for solutions with and without the impurity.

Using the solubiblity data of Linke [87] supersaturation $\sigma = (c-c_o)/c_o$ (where c and c_o are actual and equilibrium concentrations expressed in g/100g solution) was calculated. From the data on the induction period, τ, as a function of supersaturation, $S = 1 + \sigma$,

at various values of the ratio, x, of $S_2O_6^{2-}$ to ClO_3^- ions, plots of ln τ against T^{-3} $(\ln S)^{-2}$ were constructed, (cf. eq. 2.4). From these plots, values of surface free energy, γ, were calculated (eq. 2.5).

The typical dependence of ln τ on T^{-3} $(\ln S)^{-2}$ obtained in the range of relatively low supersaturations is presented in figure 5.2 for pure $NaClO_3$ solution. From the figure a large scatter in the value of the induction period is evident at all nucleation temperatures. Such a pronounced dispersion of the induction period is caused by the statistical character of the nucleation process itself and its value generally increases with decreasing supersaturation ratio. Figure 5.3 shows the surface free energy as a function of impurity content. The figure shows that there is a general increase in the values of γ and r^* (cf. eq. 2.3) with impurity concentration. This implies that dithionate ions act as obstacles to the formation of nuclei of critical size. An additional process which might happen simultaneously is the possible incorporation of a few dithionate ions into the nuclei such that they render them unstable thermodynamically compared with those formed in pure $NaClO_3$ solution. Consequently, a system containing the impurity requires a relatively large activation energy of nucleation and a large radius of the critical nucleus (cf. eqs 2.2 and 2.3).

It should be mentioned that the values of γ, obtained

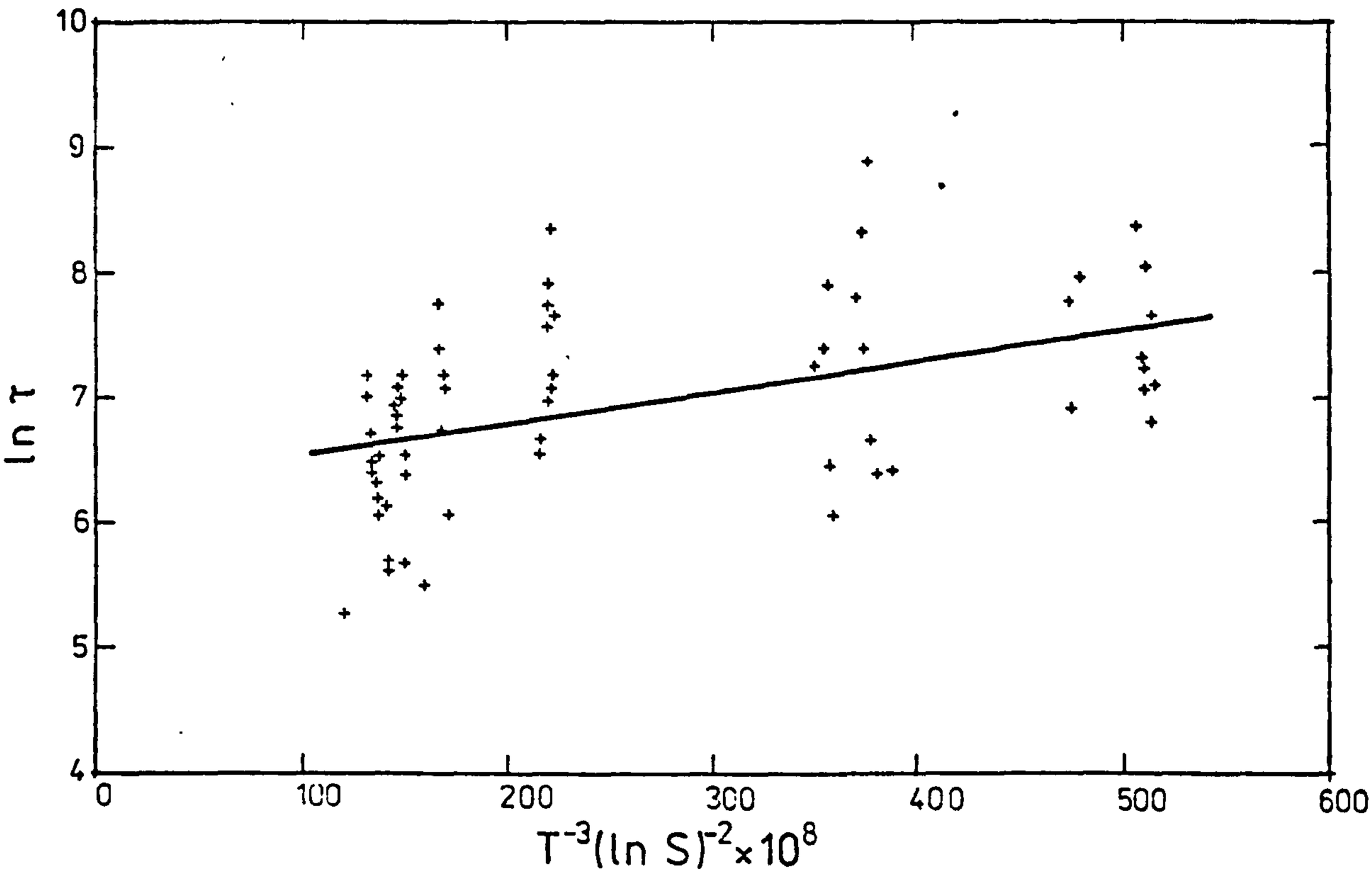

Figure 5.2. Plot of the dependence of ln τ on $T^{-3}(\ln S)^{-2}$ obtained for the nucleation of pure $NaClO_3$.

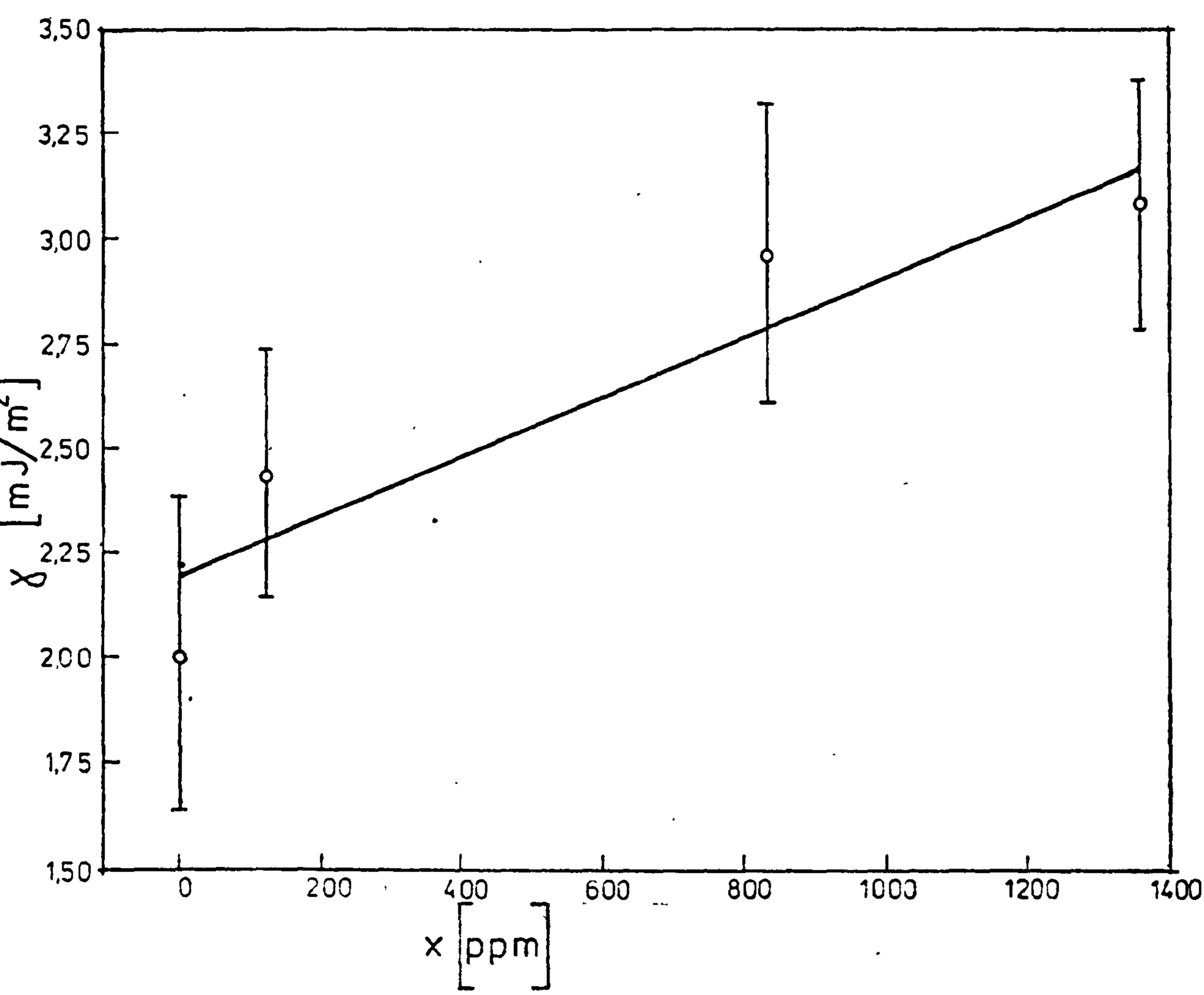

Figure 5.3. Dependence of surface free energy, γ, on impurity content, x, in the nucleating solution.

in this work, are comparable with those obtained for other water-soluble compounds (e. g. for KDP, γ = 2.8 mJ/m^2 [91]). However, these values are somewhat low in comparison with these predicted theoretically [92].

5.2. MORPHOLOGY

5.2.1. Growing of the Crystals

Crystals of sodium chlorate for the studies of morphology and characterization were grown from supersaturated aqueous solution slightly above ambient temperature. The following two methods were used for growth.

5.2.1.1. Temperature Lowering Technique

In this method the supersaturation for growth was achieved by lowering the solution temperature at a constant rate. The apparatus used for this technique is shown in figure 5.4 [69]. The long necked flask (1) filled with the solution is fitted with a ground glass seal and stirring gland (2). The solution is stirred by the glass paddle (3) fitted with a loop to suspend the seed crystal. The motion of the stirrer is kept constant at 60 rpm during every experiment to promote efficient stirring. The growth vessel is situated in a 20 litre water bath (4) heated by an infra-red lamp (5). The water bath is stirred continuously. Temperature control is achieved by using a long range contact thermometer (6).

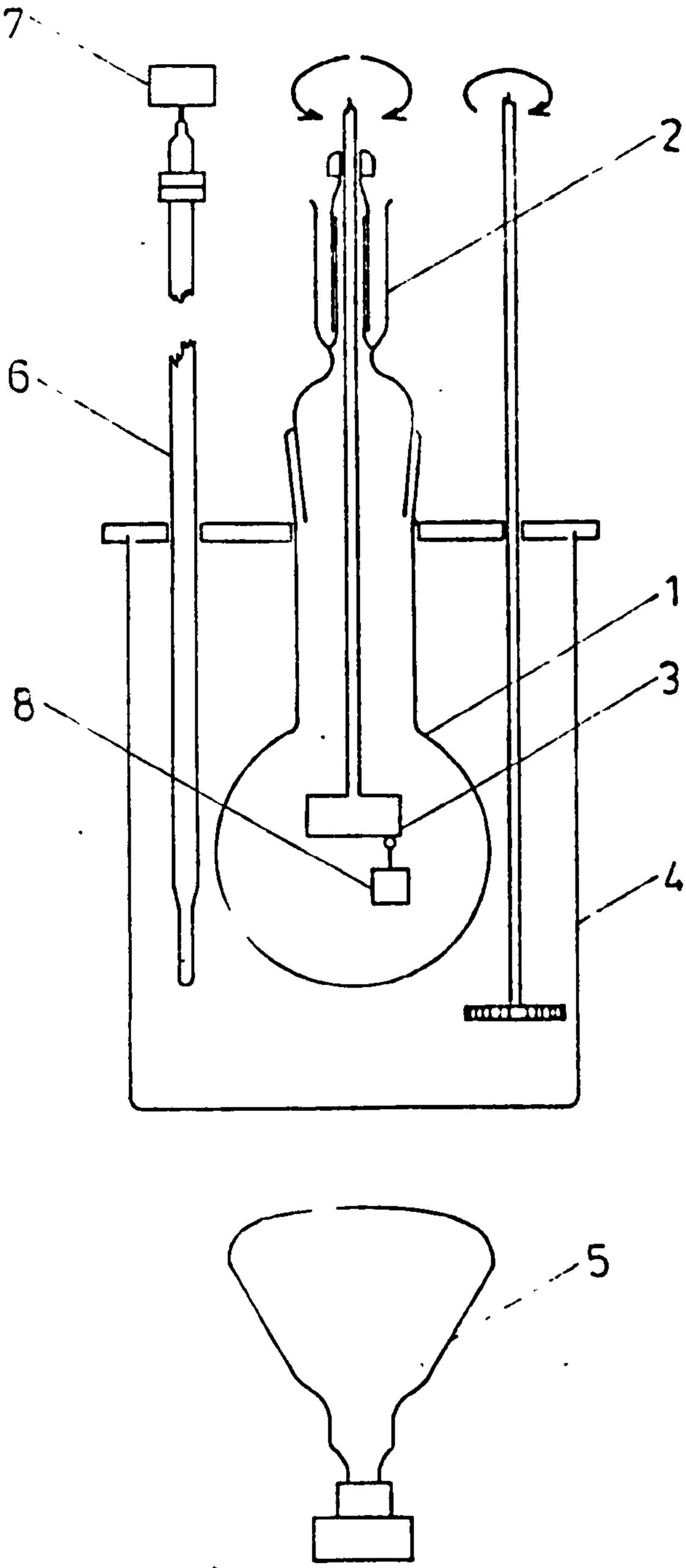

Figure 5.4. The crystallizer used for growth by temperature lowering method:
(1) crystallization flask filled with solution, (2) stirring gland, (3) stirrer, (4) water bath, (5) infrared lamp, (6) contact thermometer, (7) synchronous motor and (8) seed.

The rate of lowering of the temperature is changed by using the appropriate synchronous motor (7) of a given speed to drive down the contact thermometer. Additionally, the motor can be switched off and on for variable periods of time by a switching device to provide fine control of the temperature lowering rate. The large volume of the thermostat bath eliminates rapid fluctuations in temperature. The pulse-like heating maintains temperature control in the growth flask at ± 0.005 K [70]. Cooling rates used varied from 0.007 to 2 K/day in different experiments. All of the seeds used in the experiments were tabular in shape (only {100} form) and transparent without visible inclusions or mechanical damage.

After slightly dissolving in distilled water at room temperature, the seed (8) was hung alongside the paddle of the stirrer by using glass fibre or nylon thread. After the completion of growth, the crystal was picked up quickly from the supersaturated solution and dipped for a moment in n-hexane (kept at the same temperature as the solution) in order to remove the adsorbed solution layer from the crystal. The adhering n-hexane was then soaked up with a piece of soft tissue paper. This procedure has to be done to minimize secondary effects, e.g. local growth of the crystal. Their morphology and defect structure were subsequently investigated.

In a related series of experiments, growth was

carried out at constant temperature using fixed values of supersaturation $\sigma = (c - c_o)/c_o$ obtained by applying a constant temperature difference $\Delta T = T_o - T_g$ (T_o and T_g are the saturation and growth temperature, respectively).

5.2.1.2. Solvent Evaporation Method

In this method supersaturation was achieved by allowing the solvent of the growth solution to evaporate slowly. Solution was poured into petri dishes of 15 cm diameter and 7 cm height covered with watch glasses. The dishes were placed into a thermostated compartment and kept for the desired time to allow growth to take place. After the completion of growth, the crystals were picked up from the solution, dipped in n-hexane and dried as in the temperature lowering technique. The rate of evaporation, and therefore the supersaturation, could not be controlled accurately in this method. Additionally, vertical concentration gradients occurring under the growth conditions caused the generation of small seeds on the solution surface, which fell down after growing to a larger size.

This technique was mainly used for growing seeds of sizes up to 5 mm x 5 mm x 5 mm. Some larger crystals obtained by this technique showed typical tabular shape caused by limitations of mass transfer to the bottom face of the crystals. Examination of the seeds by X-ray topography revealed that, generally, this growth technique can be used to obtain seeds of good quality but

the quality of larger crystals of sizes 10 mm x 10 mm x 5 mm was bad.

5.2.2. Growth Habit

5.2.2.1. Pure Crystals

The form and optical perfection of sodium chlorate crystals grown at different cooling rates are presented in table 5.1. The perfection of the as-grown crystals was assessed from the amount of inclusions observed by transmission light microscopy. Obviously, the resulting crystals are cuboids modified by {110} and {111} faces in the range of cooling rate 0.007-0.03 K/day and pure {100} cuboids in the range 0.04-2 K/day. However, in the latter case {110} and {111} faces were also occasionally observed when parasitic crystals were present at the bottom of the crystallizer. The cooling rates at which this has been observed are marked by asterisk in table 5.1.

The morphological importance of the faces for crystals with {110} and {111} faces is given in table 5.2. This table indicates that with an increase in cooling rate the relative areas of {110} and {111} faces are decreased. This fact may be attributed to the differences in the kinetic coefficients of these faces [24]. The most likely explanation for the occasional observation of the {110} and {111} face at increasing supersaturation is associated with the influence of parasitic crystals in decreasing the solution

TABLE 5.1. Dependence of perfection and growth habit of pure sodium chlorate crystals grown by the temperature lowering method on cooling rate

Cooling rate [K/day]	Temperature range for growth [K]	Perfection	Habit/Forms
0.007	309.5-309.5	High	{100} and {110}
0.03	304.95-304.1	High	{100}, {110} and {111}
0.04	308.45-307.15	High	{100}
0.04 *	307.35-305.45	High	{100} and {111}
0.07	309.75-309.15	High	{100}
0.16 *	311.15-307.35	Average	{100}
0.20 **	303.95-302.3	High	{100} and {110}
0.32	300.65-298.05	High	{100}
0.48 *	311.15-308.25	Average	{100} and {111}
0.52	311.65-310.05	High	{100}
0.64	309.75-299.55	High	{100}
1.05	309.85-305.55	High	{100}
2.00	310.85-304.45	High	{100}

* Run in which a parasitic crystal grew at the crystallizer bottom.

** Run without stirring.

TABLE 5.2. Percentage area of different faces of sodium chlorate crystals in relation to cooling rate of pure solutions

Cooling rate	Percentage area		
[K/day]	{100}	{110}	{111}
0.007	64.8	34.2	1.0
0.03	51.5	47.5	1.0
0.04 *	99.6	—	0.4
0.20 **	93.4	6.6	—

* Run in which a parasitic crystal grew at the crystallizer bottom.

** Run without stirring.

supersaturation. The appearance of the {110} faces at cooling rate 0.20 K/day is connected with mass transport.

The effect of supersaturation on morphological importance was investigated at about 307 K. The results, presented in table 5.3, also show that the {110} and {111} faces are eliminated with increasing supersaturation.

The above results of the appearance of the {110} and {111} faces at low cooling rates (table 5.2) and low supersaturation (table 5.3) are in contradiction to those reported by Kern [55]. However, they are in agreement with those reported by Simon [57]. Our experiments in the growth cell (shown in figure 6.1, chapter 6) also gave pure {100} habit at supersaturations exceeding about 0.25 % but at lower supersaturations additional {110} faces appeared. Therefore, we may conclude that the transition from pure cubic habit to cuboid with {110} and {111} faces is due to decreasing supersaturation and cooling rate.

5.2.2.2. Doped Crystals

Crystals of sodium chlorate doped with sodium dithionate were grown by the constant cooling rate method using the equipment shown in figure 5.4. Solution with the required amount of admixture was prepared before every growth experiment. The admixture was added to freshly prepared pure solution saturated at 308 K. Three impurity concentrations, viz. 70, 140 and 210 ppm of

TABLE 5.3. Percentage area of different faces of $NaClO_3$ in relation to supersaturation of pure solutions

Supersaturation	Percentage area		
[%]	{100}	{110}	{111}
0.09	63.0	28.3	8.7
0.3	94.1	5.9	—
0.3	90.1	9.9	—
0.52	89.9	10.1	—
0.52	91.8	8.2	—

TABLE 5.4. Percentage area of different faces of $NaClO_3$ in relation to impurity content in solutions

Impurity content	Percentage area		
[ppm of $S_2O_6^{2-}$]	{100}	{110}	{111}
70	86.5	—	13.5
70	91.4	—	8.6
140	37.8	—	62.2
210	5.1	—	94.9

$S_2O_6^{2-}$, were used. The crystal habit varied with impurity concentration (table 5.4). It was {100} cuboid truncated by four small {111} faces for 70 ppm, {111} tetrahedron with small {100} faces for 140 ppm and {111} tetrahedron without {100} faces for 210 ppm. The maximum cooling rate used for the growth of doped crystals was 0.09 K/day. It was impossible to use larger cooling rates because the fast-growing {100} faces led to the capture of large inclusions of the mother liquor in the {111} growth sectors.

From the above results it is obvious that $Na_2S_2O_6 \cdot 2H_2O$ has a very pronounced effect on the growth morphology of sodium chlorate crystals. A concentration of only one ion of $S_2O_6^{2-}$ to every five thousands ions of ClO_3^- is sufficient to change the cuboid habit (figure 5.5) to a simple tetrahedral habit (figure 5.6).

The tetrahedral planes of sodium chlorate possess 3-fold axis passing normally through them. As there are ClO_3^- groups arranged in the structure compatible with cubic symmetry (figure 5.7a) these will be situated in the tetrahedral planes (figure 5.7b). Every such plane will therefore contain groups of three oxygen atoms arranged on an equilateral triangle and bonded together by a chlorine atom placed on the trigonal axis which passes normally through the triangle. X-ray analysis [71] shows that ClO_3^- ion is a flat trigonal pyramid having the three oxygen atoms at its base 2.38 Å apart.

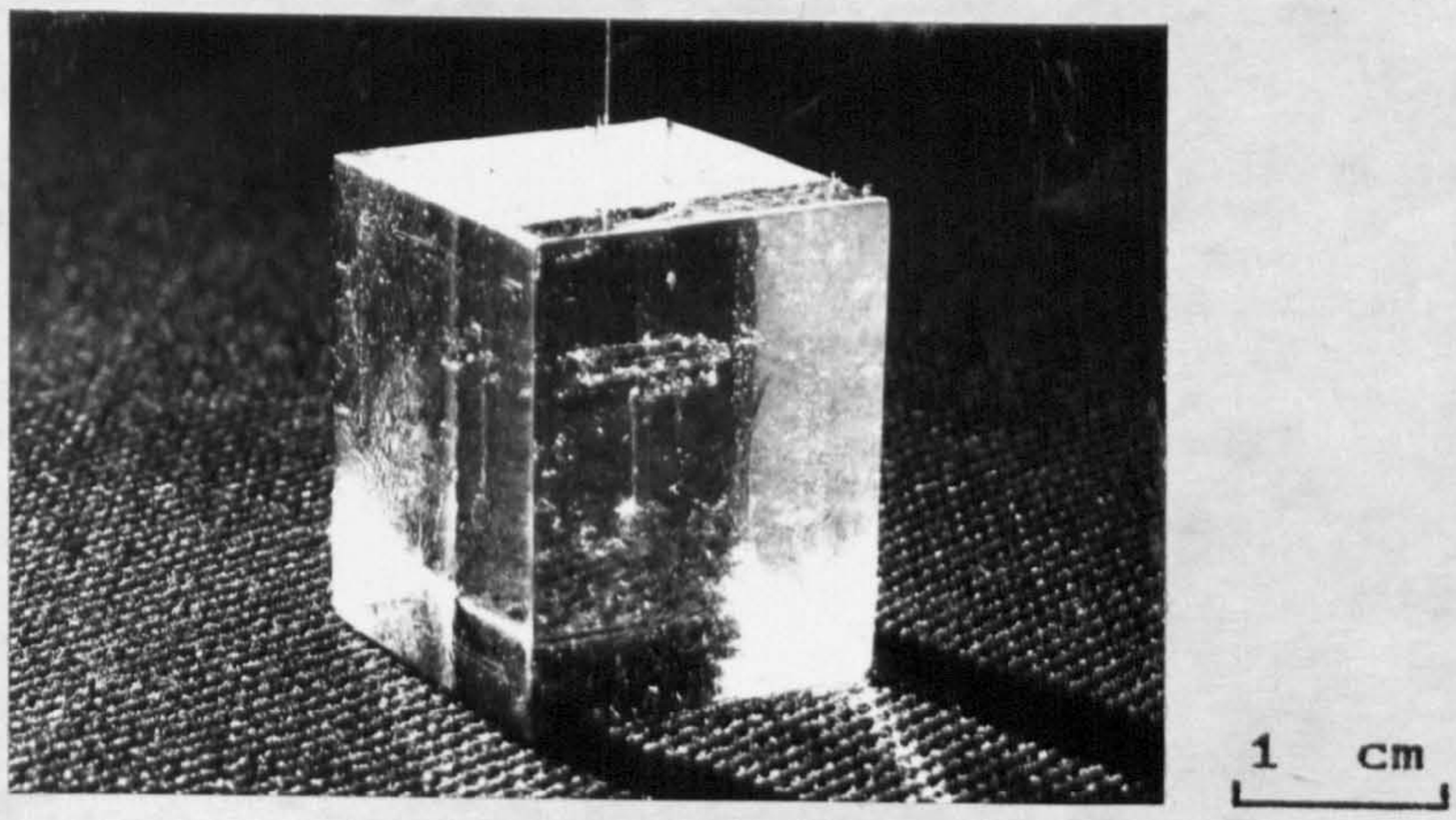

Figure 5.5. Photograph of a crystal of pure sodium chlorate exhibiting cuboid habit; cooling rate 0.64 K/day.

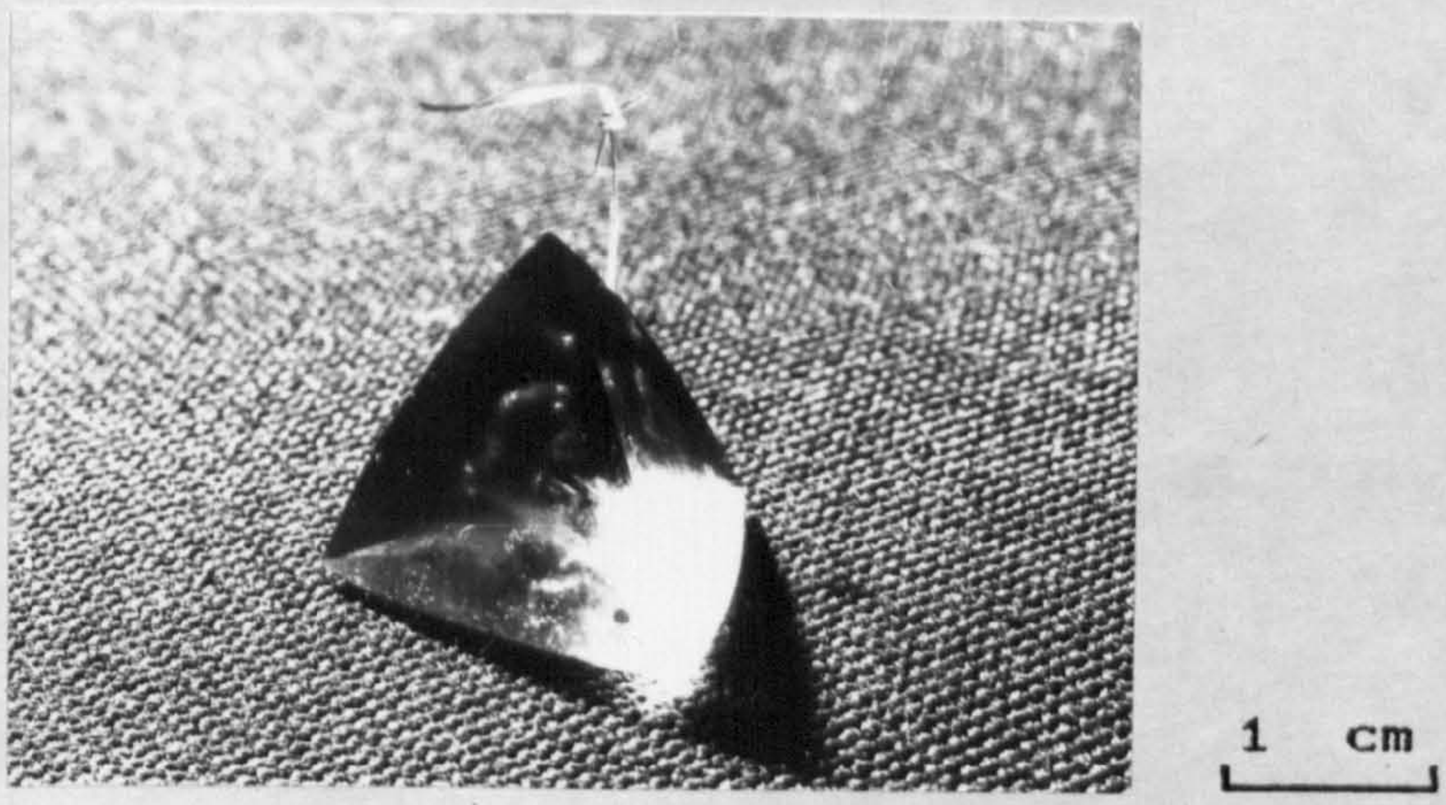

Figure 5.6. Photograph of a crystal of sodium chlorate doped with 210 ppm of $S_2O_6^{2-}$ ion exhibiting tetrahedral habit; cooling rate 0.09 K/day.

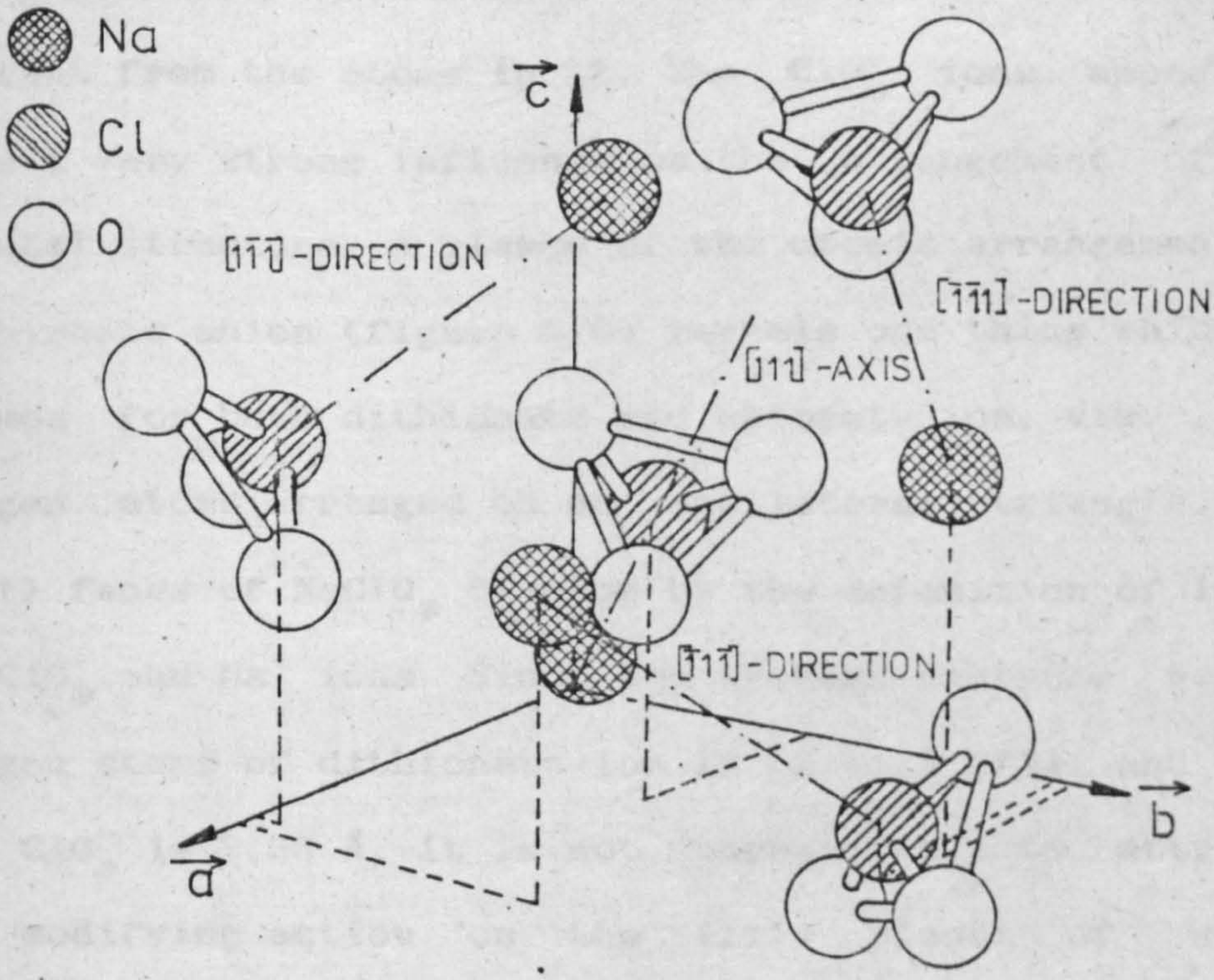

Figure 5.7 (a). Arrangement of Na^+ and ClO_3^- ions in the structure of sodium chlorate crystal.

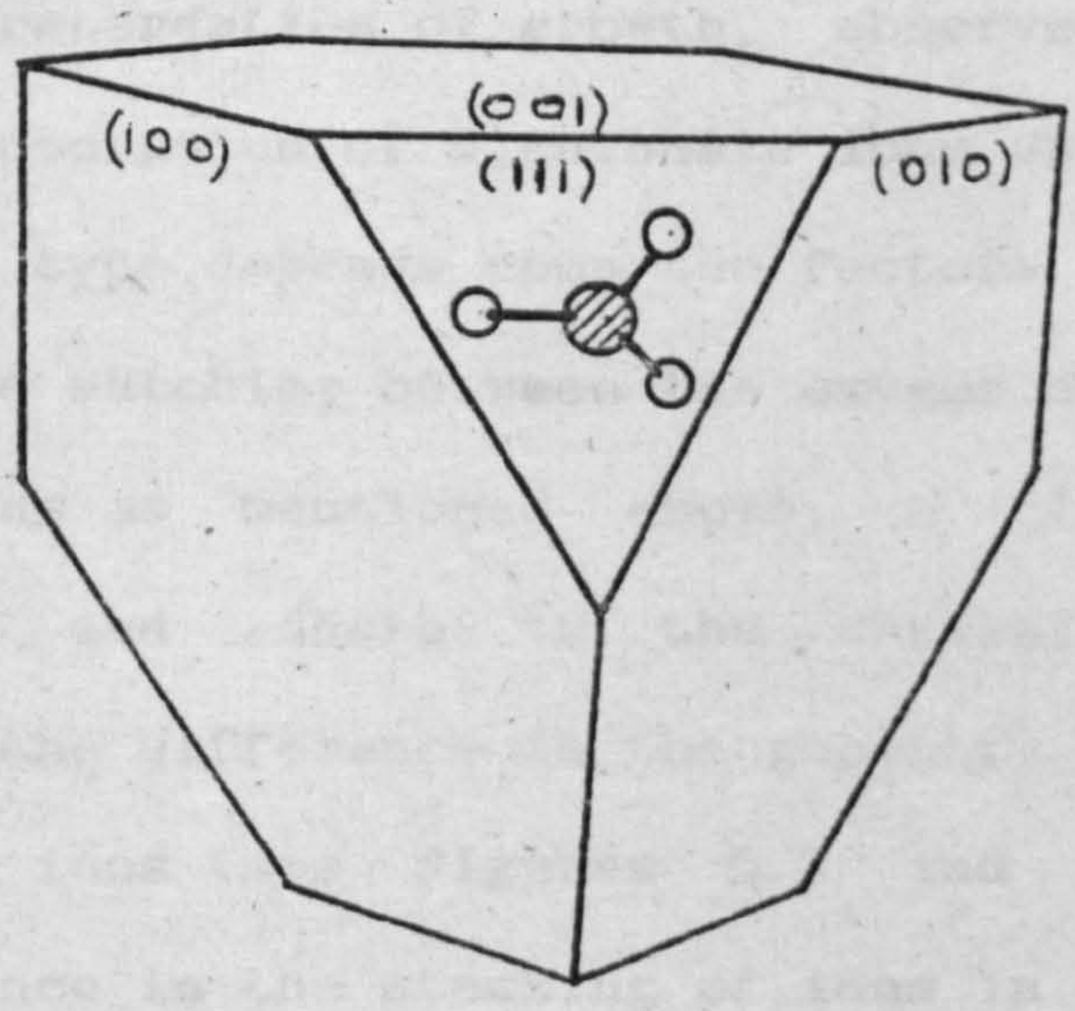

Figure 5.7 (b). Arrangement of ClO_3^- ion on the (111) face of sodium chlorate crystal.

The chlorine atom is 0.48 Å below this base and 1.455 Å distant from the atoms in it. The ClO_3^- ions appear to have a very strong influence on the arrangement of the crystal structure. A glance of the atomic arrangement of dithionate anion (figure 5.8) reveals one thing which is common for both dithionate and chlorate ion, viz. three oxygen atoms arranged on an equilateral triangle. The {111} faces of $NaClO_3$ develop by the deposition of layers of ClO_3^- and Na^+ ions. Since the average distance between oxygen atoms of dithionate ion is 2.44 Å [72] and that for ClO_3^- is 2.38 Å, it is not unreasonable to attribute the modifying action on the {111} planes of sodium chlorate to some power of attachment possessed by these ions through oxygen triangles.

The retardation of growth, observed experimentally, by the adsorption of dithionate ions on the four faces of {111} type depends upon two factors. First, because of the close matching between the oxygen atoms of ClO_3^- and $S_2O_6^{2-}$ ions as mentioned above, a dithionate ion can approach and adhere to the crystal surface easily. Second, the difference in the geometry of dithionate and chlorate ions (see figures 5.7 and 5.8) leads to a disturbance in the stacking of ions in the {111} layer. Concerning the second effect one may say that the dithionate ions, which extend far out beyond the layer of ClO_3^- ions on the {111} face, will cause much more disturbance on that account alone.

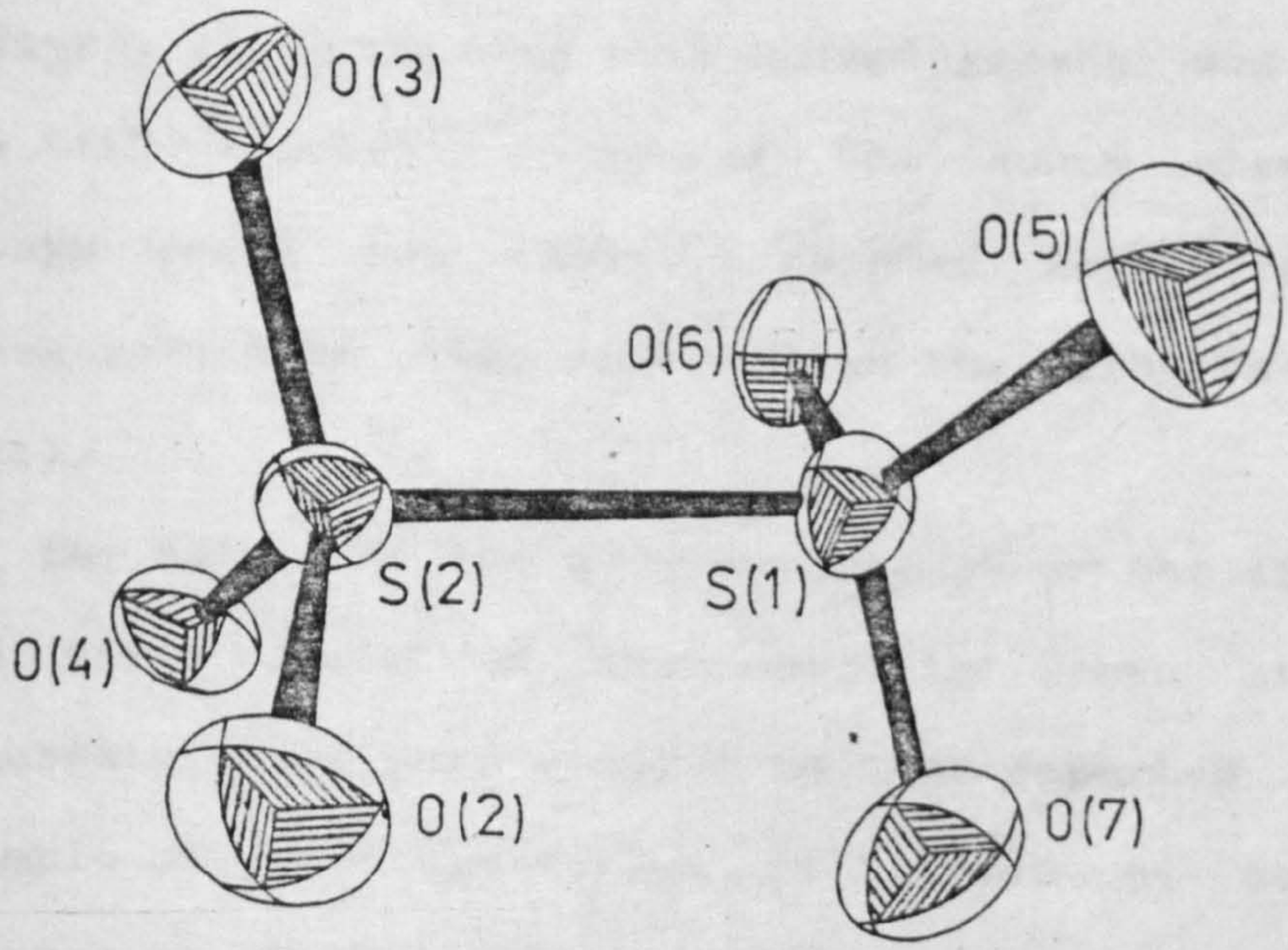

Figure 5.8. Structure of $S_2O_6^{2-}$ ion.

5.2.3. Surface Micromorphology

Microscopic examination of the {100} surfaces of crystals grown at all values of cooling rates revealed the presence of growth layers and flat-bottomed hillocks (figures 5.9 and 5.10). The crystal edges and flat-bottomed hillocks appeared to act as sources of layers (figure 5.9). The layers were especially thick on the faces grown at higher cooling rates (figure 5.10). However, at no cooling rate spiral growth was observed. The {110} and {111} faces of the above crystals were always rough but kinked, rounded layers emitted by elevations were often observed on the {110} faces (figure 5.11).

The nature of the micromorphology of the {100}, {110} and {111} faces of the crystals grown at constant supersaturation were similar to that reported above. An example of the initiation of layers by dark-looking sources is shown in figure 5.12).

The presence of $S_2O_6^{2-}$ impurity ions in the solution was observed to have a significant influence on the micromorphology of the {100} and {111} faces of the doped crystals. On the {100} faces thick layers with saw-teeth-like structure were observed (figure 5.13). The thickness of these layers increases with increasing impurity concentration. The layers originate from the edge common with the (111) face (see figure 5.7b). The {111} faces became more rough with increasing impurity

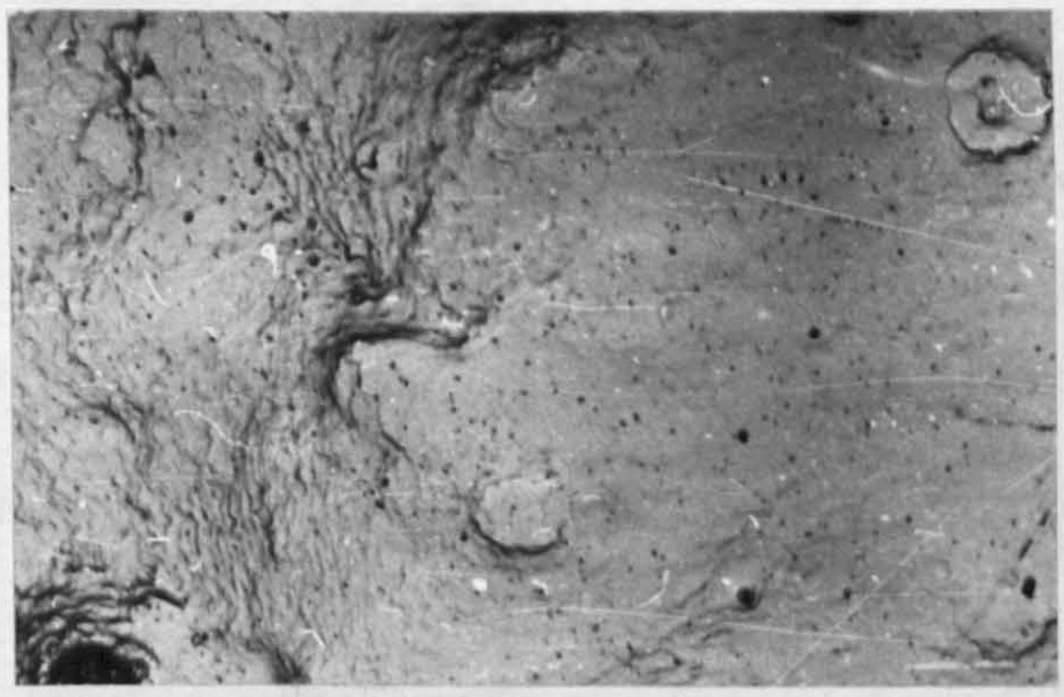

Figure 5.9. The (100) face of a pure sodium chlorate crystal, grown at cooling rate 0.007 K/day, showing the movement of growth layers and the appearance of flat-bottomed growth hillocks. The initiation of layers in hillock-free areas took place at the edge of the crystal situated on the left side of the photograph.

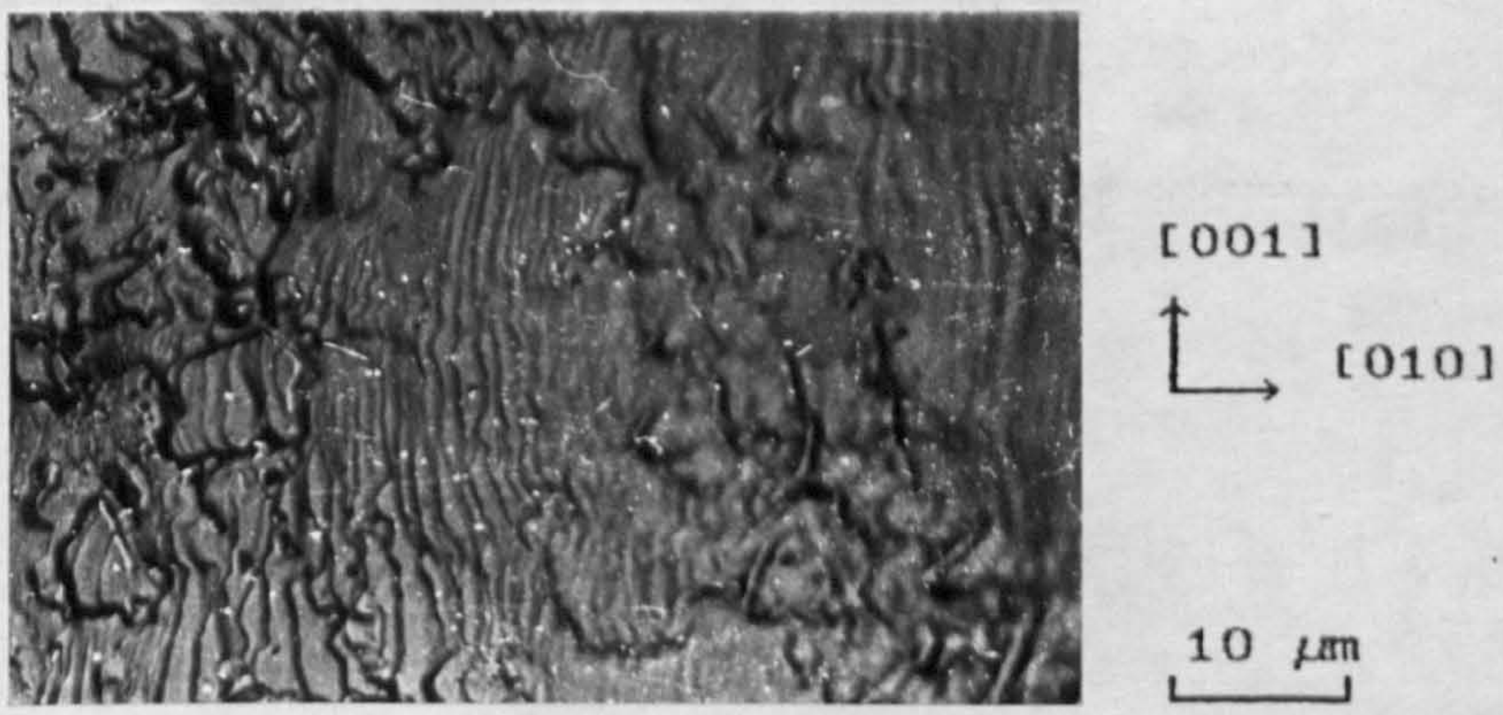

Figure 5.10. Bunching of layers observed on the (100) surface of a pure sodium chlorate crystal grown at cooling rate 0.16 K/day.

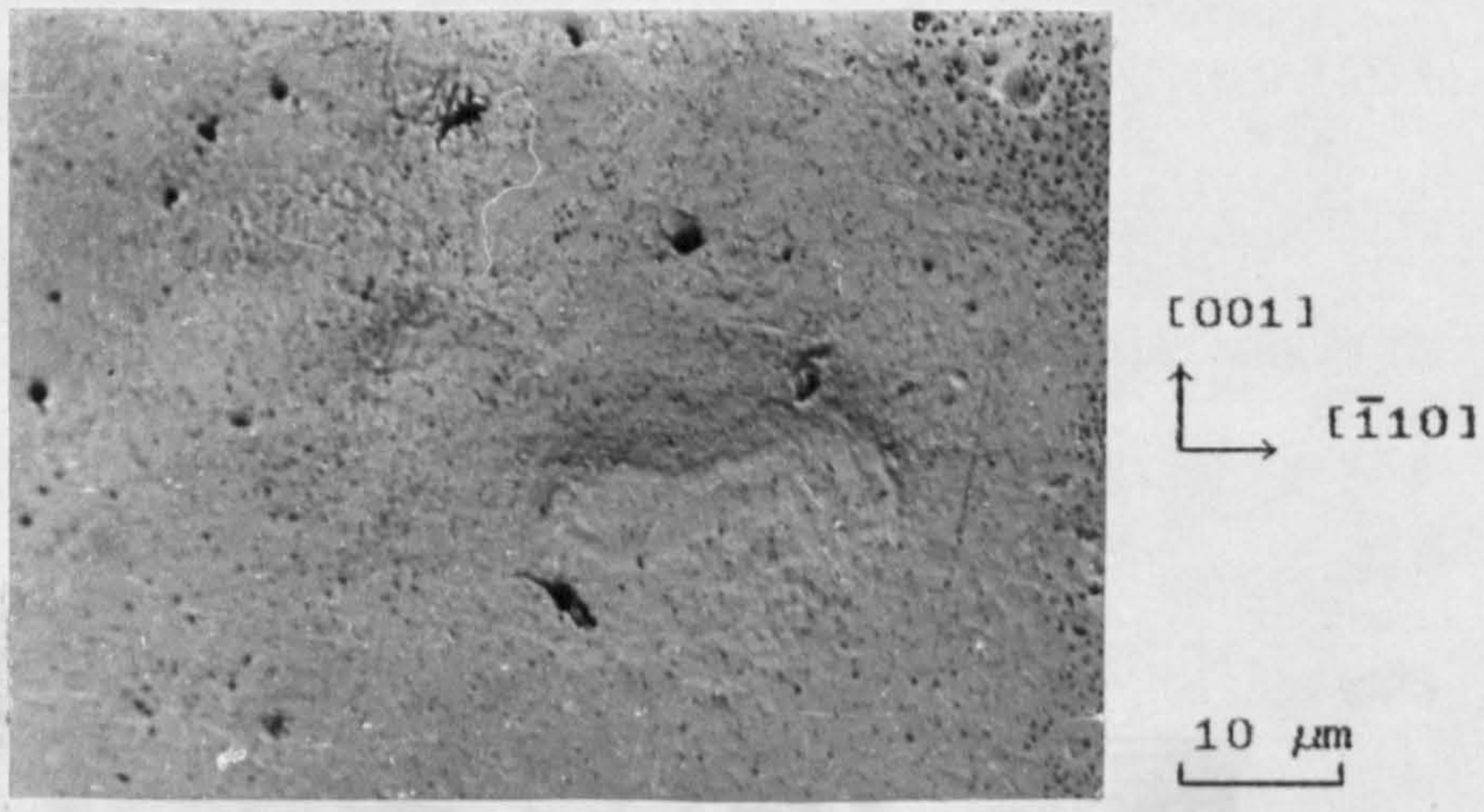

Figure 5.11. The (110) surface of a sodium chlorate crystal grown at cooling rate 0.007 K/day showing rough nature. The layers emitted by the irregularly shaped hillock are rounded and kinked.

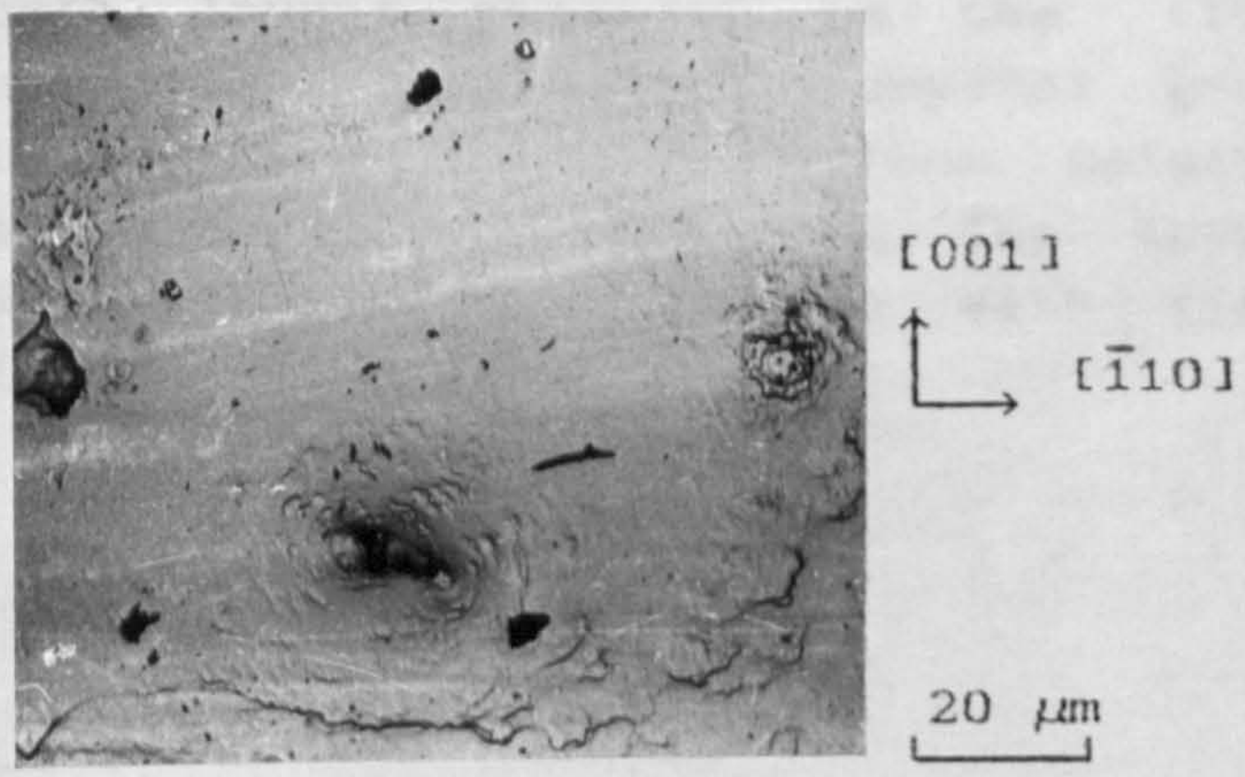

Figure 5.12. Example of layers originating from an elevation (probably large dirt particle) on the (110) surface of sodium chlorate crystal grown at a constant supersaturation of 0.52 %.

Figure 5.13. Saw-teeth layers observed on the (100) surface of a sodium chlorate crystal grown at cooling rate 0.5 K/day from solution containing 70 ppm of $S_2O_6^{2-}$ ions. The layers initiate from the edge common with (111) face (see fig. 5.7 b).

concentration (figure 5.14a). Examination of these surfaces at higher magnification revealed the presence of block-like structure composed of tiny flat hillocks (figure 5.14b).

The only {111} faces of crystals grown by the solvent evaporation method from solutions containing impurity revealed block-like structure similar to that described above in the case of {111} faces of doped crystals grown by the temperature lowering method. An example of this structure is shown in figure 5.15 for a crystal grown from solution containing 68 ppm $S_2O_6^{2-}$ ions. At still higher impurity concentration the surface became uneven with hillocks of various sizes as shown in figure 5.16.

From the photographs of the surface micromorphology presented above it follows that the free movement of layers takes place on the {100} faces of pure crystals. The {111} faces are rough microscopically while the {110} faces appear to have a character in between. The effect of impurity ions is to suppress the lateral development of the rough {111} faces drastically in comparison with that of the {100} faces.

5.3. CHARACTERIZATION

5.3.1. X-ray Topography

Topography work was done on crystals grown from pure solutions at cooling rates 0.03 ,0.48 and 1.05 K/day. The

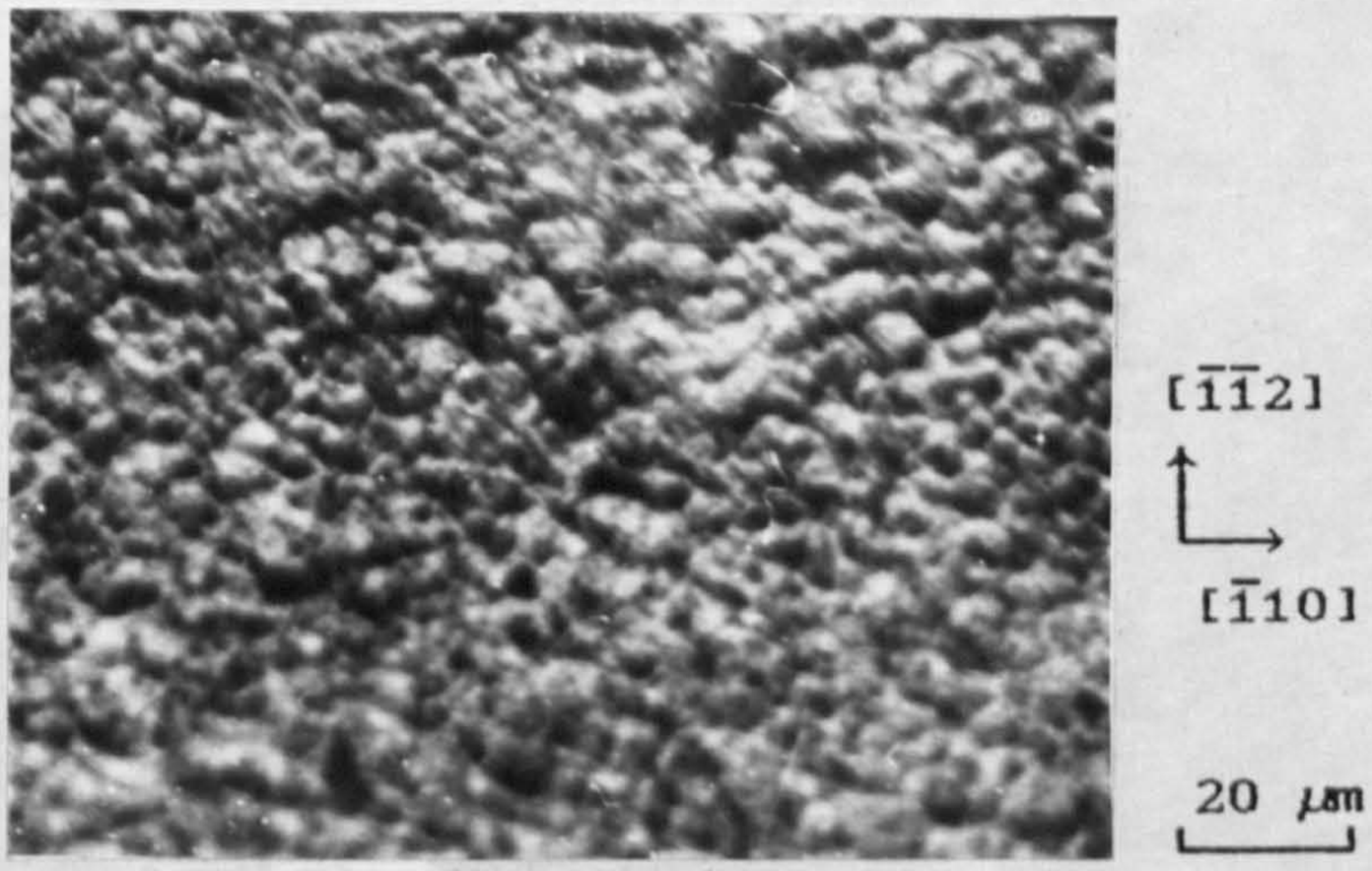

Figure 5.14 (a). Rough nature of (111) surface of a sodium chlorate crystal grown by temperature lowering method at cooling rate 0.09 K/day from solution containing 210 ppm of $S_2O_6^{2-}$ ions.

Figure 5.14 (b). A magnified part of the surface shown in (a) revealing tiny, flat hillocks.

Figure 5.15. Block-like structure observed on the (111) surface of a sodium chlorate crystal grown by solvent evaporation from solution containing 68 ppm of $S_2O_6^{2-}$ ions.

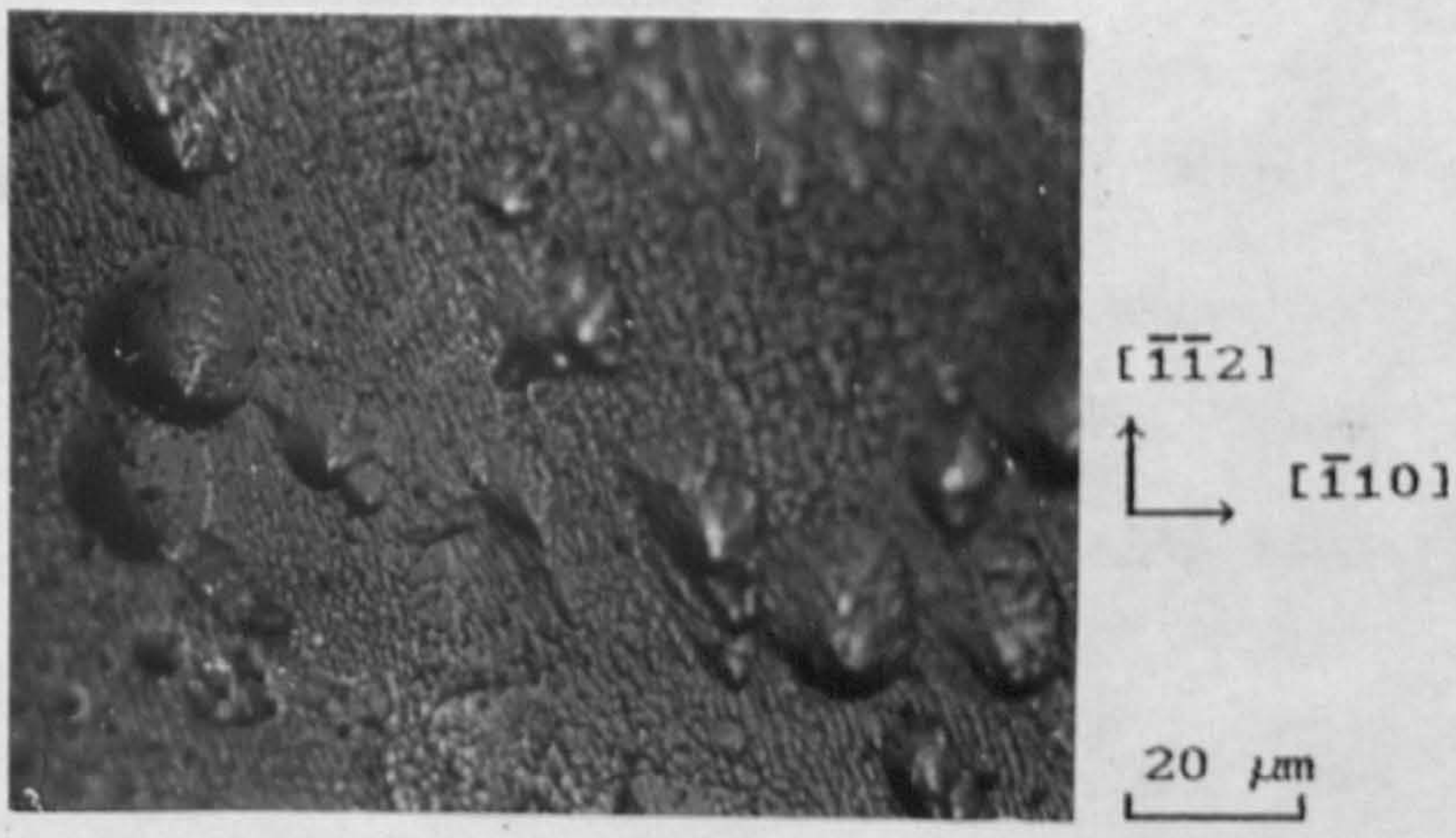

Figure 5.16. Growth hillocks of various sizes formed on the (111) surface of a sodium chlorate crystals grown by solvent evaporation from solution containing 808 ppm of $S_2O_6^{2-}$ ions.

corresponding Lang topographs taken with Mo $K\alpha_1$ radiation are presented in figures 5.17, 5.18 and 5.19, respectively.

Figure 5.17 shows topographs ($00\bar{2}$ and 110 reflections) of the ($1\bar{1}0$) slice of a crystal grown at cooling rate 0.03 K/day. Two types of dislocation structures, curved and straight, are visible in these topographs. The curved dislocation lines A seen in the ($\bar{1}\bar{1}0$) sector are mainly of mixed character, while the isolated straight dislocations B and C running in [$00\bar{1}$] and [001] directions in the ($00\bar{1}$) and (001) growth sectors are mainly of pure screw character. The climbed segments of straight dislocations, D, running in [110] direction are mainly of edge character. In the ($11\bar{1}$) growth sector the character of isolated straight dislocation line, E, cannot be established because of the limited number of reflections. After arriving at the growth sector boundary between ($11\bar{1}$) and ($00\bar{1}$) growth sectors this dislocation enters another growth sector. In the (110) growth sector weak growth bands are seen. However, the ($11\bar{1}$) and (110) sectors are practically dislocation free.

Figure 5.18 shows topographs, with 200 and 020 reflections, of a (001) slice of a crystal grown at cooling rate 0.48 K/day. The central area of the topographs shows the strained region around the seed. Apart from a few straight dislocation lines most of which

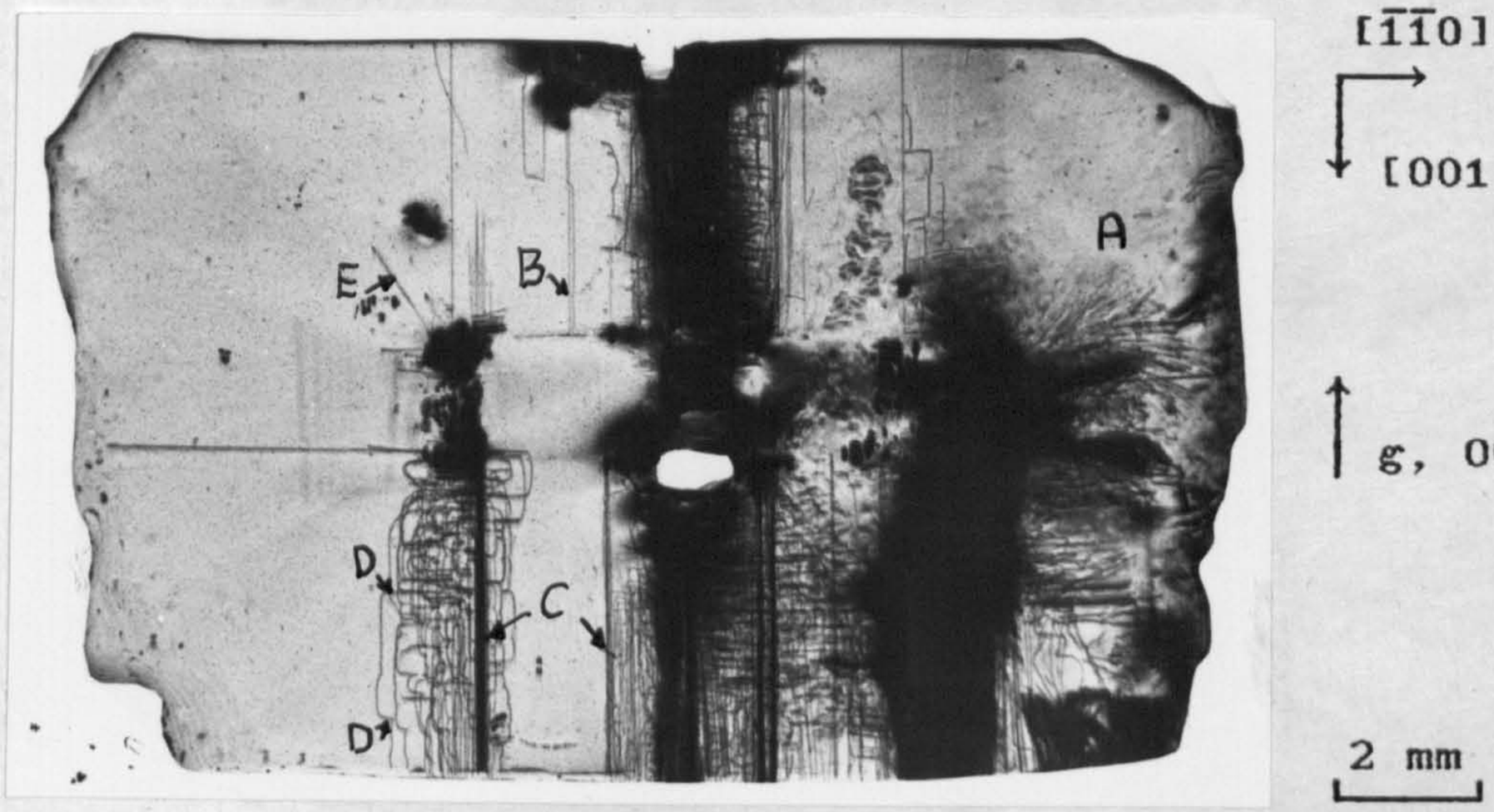

(a)

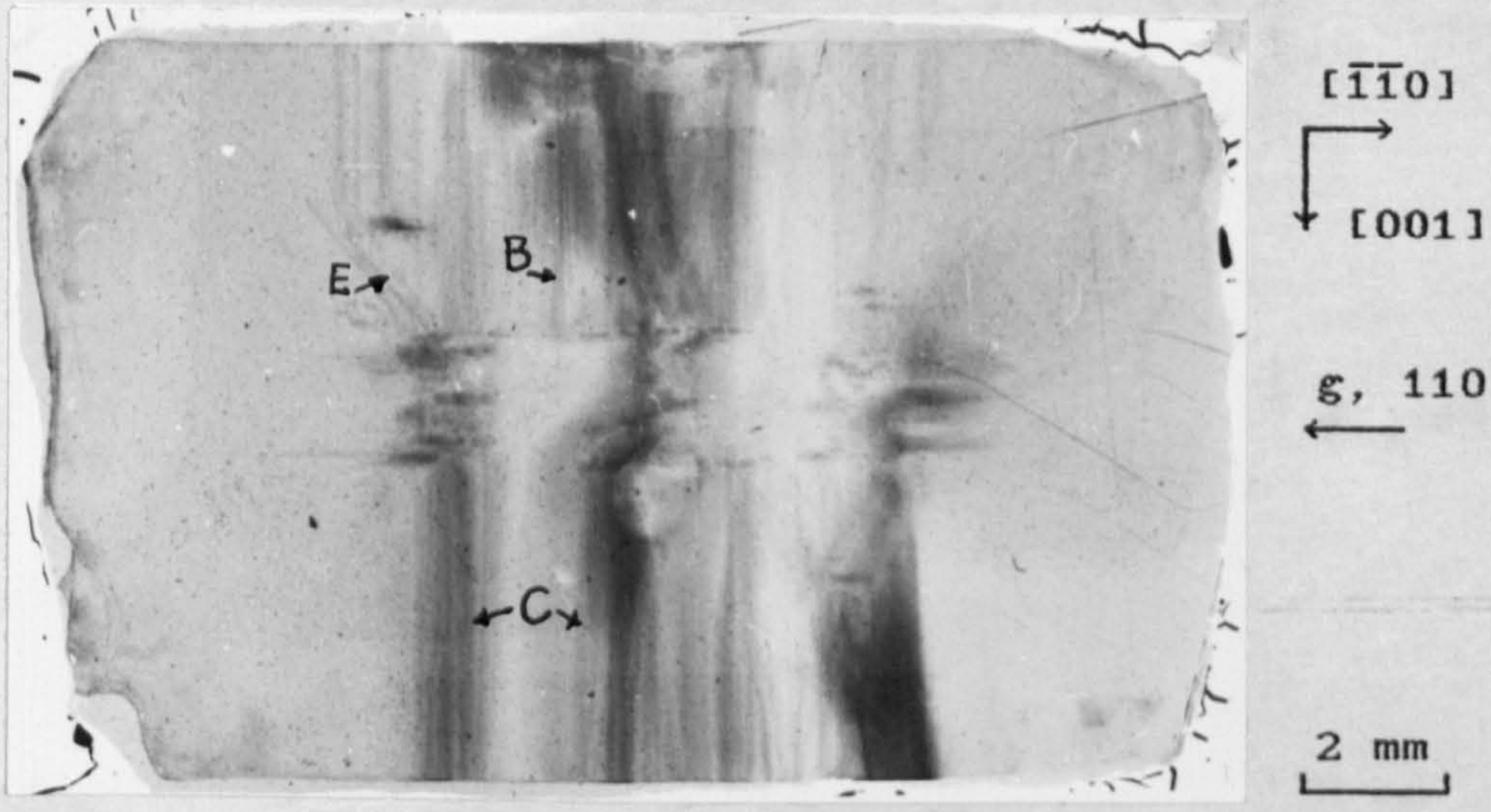

(b)

Figure 5.17. Lang topographs of a (1$\bar{1}$0) slice of a crystal grown at cooling rate 0.03 K/day; reflections: (a) 00$\bar{2}$, (b) 110.

(a)

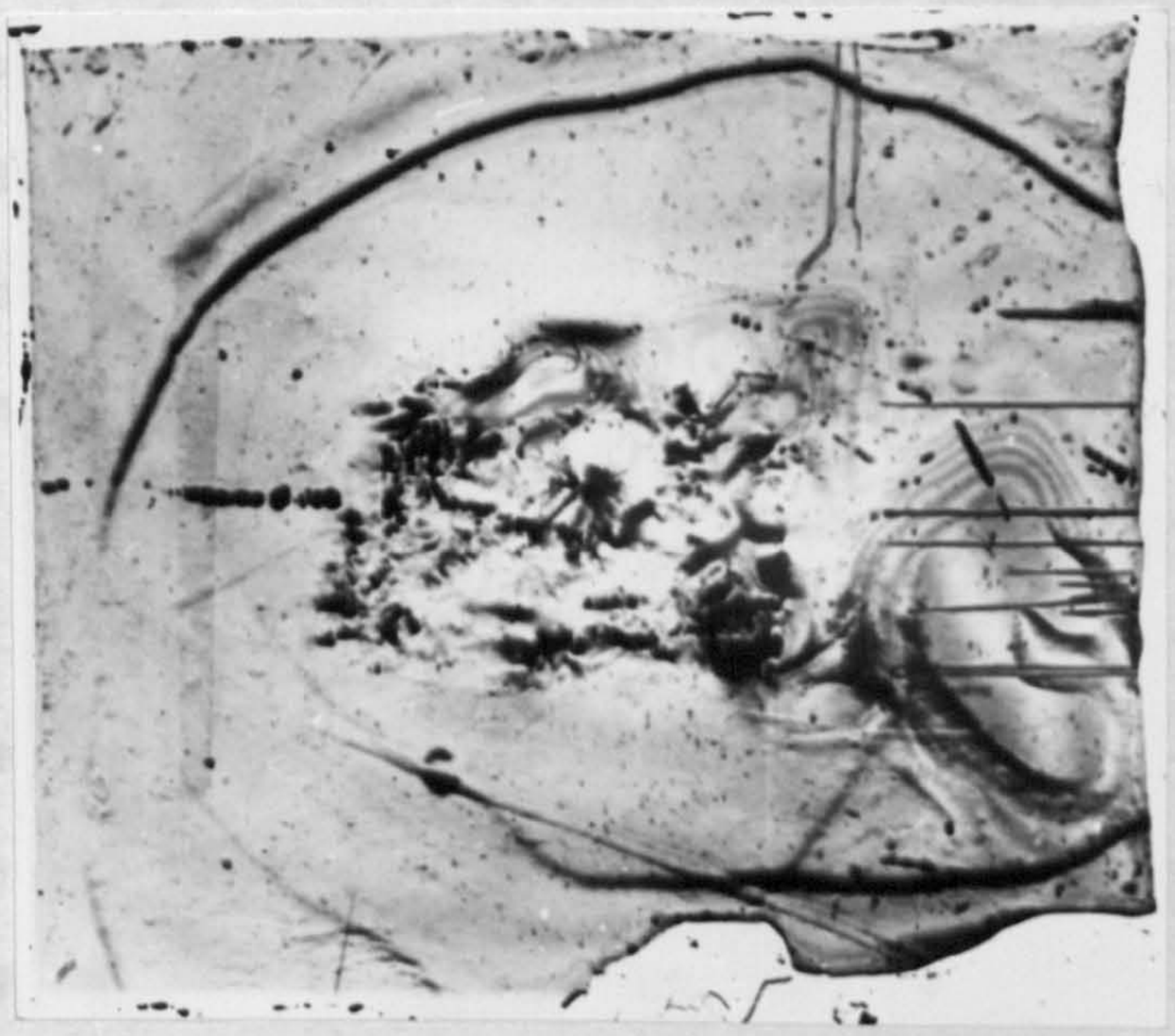

(b)

Figure 5.18. Lang topographs of a (001) slice of a crystal grown at cooling rate 0.48 K/day; reflections: (a) 200, (b) 020.

are mainly of edge character, the crystal sector is dislocation free.

Figure 5.19 illustrates topographs, with 002, 020 and 011 reflections, of a (100) slice of a crystal grown at cooling rate 1.05 K/day. It is obvious from the topograph that most of the dislocations are straight and in bundles. Some of them in $(0\bar{1}0)$ and (001) growth sectors have climbed. Almost all the dislocations, irrespective of whether isolated or in bundles, are of pure screw or edge character. The growth bands are seen only in the seed region of the topographs.

All the topographs in the above figures corroborate the common observation of the dislocation structure in solution-grown crystals that, generally, dislocations run perpendicular to the growth interface. Curved dislocations are observed only at low cooling rates. This observation is in agreement with the results obtained by Matsunaka et al. [47]. The complicated dislocation structure (curved and markedly climbed dislocations) in crystals grown at low cooling rates is similar to that reported by Hooper et al. [73] in the case of the self-nucleated $NaClO_3$ crystals of complex forms obtained by solvent evaporation.

5.3.2. Lattice Parameter Measurements

In order to obtain information about lattice distortion caused by dithionate ion, powder diffraction analyses of pure and doped crystals with silicon as an

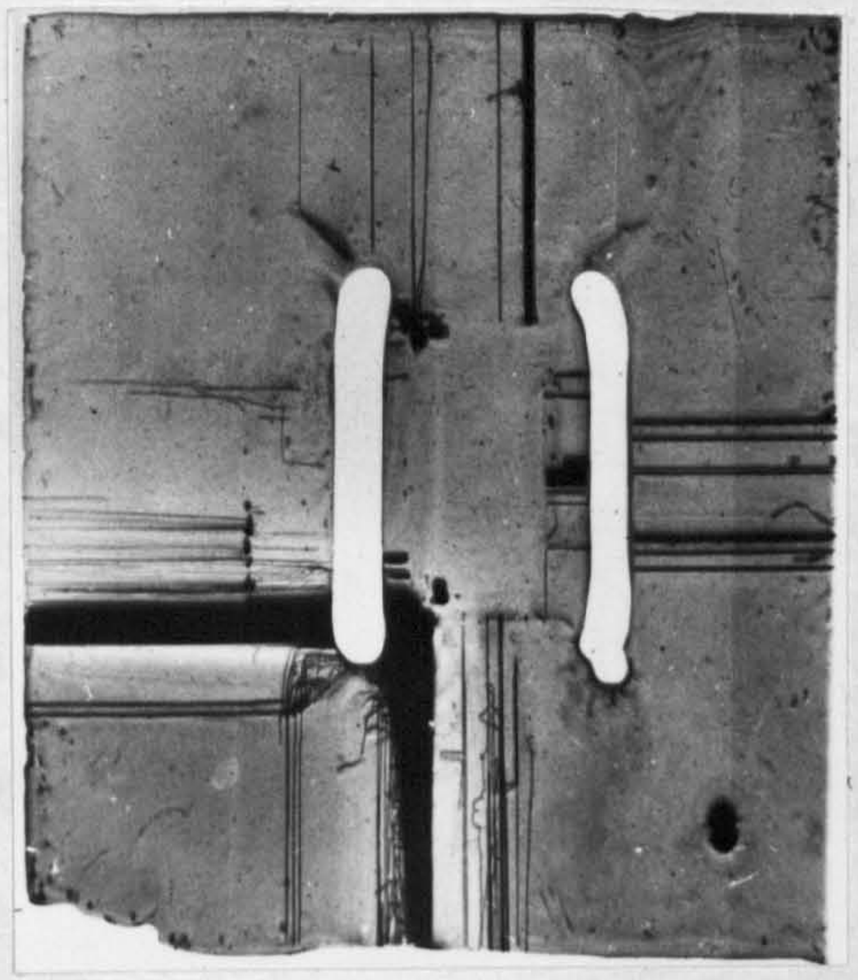

g, 002

2 mm

(a)

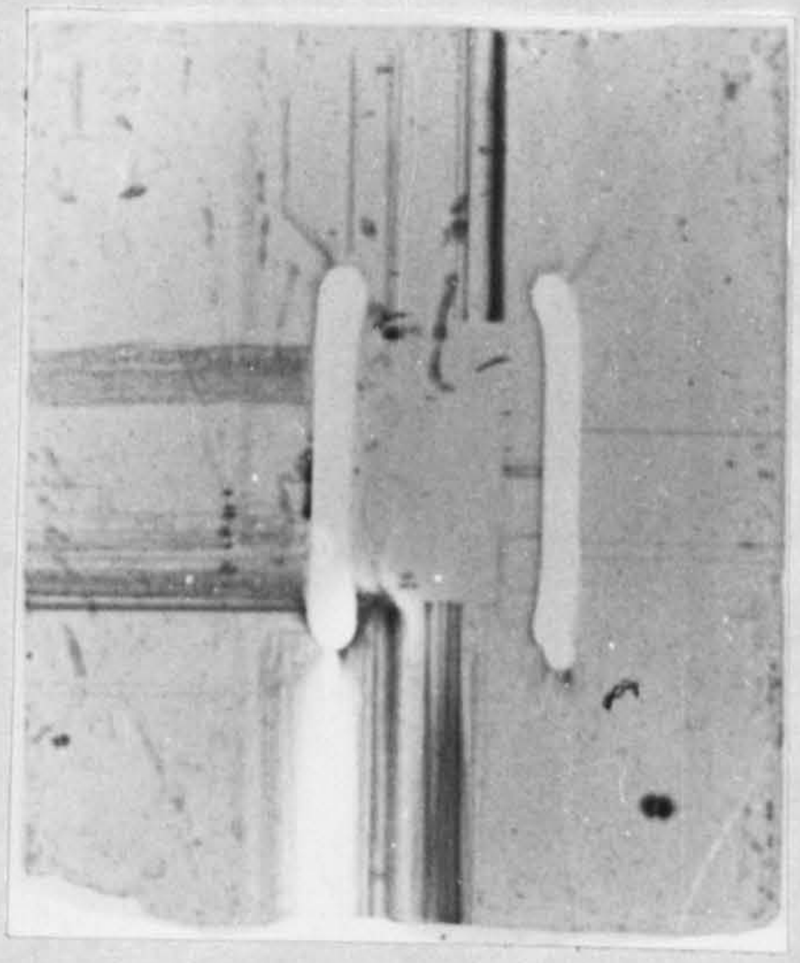

g, 011

2 mm

(b)

[010]

[001]

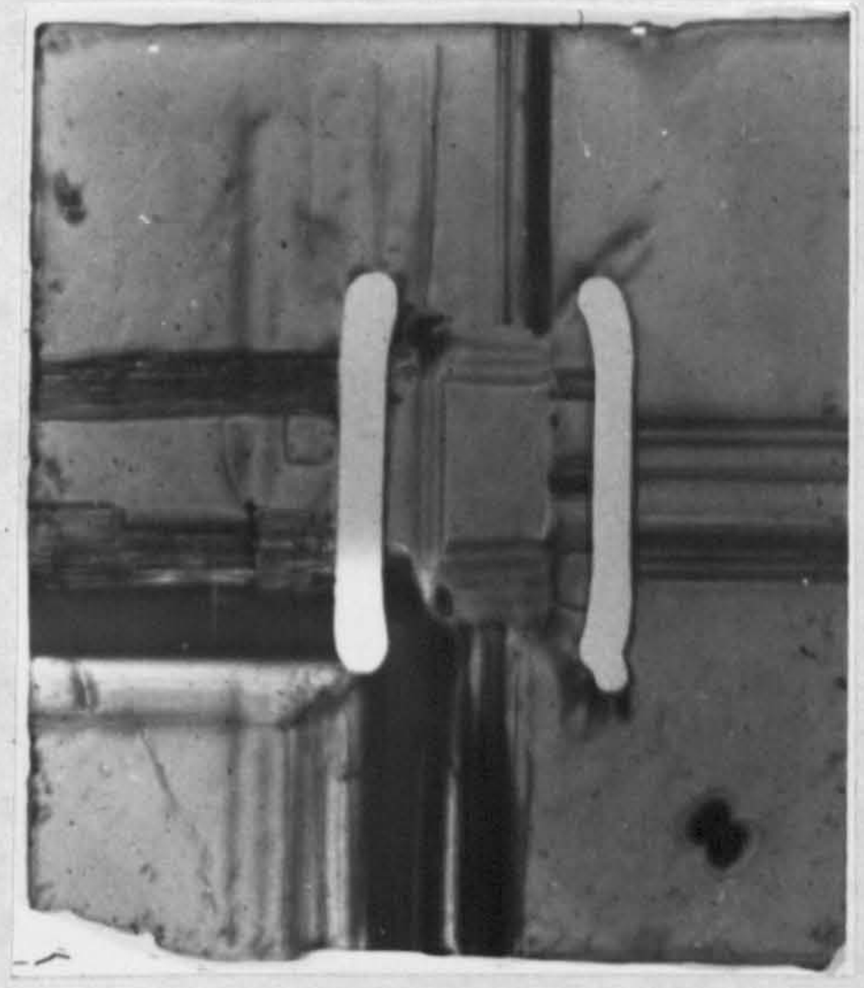

⟶ g, 020

2 mm

(c)

Figure 5.19. Lang topographs of a (100) slice of a crystal grown at cooling rate 1.05 K/day; reflections: (a) 002, (b) 020, (c) 011.

internal standard were made. For lattice distortion measurements a crystal grown by the solvent evaporation method from solution containing 10040 ppm of $S_2O_6^{2-}$ impurity was selected. To minimize the total error in d-spacing measurements, arising, firstly, from the incorrect centring of the specimen in the diffractometer and, secondly, from the absorption of X-rays in the sample, the graphical extrapolation method of Bradley and Jay [74] was applied. The first part of the error is given by

$$\Delta d/d = C_1 \cos^2\theta \qquad (5.1)$$

where C_1 is a constant for all lines, while the second by

$$\Delta d/d = C_2 \cos^2\theta \,/\, \theta \qquad (5.2)$$

where C_2 is another constant for all lines. Both errors approach zero at $\theta = 90^\circ$, as does the sum of the two, and very approximately in proportion to the factor $\cos^2\theta$. The computed values of a_o, obtained for high order reflections, against $\cos^2\theta$ for both pure and doped crystals are shown in figure 5.20 (a,b), respectively. Each of these two lines extrapolates to the corrected value of a_o at $\cos^2\theta = 0$. The lattice parameters of the doped crystals is larger by (0.0130 ± 0.0005) Å than that of the pure crystals. This distortion may be attributed to the incorporation of dithionate ions into the doped crystals during their growth.

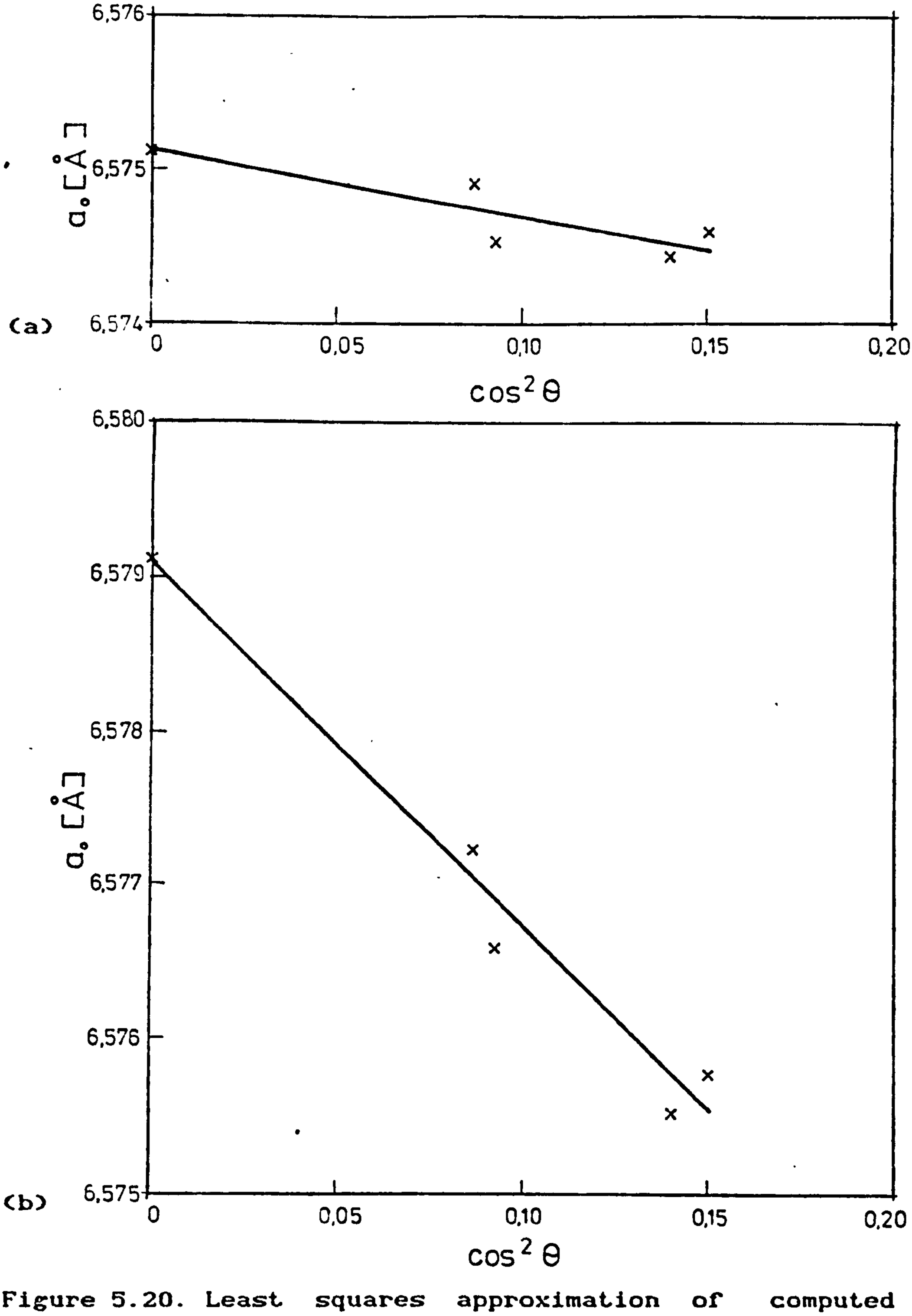

Figure 5.20. Least squares approximation of computed values of lattice parameter, a_o, of $NaClO_3$ crystal grown from (a) pure solution, (b) a solution containing 10040 ppm of $S_2O_6^{2-}$ impurity. Both crystals were grown by the solvent evaporation method under identical conditions.

5.4. COMMENTS ON THE MECHANISM OF GROWTH AND IMPURITY ADSORPTION

According to Kern [55], the {100} faces of $NaClO_3$ are of F type with two PBCs, the {110} aces are of S type with one PBC and the {111} faces are of K type without a PBC. Consequently, it is expected that the morphological importance of these faces of the crystals follows the sequence: {100} > {110} > {111}. This inference is in agreement with the experimentally observed morphological importance of the growth habit of $NaClO_3$ crystals obtained from pure solutions (Subsec. 5.2.2, tables 5.2 and 5.3).

It is interesting to compare the dependence of growth habits of $NaClO_3$ and NaCl crystals on supersaturation. The PBCs in NaCl are similar to that in $NaClO_3$. Therefore, it is expected that their supersaturation dependence of growth habits are also similar. However, in contrast with the occurrence of S and K faces on $NaClO_3$ at low supersaturations, K faces occur at high supersaturations in the case of growth of NaCl crystals from aqueous solutions [12]. In the latter case, the effect has been attributed to a strong adsorption of water dipoles on the (111) face due to an electrostatic field strength caused by a rearrangement of the surface normal to it. The adsorption on the cube face is much weaker because of a much lower field strength. Hence at

high supersaturation values when the removal of the water dipoles is the possible rate-determining step, the growth rate of the (11) face is slowed down.

In the case of $NaClO_3$ crystals, the opposite effect of supersaturation on the crystal habit may be attributed to the difference in the structure of the surfaces caused by the complex ClO_3^- ion.

From the crystallographic structure of $NaClO_3$, it is expected that the {100} faces will exhibit the free development of growth layers by a two-dimensional nucleation or spiral growth mechanism, the {110} faces should show striations parallel to the <100> directions, and the {111} faces, present a rough appearance without any structure. The observations of the surface micromorphology of the {100} and {111} faces are indeed in accord with these expectations. However, in contradiction with the expected striations, the {110} faces show a rough micromorphology resembling that of the {111} faces. This apparent contradiction may be reconciled if one considers the nature of the PBCs in the structure (see figure 5.21). The PBCs are not straight but zig-zag, which can serve as additional source of kinks for growth. A similar reasoning explains why the layers observed on the {100} faces are circular rather than being oriented parallel to the predicted PBCs, i. e. along <010> and <001> directions.

Bennema [39] found that his kinetic data of the

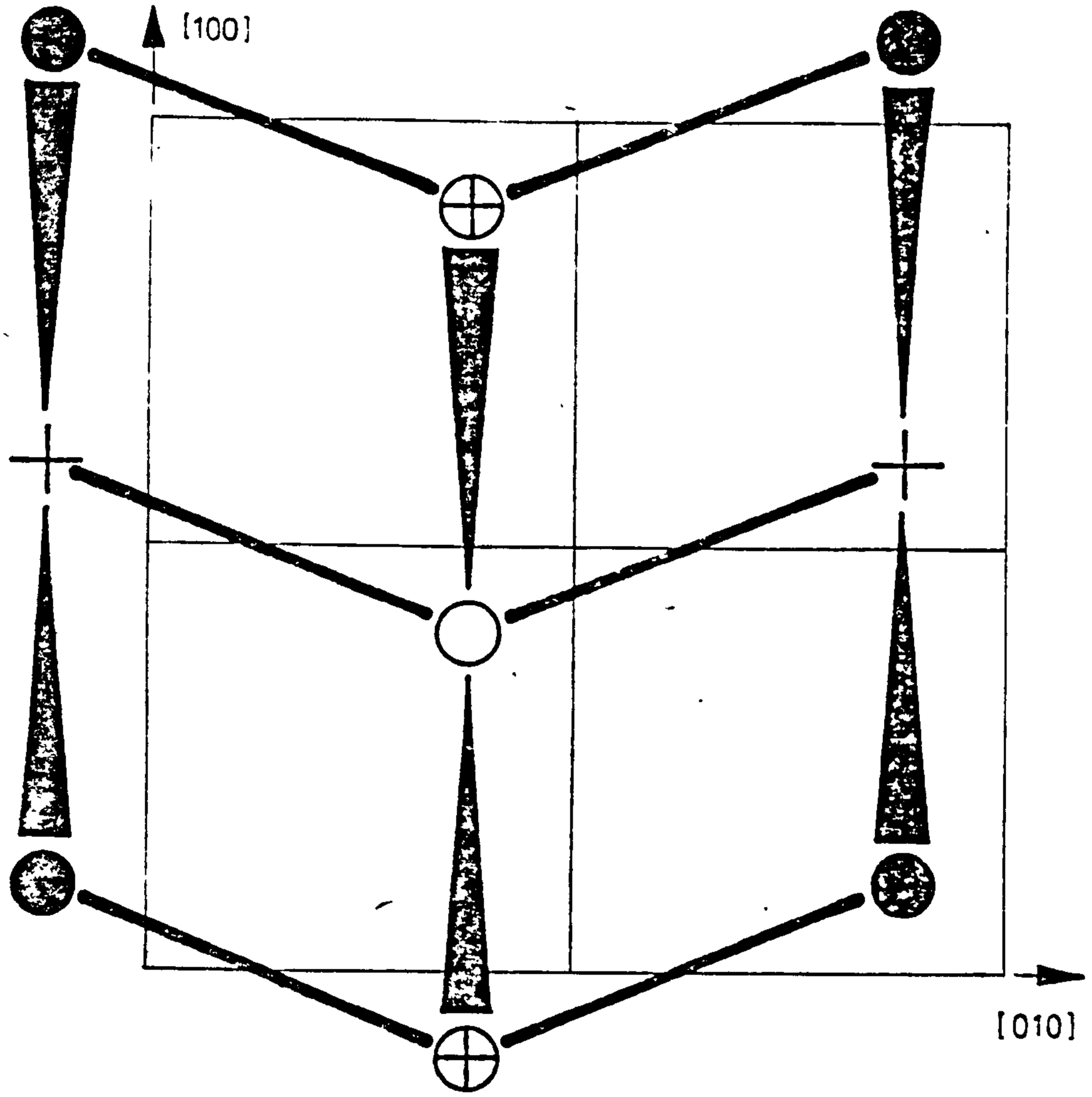

Figure 5.21. Periodic Bond Chains in $NaClO_3$ crystals; ● - Na^+ ion (coordinate u); ⊕ - ClO_3^- ion (coordinate v), ○ - ClO_3^- ion (coordinate $\bar{u}$), ┼ - Na^+ ion (coordinate $\bar{u}$); u = 0.08, v = 0.07.

dependence of R on σ can be interpreted by the BCF theory and a transition from parabolic to linear dependence was observed at $\sigma = 6 \times 10^{-4}$. Hosoya et al. [40] interpreted their kinetic data of {100} faces of $NaClO_3$ in terms of both BCF and B+S models and noted the transition from BCF to two-dimensional mechanism at $\sigma = 2\text{-}3 \times 10^{-2}$. Matsúnaka et al. [47] concluded that the crystal with curved dislocations grow by the BCF spiral growth mechanism while those with the straight dislocations grow by the two-dimensional nucleation mechanism. Our X-ray topography results do show the occurrence of curved dislocations in crystals grown at low cooling rates i. e. at low supersaturations (figure 5.17), but no growth hillocks or spirals typical of spiral growth mechanism are observed on the as-grown {100} faces (figures 5.9, 5.10 and 5.12). These facts and the fact that kinetic data can be fitted to different growth-rate equations shed doubts on the operative growth mechanisms in $NaClO_3$ crystals deduced by the previous workers. Our observations of the surface micromorphology of the crystals grown at low supersaturations suggest that $NaClO_3$ crystals grow by the two-dimensional nucleation mechanism.

The apparent effects of $S_2O_8^{2-}$ ions on the growth of $NaClO_3$ crystals are the following:

(1) It causes a change in their growth habit by an increased importance of {111} faces with increasing

impurity concentration.

(2) It changes the micromorphology of both {100} and {111} faces. It leads to the bunching of growth layers on the {100} faces (figure 5.13). The {111} faces are rough for crystal grown from pure solution but there appear rugged, rounded hillocks on them when grown from solutions containing the impurity (figures 5.14b and 5.16). The hillocks become point-bottomed and better defined at increased impurity concentration, but the general surface background remains rough (compare figures 5.14b and 5.16).

(3) The impurity leads to an increase in the lattice parameter of the growing crystal and is caused by its incorporation into the crystal lattice (Subsec. 5.3.2).

In order to explain the above points, it can be supposed that the inhibition of the {100} faces by the impurity ions is caused by their adsorption on the layers while that of the {111} faces is a consequence of the physical blocking of regular lattice sites by the impurity ions in a manner described in Subsec. 5.2.2.2. At higher impurity concentrations, the impurity ions not only block the development of the {111} face but can produce local three dimensional clusters which may provide sites for the attachment of growth units. Consequently, the hillocks grow laterally along the surface and upward perpendicularly to it. Because of the statistical nature of the formation of impurity clusters,

the sizes of the hillocks are expected to be different, as has been observed experimentally (figure 5.16). The above mechanism of adsorption also implies that impurity ions may be incorporated into the lattice of the growing crystal, a fact substantiated by an increase in the lattice parameter of doped crystals (Subsec. 5.3.2).

Finally, it should be mentioned that the above mechanism of habit modification by impurities is similar to the one suggested by Buckley [21], but the effect of $S_6O_6^{2-}$ in modifying the habit of $NaClO_3$ is much stronger (ratio of ClO_3^- to $S_2O_6^{2-}$ ions is 5000:1) than that (1000:1) reported by him.

CHAPTER 6

GROWTH KINETICS OF SODIUM CHLORATE CRYSTALS

Knowledge of relative growth rates is of vital importance in the prediction of growth morphology of crystals. Depending on the external conditions such as supersaturation, growth temperature, flow rate of the solution, impurities etc., not only the growth rates of a crystal are changed but its habit can be modified as a result of the appearance of additional sets of planes due to changes in the growth mechanism of the crystal. During the last decade data on the dependence of R on σ has been used to establish uniquely the mechanism of growth of crystals. However, Garside et al. [75] and van Enckevort [18] showed that conclusions of growth mechanism from the dependence of R on σ alone may be misleading and that supplementary experimental evidence has to be obtained to prove the actual growth mechanism.

The aim of the present chapter is to look for correlation between defect structure (especially dislocations) and applied supersaturation and between growth rate and tensile strain applied during growth.

6.1. THE FLOW CELL AND THE MEASUREMENT OF GROWTH RATES

The growth cell used in the whole series of kinetic

experiments is presented in figure 6.1. It has a double-walled construction with an internal vessel for the growth solution (1) with working volume of 27.2 cm^3 and an external cylindrical compartment (2) for circulation of thermostated water. The temperature of the cell was monitored by a platinum resistance thermometer (3) connected to a digital display. Additionally, stainless-steel rods (4) were used to mount seed crystals inside the working volume. The scheme of the whole system used for kinetic measurements is presented in figure 6.2. Saturated solution was kept with excess crystalline material in the thermostated water bath (1) at a constant temperature. The solution was pumped through the first heat exchanger (2), the cell (3), the second heat exchanger (4) and a flowmeter (5) back to the reservoir (1) by a centrifugal pump (6). Two water circuits were formed. The first consisted of the thermostated water bath (7) and the first heat exchanger (2) placed before the cell, and the second with the water bath (8) and the second heat exchanger (4) placed after the cell. Thus by setting the temperatures of the water baths (7, 8) it was possible to achieve the required working temperature and supercooling, respectively, within half an hour and then carry out the kinetic measurements using a traveling microscope at a magnification of x40. The total time of observation varied from 24 hours for the lowest supersaturation to 8 hours for the highest one.

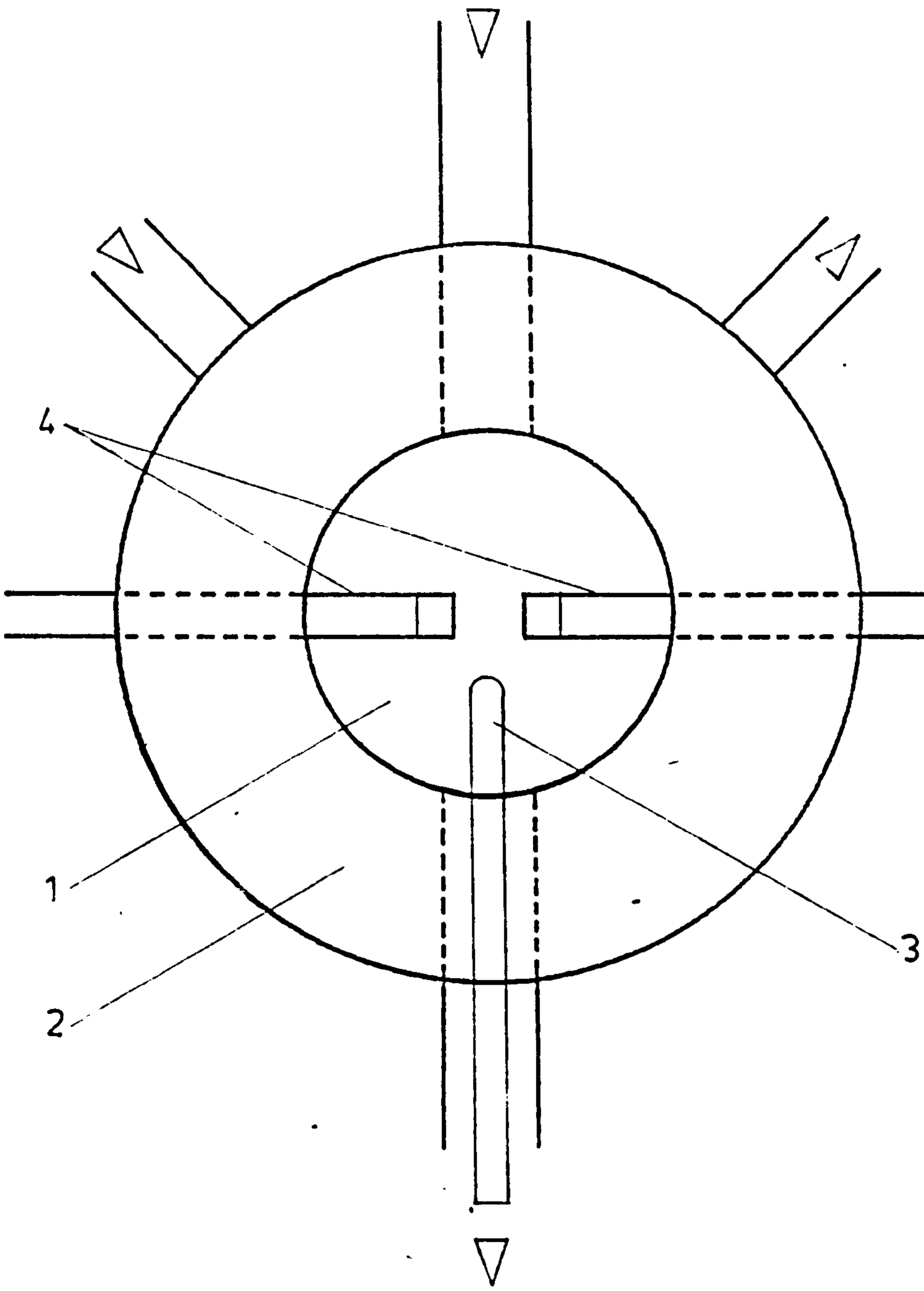

Figure 6.1. Schematic diagram of growth cell: (1) internal compartment for solution flow, (2) external compartment for circulation of water (3) platinum resistance thermometer, and (4) rods for mounting the crystal.

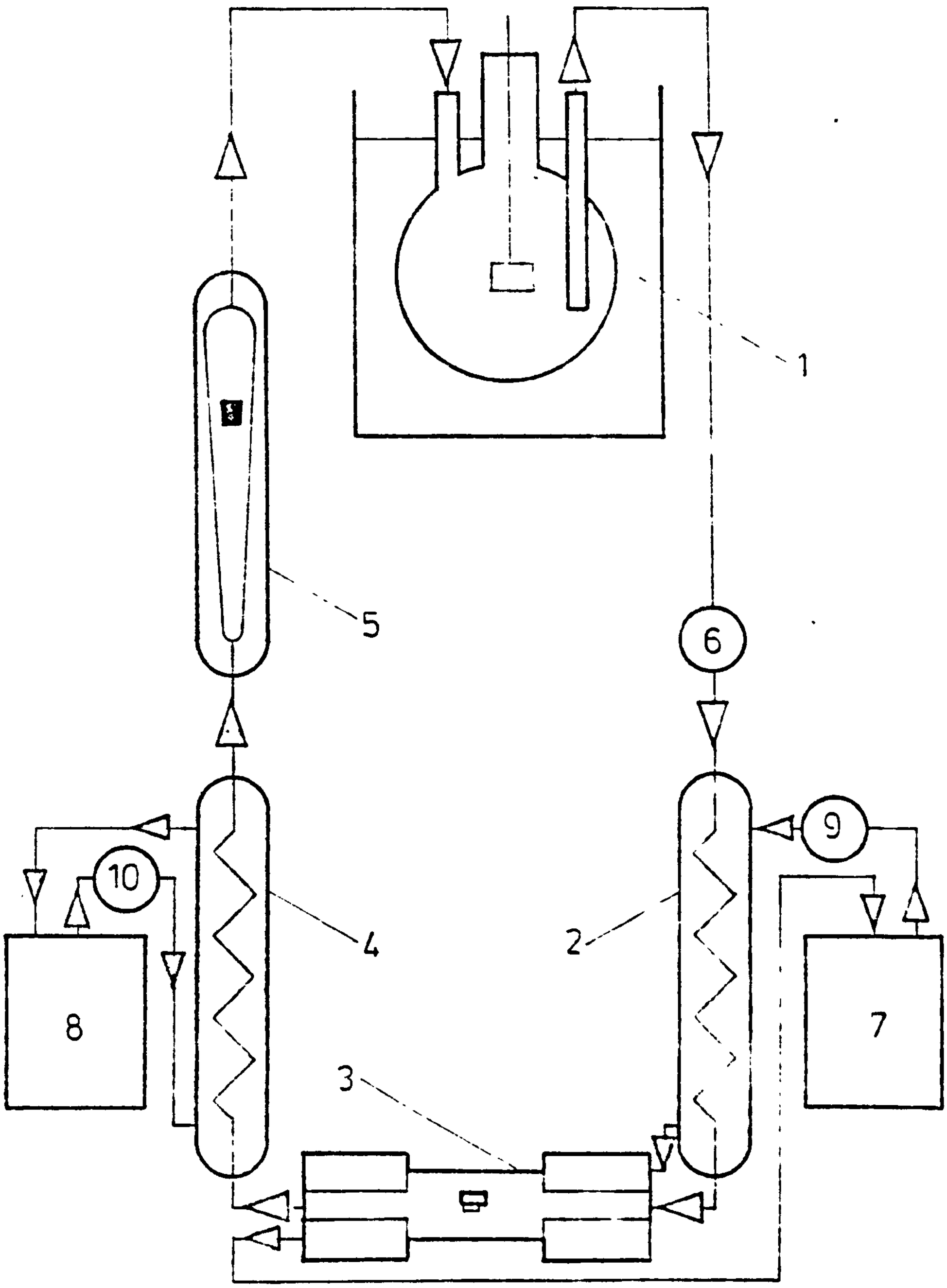

Figure 6.2. Schematic diagram of the experimental set-up for measurements of growth kinetics: (1) thermostated water bath, (2, 4) heat exchangers, (3) growth cell, (5) flowmeter, (6, 9, 10) centrifugal pumps, and (7, 8) water baths.

In order to check the effect of volume diffusion, different flow rates of the solution were applied in the preliminary series of experiments. It was found that a flow rate of 300 ml/min was sufficient to achieve growth controlled by surface diffusion at all supersaturations used during the measurements.

6.2. RECOVERY PROCESS AT DIFFERENT SUPERSATURATION LEVEL

The aim of the kinetic measurements presented in this section was to establish the dependence of growth rate on total strain built in the crystal. Therefore, attention was paid principally to the correlation of the individual growth rates and dislocation content in particular crystals. Below we describe the experimental procedure for the measurement.

A tabular seed of the {100} form, obtained in a petri dish by the solvent evaporation technique, was mounted on the rod by means of an epoxy resin (araldite) in such a way that the (100) face was facing the flow direction. The solution flow was switched on and the circulation took place out of the cell. The temperature of water passing through the first heat exchanger was decreased in order to obtain the required supersaturation. The seed crystal was placed into the cell which was subsequently sealed firmly. Then the solution flow was switched through the cell and after the system attained the

dynamical thermal balance the growth rate measurements were started. The solution was overheated while passing through the second heat exchanger (becoming slightly undersaturated after the cell) and was pumped back to the reservoir. This method worked successfully but due precautions of cleaning the tubing and the cell were taken before each run. Nevertheless, as indicated by a decrease in flow rate, blocking of the tubing occurred occasionally at high supersaturations. Such runs were excluded from analysis.

Six representative runs subjected to the analysis are presented in table 6.1. It is worth noting that in all runs in this series of experiments refacetting of the seed took place on suspending the latter into a supersaturated solution and that supersaturation differed in each run.

We expected that the newly formed interface will be a source of strain which will be released at later stages of growth by the generation of growth dislocations. Also that the higher the supersaturation the more strain is built in crystals and the higher the numerical density of dislocations. Therefore, in order to check this hypothesis, the newly grown crystals were subjected to Lang topography. Topographs of crystals grown at different supersaturation are illustrated in figure 6.3. In general, the topographs of the regrown crystals confirmed the above assumption.

Table 6.1. Experimental data on growth rates of $NaClO_3$ crystals grown in the flow cell at flow rate 300 ml/min and saturation temperature 302.9 K.

Supersaturation [%]	Growth rate [μm/sec]
0.20	0.005
1.5	0.076
2.05	0.079
2.27	0.128
2.59	0.111
3.64	0.116

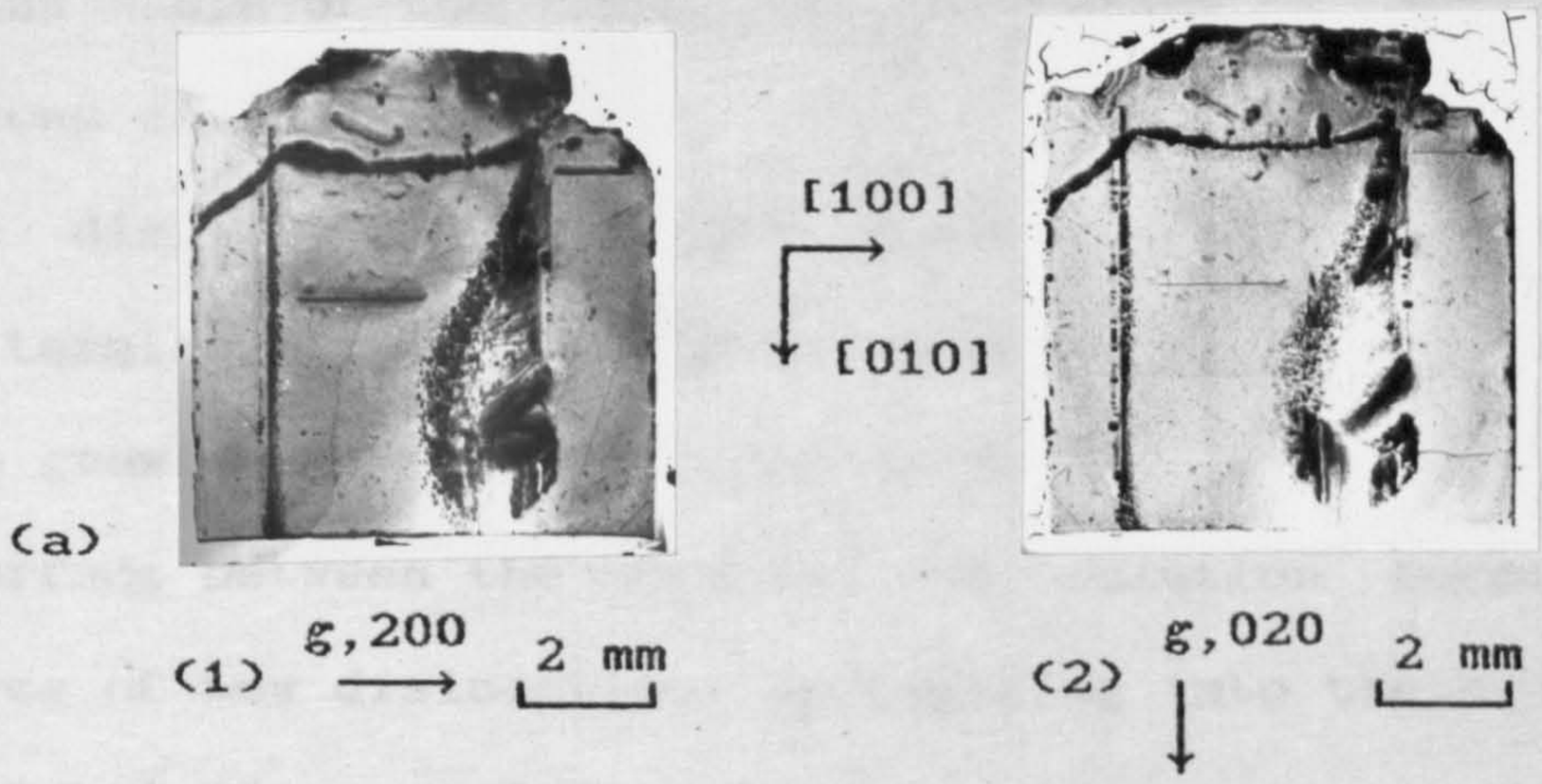

Figure 6.3. Lang topographs of (001) slices of crystals grown at different supersaturations: (a) 1.5 %, (b) 2.05 %, (c) 2.27 %. Reflections: (1) 200, (2) 020.

On the basis of the topographs the following general conclusions can be drawn:

(1) The dislocation structure existing in the seed usually terminates at the interface and do not propagate into the growing crystal (figures 6.3b,c).

(2) Interface between the seed and the solution becomes the source of new dislocations propagating into the newly grown crystal (figures 6.3a-c).

(3) The (100) sector, facing the flow, grows faster than the ($\bar{1}$00) sector (figure 6.3a-c).

(4) The dislocations observed in the whole range of supersaturation are straight and are of pure edge or screw type (figure 6.3a-c).

The second series of experiments was performed under constant supersaturation but the refacetting conditions varied for every run. The aim of this approach was to establish a correlation between the degree of strain generated during refacetting and the numerical density of dislocations. The results summarized in table 6.2 reveal that this is indeed the case. When a supersaturation employed for refacetting was low the density of dislocations was also low (figure 6.4a). Analysis of the topographs revealed, as in the previous series of experiments, that dislocations usually terminate at the interface, but there are cases, when they propagated into the newly grown crystal figure 6.5). This phenomenon was observed when a gradual, slow change of temperature of

Table 6.2. Experimental data on growth rates of $NaClO_3$ crystals after the refacetting process at different supersaturations: flow rate 300 ml/min, saturation temperature 303.70 K, growth temperature 302.27 K, supersaturation 1.5 %.

Refacetting supersaturation [%]	Growth rate [μm/sec]
0.4	0.036
1.2	0.046
1.4	0.052
2.0	0.059
2.3	0.070
2.6	0.086

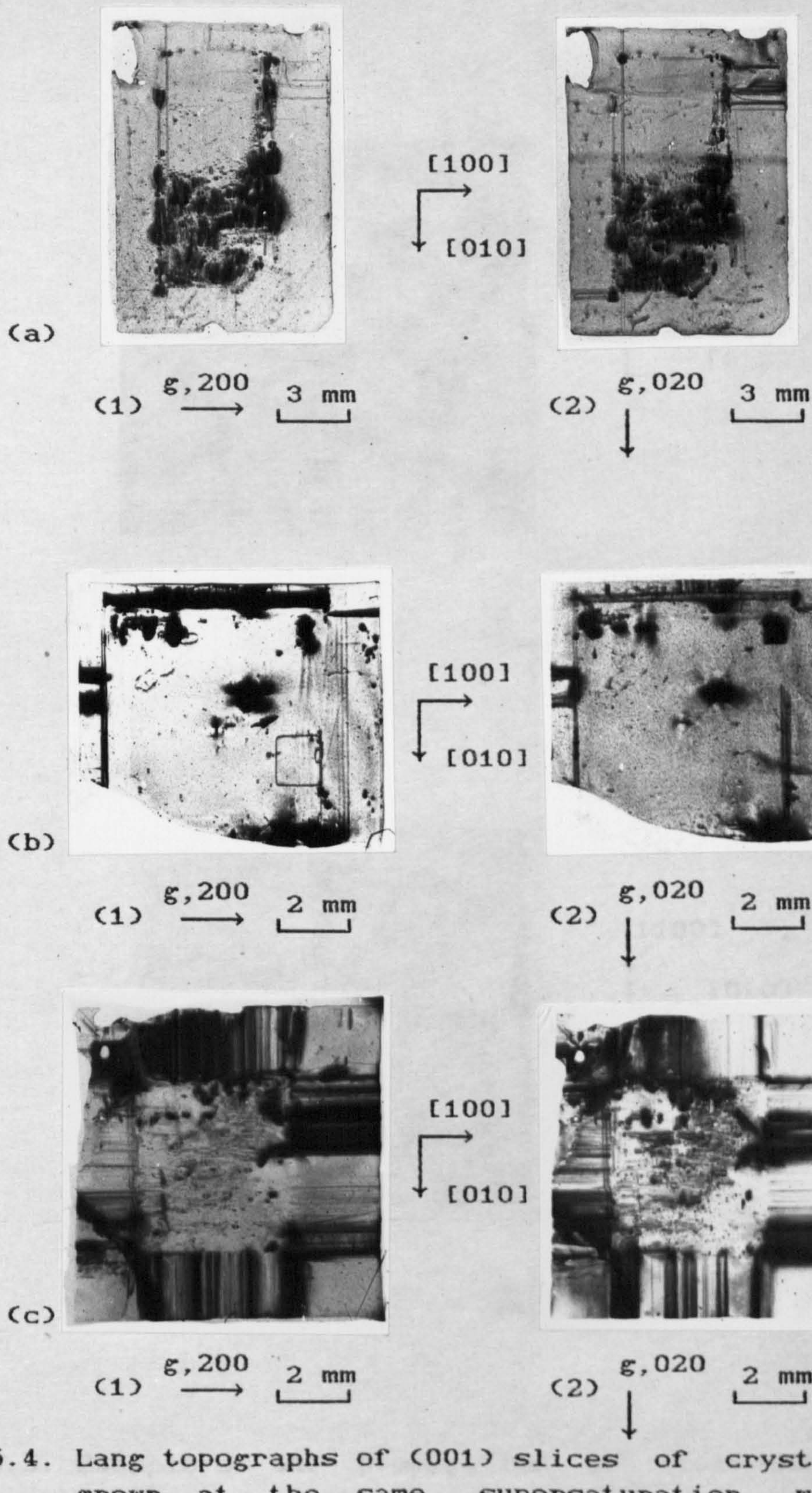

Figure 6.4. Lang topographs of (001) slices of crystals grown at the same supersaturation with different initial supersaturation at the beginning of the growth process: (a) 0.4 %, (b) 2.0 % and (c) 2.6 %.
Reflections: (1) 200, (2) 020.

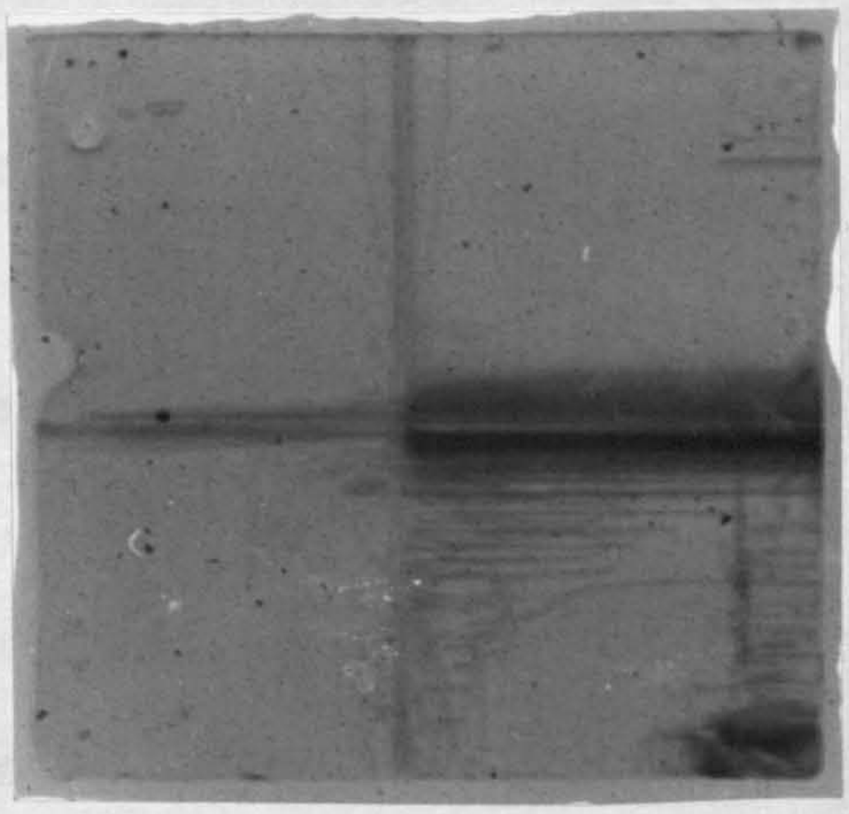

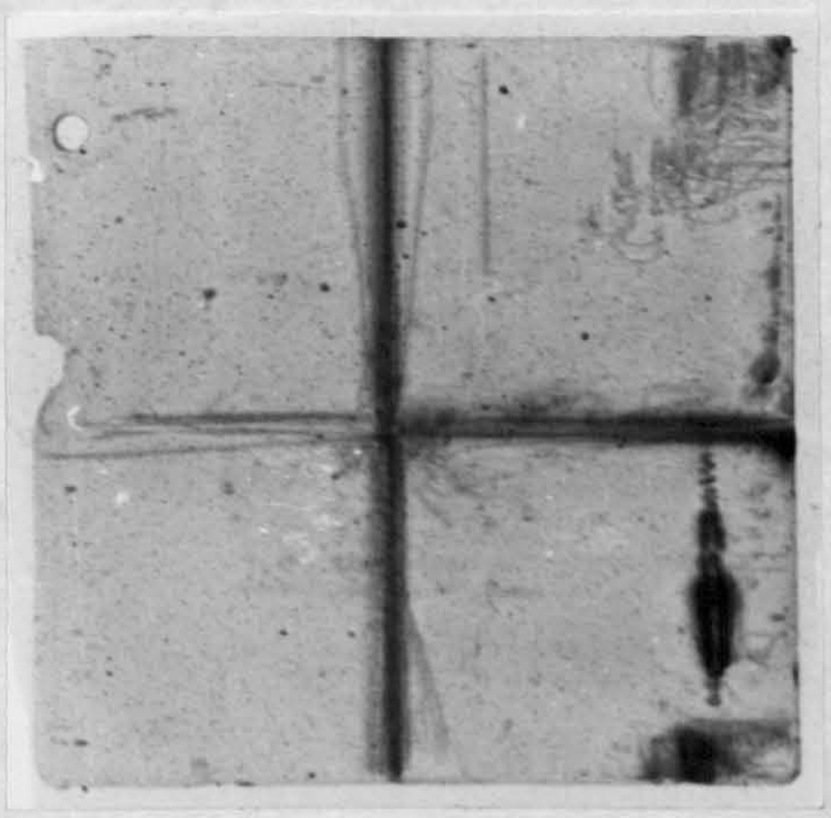

Figure 6.5. Example of the propagation of dislocations originated in the seed through the newly formed interface. The crystal was grown by a gradual change of solution temperature from undersaturation to supersaturation state. Reflections: (a) 200, (b) 020.

the working solution from undersaturated to supersaturated state was applied. Generally, the higher was the value of refacetting supersaturation the more strain (i. e. dislocations) was generated at the newly-formed interface (figure 6.4a-c). Similar observation have been made by Bhat et al. [82] on potash alum crystals.

Another interesting feature was observed when a crystal rounded due to slight dissolution was subjected to growth (figure 6.6). When the regenerating rounded plane was close to the {111} a succession of thick kinked layers was observed (figure 6.6a), but when it was close to the {110} flat facets were grown (figure 6.6b). Prolonged growth of these faces leads to the capture of inclusions by the regenerating face (figure 6.7). In the former case the inclusions were dendritic (figure 6.7a) while in the latter case they were parallel to the growing interface (figure 6.7b). These observations of the difference in the regenerated interfaces and in the type of inclusions may be attributed to the formation of block structures with natural facets formed from macrosteps [76]. The mechanism of regeneration of a plane close to {111} of $NaClO_3$ and capture of inclusions in the regenerating face is similar to that of the capping process on the (001) face of KDP-type crystals [77, 78] and of the capture of liquid inclusions on the regenerating {101} faces [77]. It should be noted that

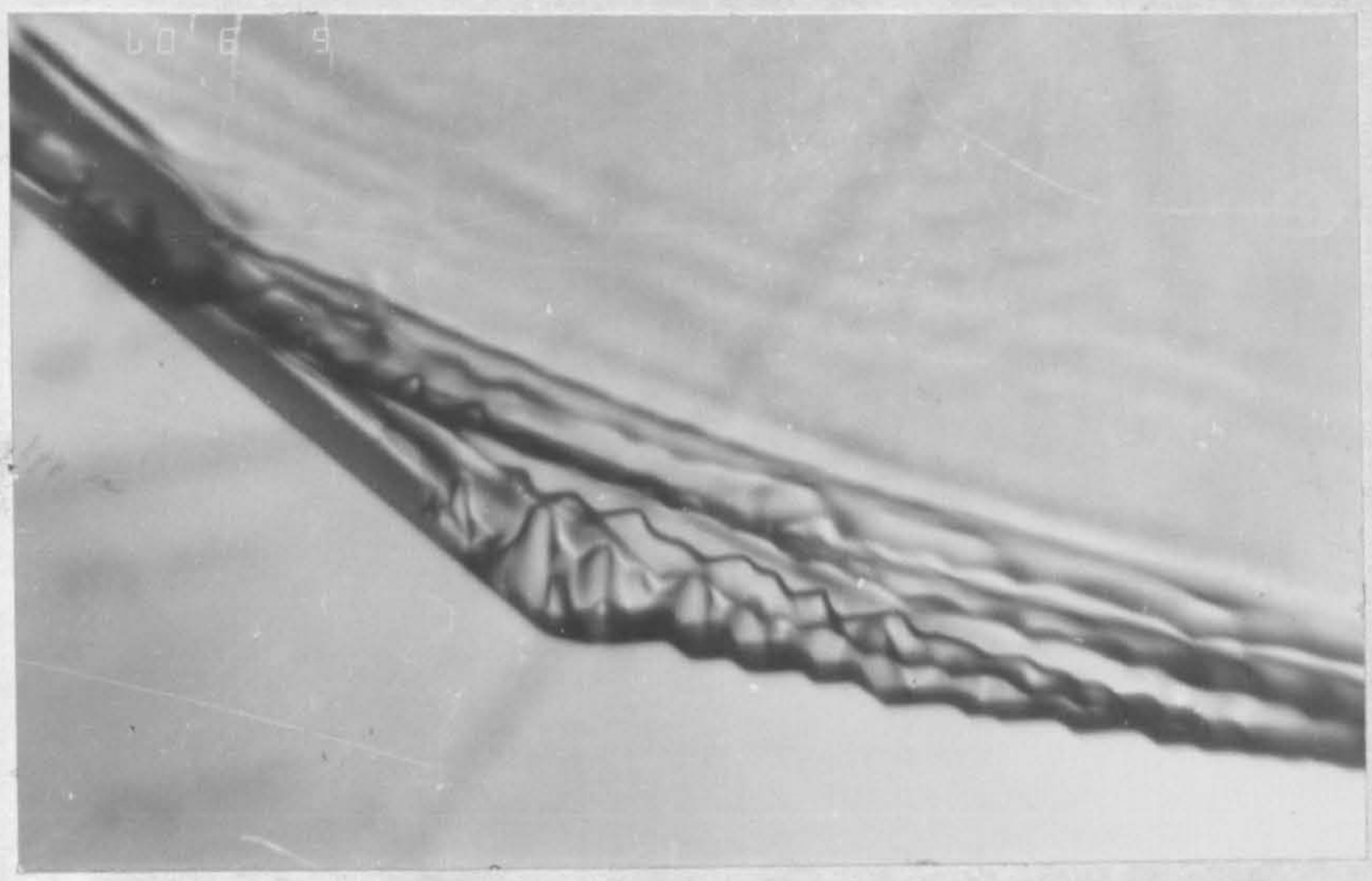

100 μm

(a)

100 μm

(b)

Figure 6.6. Example of difference in recovery process during the growth of $NaClO_3$ crystal rounded after slight dissolution. The steps of the type seen in (a) and (b) appear when the rounded face is close to (a) (111) and (b) (110).

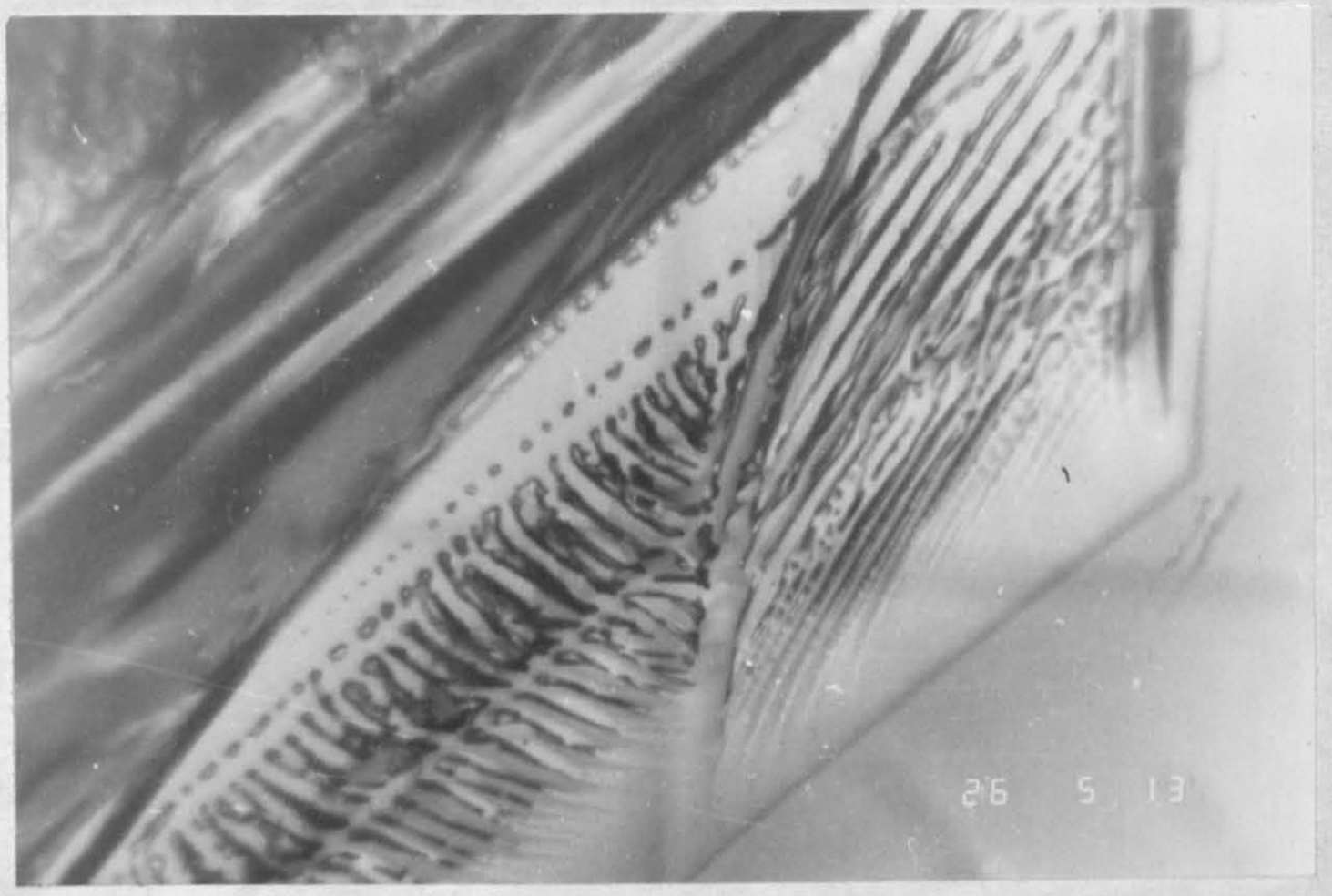

100 μm

(a)

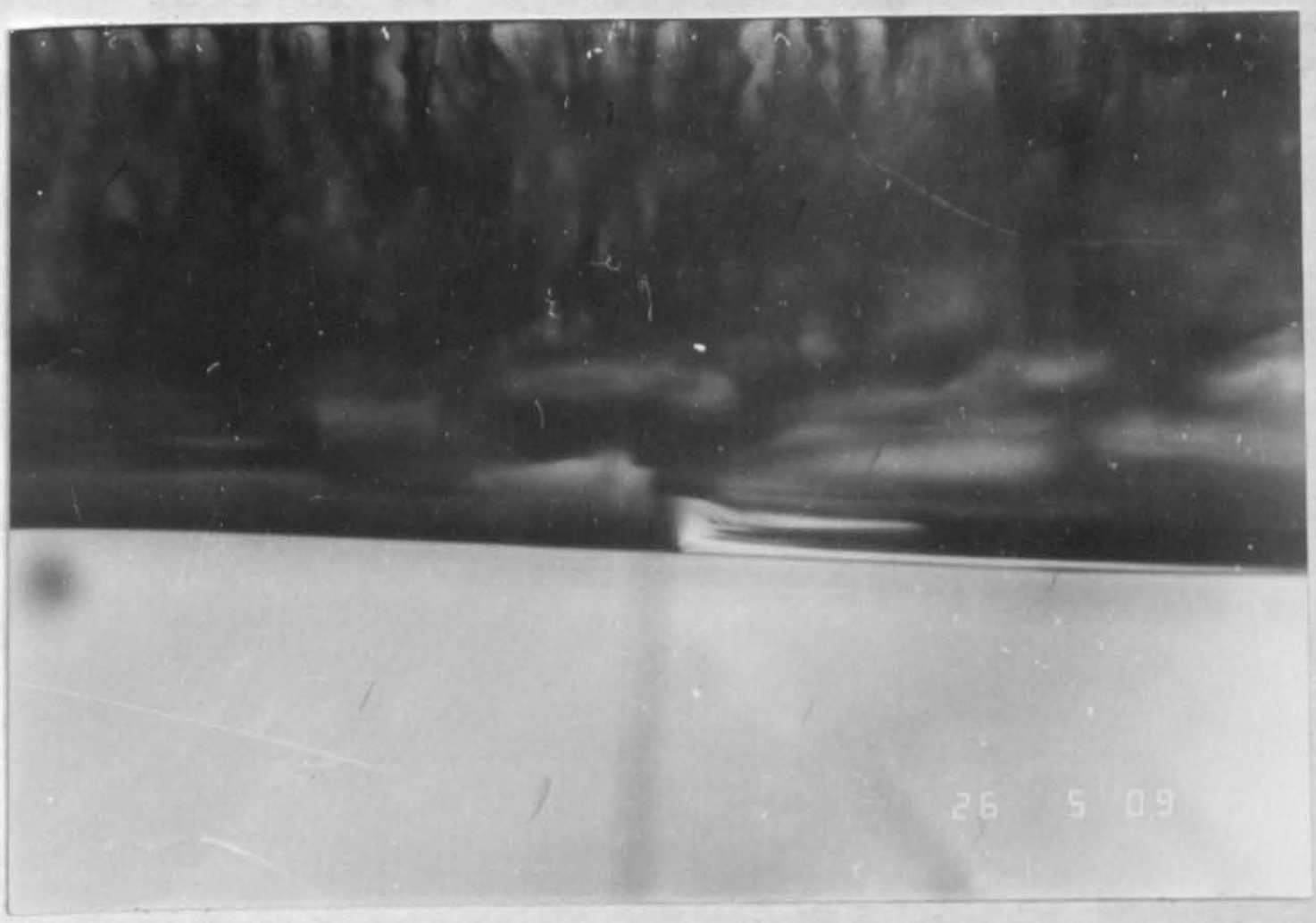

100 μm

(b)

Figure 6.7. Different types of inclusions captured during the recovery process of (a) (111) and (b) (110) faces of the crystal rounded after slight dissolution and grown in the flow cell.

both the {111} faces of $NaClO_3$ and the {001} faces of KDP-type crystals are K faces.

The experimental data on growth rate as a function of supersaturation employed for the development a crystal (Table 6.1) or for the regeneration of a seed (Table 6.2) may be represented by a linear relation

$$R = C\,\sigma$$

where the values of C are, respectively $3.43(\pm 0.86)\times 10^{-8}$ and $2.56(\pm 0.20)\times 10^{-8}$ m/s for the two cases. The linear dependence of growth rate on supersaturation with essentially the same value of C may be attributed to a growth mechanism controlled by bundles of screw dislocations [89] or to the rough nature of the (100) face [90].

In the case of potash alum, Bhat et al. [62] found that edge dislocations alone can yield a linear dependence of growth rate on supersaturation. Lang topographs of $NaClO_3$ crystals (figures 6.3 and 6.4) reveal the presence of both screw and edge dislocations. However, it is difficult to determine the density of screw and edge dislocations separately from these topographs, consequently, it is not possible to say whether one type of dislocations (i. e. screw or edge alone) or both collectively govern the growth mechanism of $NaClO_3$ crystals and assess the role of dislocations from the kinetic data and Lang topography.

6.3. GROWTH OF THE CRYSTALS WITH APPLIED TENSILE STRAIN IN THE KINETIC CELL

A specially designed growth cell with a device for in-situ straining of the crystal in tension during its growth was used in the whole series of experiments. The construction of the cell was similar to that described in Sec. 6.1. The same system for circulation and temperature control of the solution was used. An additional attachment, a strain gauge, enabled the assessment of tensile microstrain applied during the growth of the crystal. The solution flow was set at a constant rate of 300 ml/min.

Sodium chlorate crystal is a highly brittle material and because of its structure the typical (111) slip plane of alkali halides is not present. This leads to the situation that there is no slip pattern observed under the tensile strain. The inference was confirmed from the topographs of the strained crystals. No slip patterns were detected even at very high tensile strains applied to the grown crystals. Brittle fracture occurred before plastic deformation. The most interesting feature was the observed reduction of growth rate of the crystal under increasing applied strain. Moreover, after the brittle fracture had occurred, the growth rate increased to a value greater than the original zero strain value. This observation can be attributed to the possible generation

of new growth centres on the fractured surface.

Dislocation structure of the strained crystals was similar to that reported by Hooper et al. [73] in self-seeded crystals and comprises edge and screw dislocations of the Burgers vector $\bar{b}\langle 100\rangle$. This dislocation structure is similar to that observed in crystals of growth experiments described in Sec. 6.1. Thus it may be concluded that applied tensile strain is not responsible for the generation of new dislocations in the crystal and the latter remains elastic until the strain exceeds a certain value when it undergoes fracture. This conclusion is in agreement with the results reported in the next chapter on the growth rate retardation of small strained crystals.

CHAPTER 7

GROWTH RATE DISPERSION OF SMALL SODIUM CHLORATE CRYSTALS

A wide range of evidence exists to show that under constant external conditions of supersaturation, temperature and hydrodynamics, different crystals of the same material frequently, and perhaps usually, grow at different rates. This phenomenon is termed growth rate dispersion. It was first noted in the growth of secondary nuclei produced by attrition during bulk recrystallization [79, 80]. Confirmation of this observation and its association with the attrition process were obtained from small-scale laboratory experiments in which particles fractured from larger crystals were observed to grow at vastly different rates [81-84]. The later studies [81-84] were carried out under very well controlled conditions which eliminated the possibility that variations in the nature of the solution might have a dominant influence on the process. The phenomenon has since been presumed to be associated with some varying property of the solid particle.

Understanding of the mechanism of the occurrence of growth rate dispersion is important for at least two reasons. Firstly, it is a reflection of the growth process taking place at the crystal surface. Consequently, the nature and magnitude of the effect

gives information about the growth mechanism. Secondly, its occurrence has a major influence on the crystal size distribution and quality of the product obtained from industrial crystallizers.

Current speculations have centred around the belief that the origin of growth rate dispersion lies in the mechanism of the rate-controlling surface integration process and the role of dislocations in it. Since dislocations are active sources of growth [16], their uneven distribution in growing crystals has led to the suggestion that fractured fragments could contain different numbers of dislocations [85]. These, in turn, could yield different growth rates for the particles.

Recent work [86] on the defect structure of the regrowth of fractured crystals has shown that dislocations do not propagate into the growing crystal, but terminate at the new interface. New dislocations, the density of which depends on the condition used for the refacetting, form at the interface and propagate. Dislocation mechanism does not, however, account for zero growth rates [85]. It was also shown [62] that the application of elastic strain to a growing crystal causes a reduction in the growth rate even to zero. This suggests that the presence of elastic strain in a fractured fragment of the crystal developed from a secondary nucleus could contribute to growth rate dispersion. This speculation is also consistent with

recent observations that milled (and hence potentially strained) seed microcrystals of potash alum, on an average, grow more slowly than unmilled crystals [85]. It concurs also with the demonstration by Andrews et al. [86] that crystals of more complicated structures such as proteins and zeolites often cease to grow after achieving a certain size. X-ray analysis of these crystals showed them to be more defective and strained than those which continued to grow. To test this speculation, the growth rates of individual, 50 - 150 μm sized particles of sodium chlorate have been examined in the present work. Subsequently, using X-ray technique the strain in a range of crystals showing different growth rates has been assessed. By comparing this strain with the growth rate dispersion of the crystals concerned, it has been shown that elastic strain plays a major role in growth rate dispersion during the early stages of crystallization of small particles.

7.1. MEASUREMENTS OF GROWTH KINETICS OF SMALL SODIUM CHLORATE CRYSTALS

Crystals were nucleated, grown and observed in a flow cell, similar to that described previously [62], shown in figure 6.1. The cell was connected with the external system of water baths and solution reservoir, shown in figure 6.2, in order to maintain constant supersaturation

and temperature conditions during every experiment. The cell itself had solution capacity of 13.6 ml (diameter = 34 mm, depth = 15 mm). A platinum resistance thermometer inserted in the solution enabled the temperature to be measured to ± 0.05 K. A crystal of sodium chlorate of dimensions 7 mm x 7 mm x 3 mm used as a source of secondary nucleation was stuck to the end of a stainless steel rod and inserted into the central growth chamber of the cell before solution flow was commenced. All measurements were made at a solution temperature of 303.15 ± 0.05 K.

Crystal nuclei were produced in the cell by the "apparent secondary nucleation mechanism" [9] whereby flow of the solution through the cell at 150 ml/min results in the detachment of sub-microscopic fragments from the surface of the crystal. These nuclei fell on to an "England Finder Graticule" inserted in the cell. This glass slide was marked with a grid comprising 1 mm squares. Each square contains a centre ring bearing a letter reference and a number, which allowed observation of the growth of specific crystal and their later retrieval for X-ray analysis. The growth of small crystals was followed by observation through a optical microscope (magnification x100), the crystals being photographed as growth proceeded. The total time of observation was about 30 min.

Measurements of growth rates were made at 302.35 ±

0.05 K (undercooling 0.80 K). Using the solubility data of Linke [87], the supersaturation σ was calculated to be 0.35%. Following the observation of growth kinetics and when the crystals had grown to a size between 30 and 150 μm, they were quickly removed from the solution through a layer of n-hexane floating on the surface and washed for a few minutes in n-hexane having the same temperature as the solution. This removed all solution from the surfaces of crystals and prevented their damage by further growth or dissolution.

Using stereographic microscope, specifically small crystals were removed from the graticule and mounted on fine glass needles (diameter 30 μm, length 10 mm) using a quickly setting epoxy resin, "Devcon". Laue diffraction patterns of the crystals were taken on the high intensity wiggler beam line of the SRS at Daresbury, using equipment set up by Andrews et al. [86]. At 2 GeV, the effective wavelength of the emitted synchrotron X-rays lies in the range 0.3 - 2.5 Å. Exposure times were short, lying between 10 and 20 seconds even for a 50 μm crystal. A specially designed backstop and a screen were used to reduce the background scattered intensity and to improve the signal to noise ratio. Most of the patterns obtained showed considerable asterism with "spots" spreading up to 15 mm in length and elongated radially (see figure 7.4). This asterism could be used to define the mosaic spread (lattice plane mismatch, strain, defect

content) of the crystal. The mosaic spread, η, can be calculated [86] from the geometry of the Laue diffraction patterns using the expression

$$R = 2 \cdot \eta \cdot d / \cos^2(2\theta), \qquad (6.1)$$

where R is the radial Laue spot extension, d is the distance between the flat film and the sample, and θ is the angle of reflection. The radial spread of the reflections was estimated visually using a traveling microscope with an eyepiece graticule. Several reflections measured at different radii from the incident beam and at different angles of reflection θ were analysed and their results combined to give an average mosaic spread for a particular crystal. Selection of these reflections ensured assessment of the mosaic spread at different X-ray wavelengths in the range recorded. Thus full penetration of each particle is assured.

7.2. GROWTH RATE DISPERSION

Crystal growth rates were determined by measuring the change in overall crystal size between opposite prismatic {100} faces with time. For any particular crystal, this growth rate, R, was constant over the period of observation (~ 30 minutes). Figure 7.1 shows a typical growth rate curve for a particle of initial size of 65 μm. Similar experiments were carried out for a total

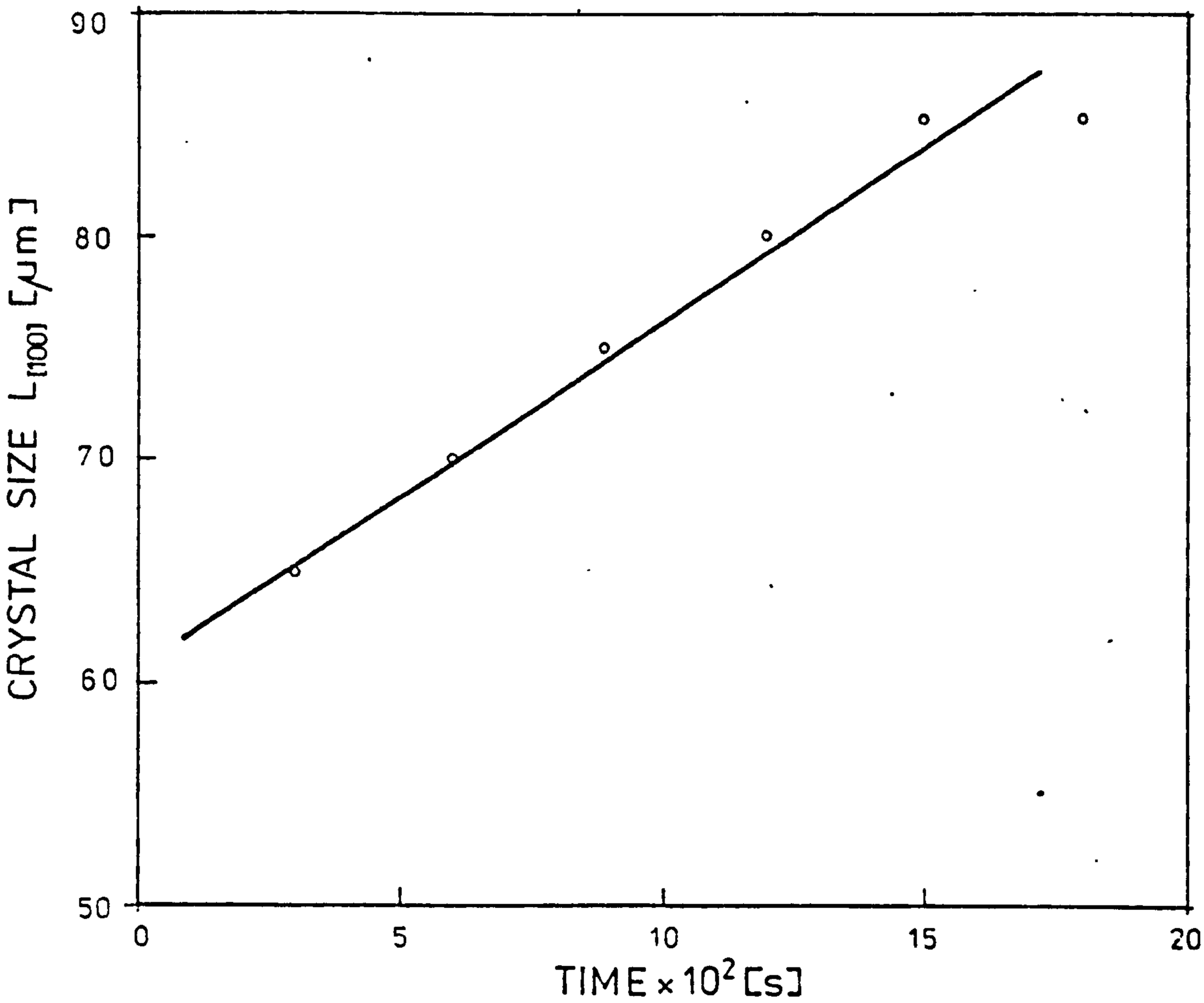

Figure 7.1. An example of the dependence of crystal size along [100] direction on growth duration.

of 90 crystals. The initial sizes of the crystals lay in the range 5-100 μm. The results are collected in figures 7.2 and 7.3. Figure 7.2 confirms the existence of a pronounced growth rate dispersion, with many crystals growing slowly and a few not growing at all. Figure 7.3 shows the distribution of growth rates as a function of initial size. The wide dispersion is again apparent. It is noticeable, however, that those crystals which show the lowest growth rate lie mostly in the lower size range.

7.3. ASSESSMENT OF STRAIN AND ITS RELATION TO GROWTH RATE

Laue diffraction patterns of eighteen crystals chosen at random from the distribution shown in figures 7.2 and 7.3 were recorded. The crystals chosen were of sizes between 30 and 150 μm. The very pronounced variation in radial asterism over the range is shown in the patterns reproduced in figure 7.4. These represent the extremes of behaviour. Figure 7.4a, for the larger, more perfect sample (150 μm), shows a small degree of radial streaking corresponding to a mosaic spread of 0.5°. The growth rate of this crystal was 7.17×10^{-8} m s^{-1} and lay at the upper end of the range recorded. In contrast, figure 7.4b reflects the unusually large mosaic spread of 4.61° recorded for a crystal, the growth rate of which was 0.14×10^{-8} m s^{-1}. In general, it was found that the growth

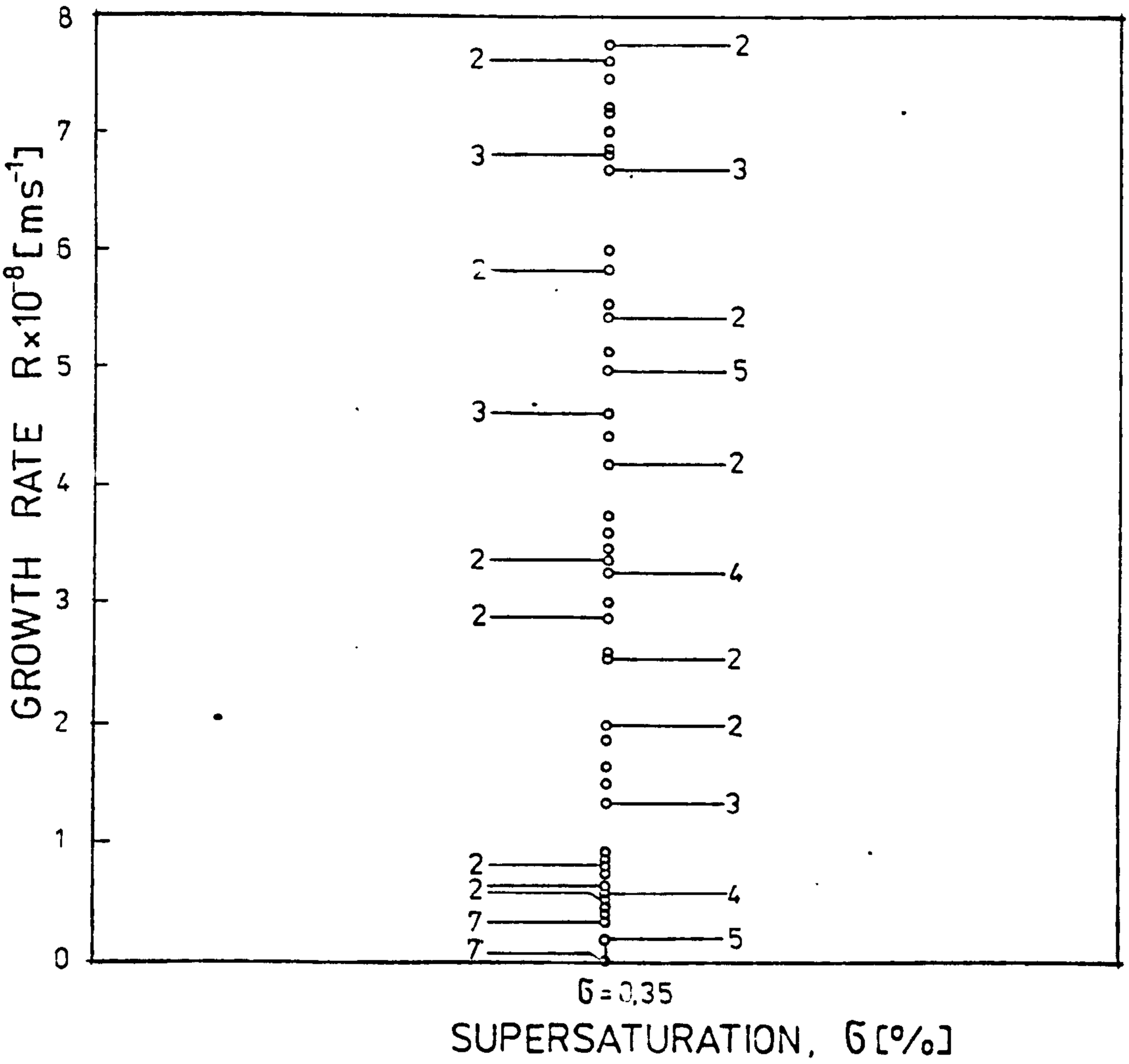

Figure 7.2. Growth rate dispersion of crystals grown at the same experimental conditions. The numerals indicate the number of crystals showing the same growth rate.

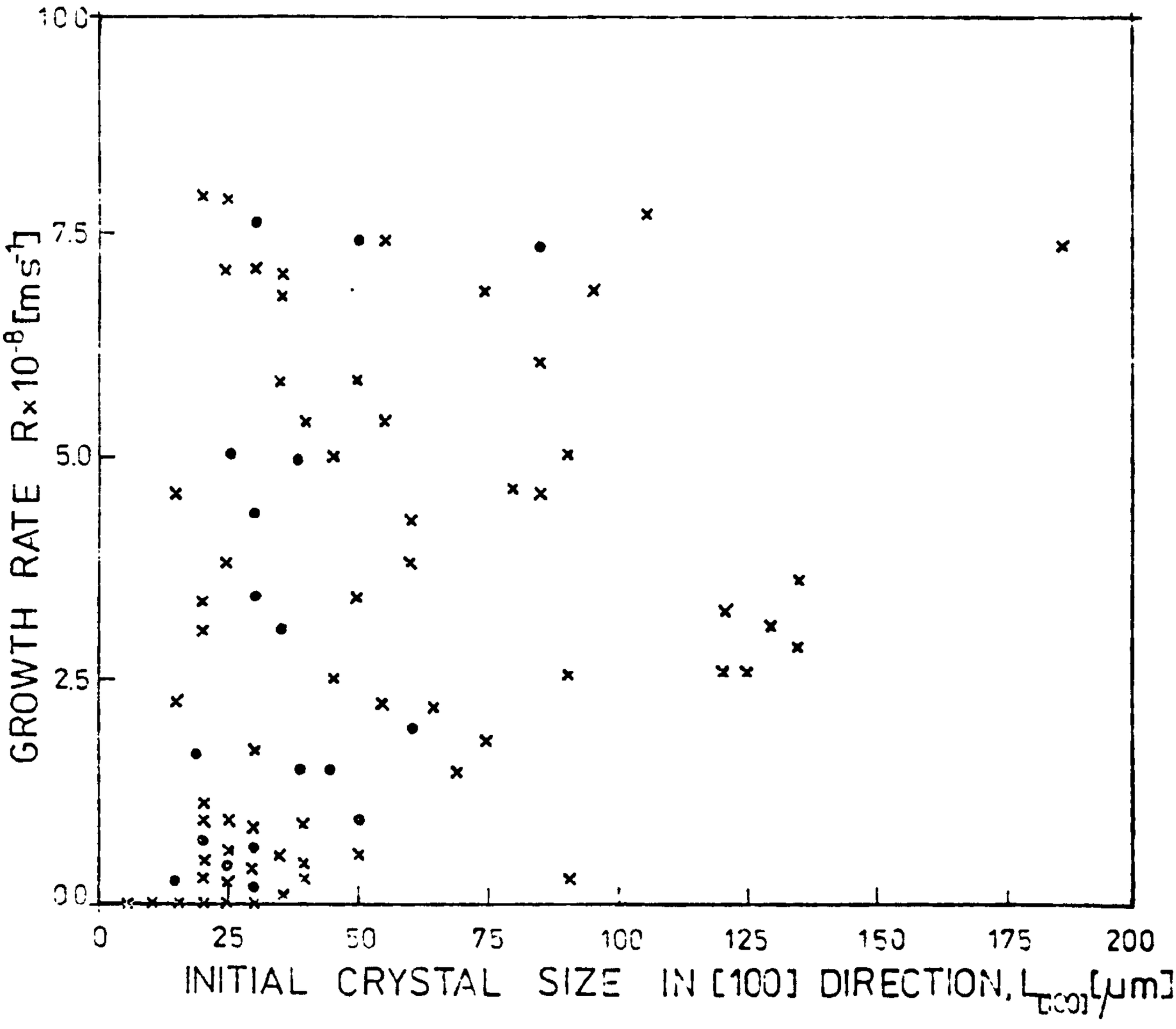

Figure 7.3. Growth rates of crystals as a function of their initial size in [100] direction. The full circles indicate the crystals used for Laue diffraction studies.

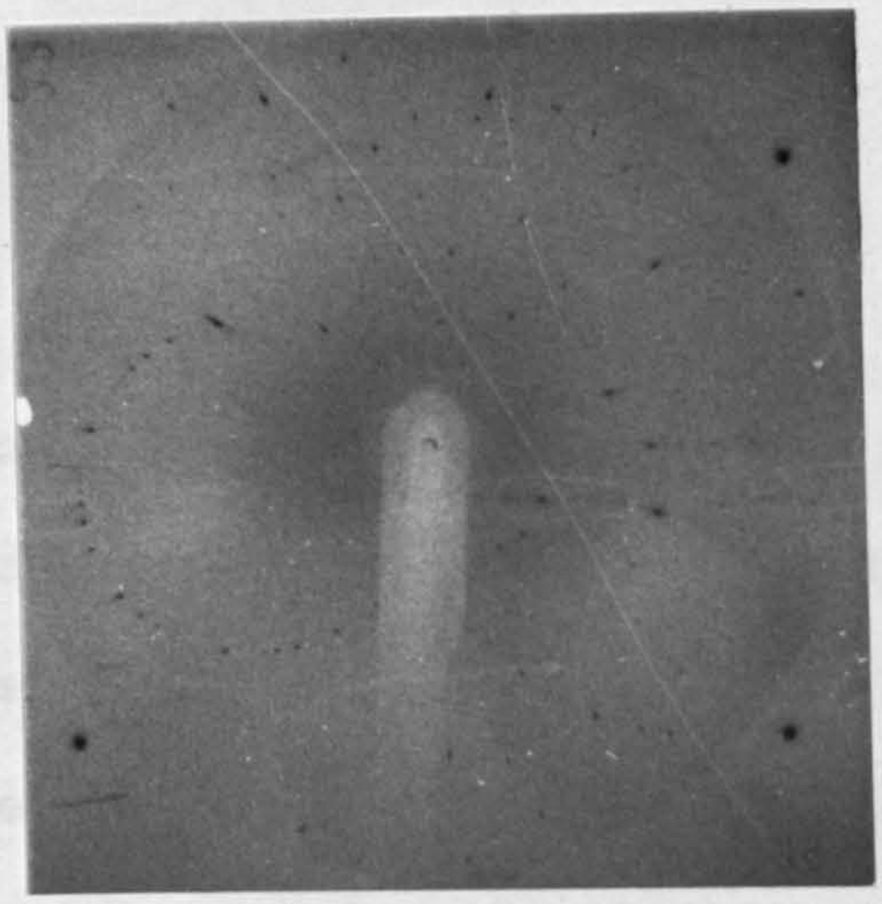

(a)

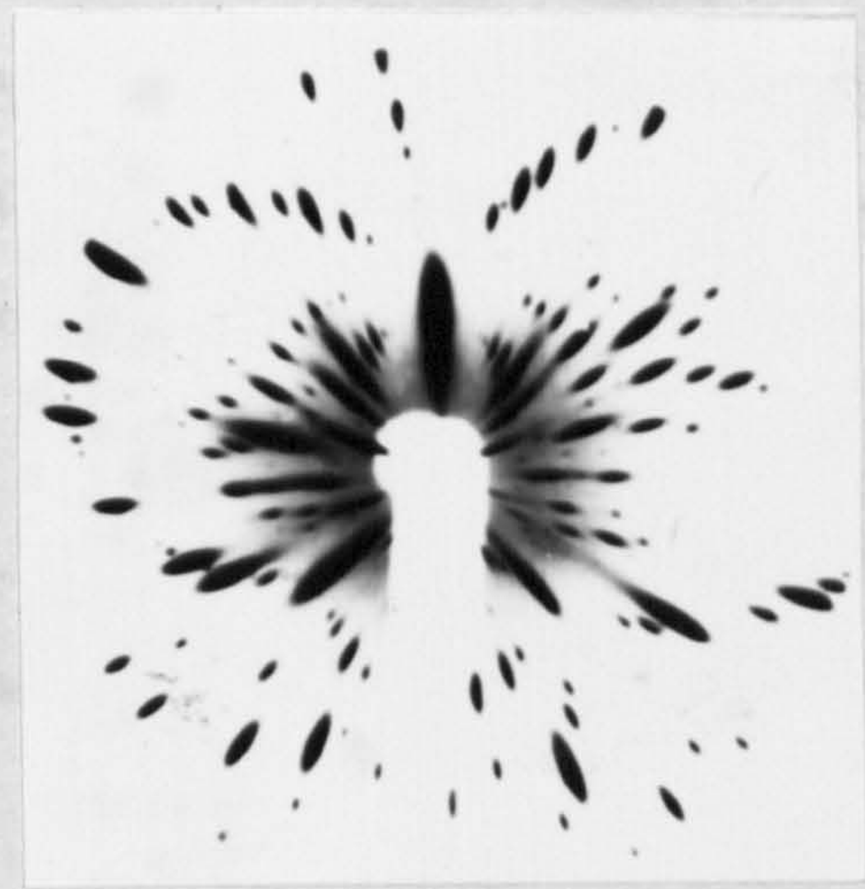

(b)

Figure 7.4. Laue diffraction patterns of crystals with built-in strain corresponding to a mosaic spread of (a) 0.5° and (b) 4.61°.

rate of a crystal was inversely proportional to its mosaic spread. The full data are recorded in figure 7.5.

7.4. INTERPRETATION OF THE OBSERVED LAUE PATTERNS AND CONCLUSIONS

The mosaic spread of a crystal reflects the total disorder. This disorder may comprise the effects of defect structure such as dislocations or general periodic lattice disorder or strain. It is unlikely that dislocation structure would have a dominant influence on such small crystals. We propose that general lattice strain is the principal disorder which is monitored and that it is this which influences crystal growth. This conclusion is supported by an increase in dislocation content in $NaClO_3$ (chapter 6) and other materials (sodium nitrate [61], potash alum [62] and ammonium dihydrogen phosphate [88]) occurring on the refacetting of fractured large crystals. This increase causes an equivalent increase in growth rate, an effect opposite to that observed in the present study.

Recent examinations of the influence of tensile stress on the growth of large crystals of sodium chlorate (chapter 6), potash alum [62] and sodium nitrate [88] provide further support to the above inference. In all cases, the application of a tensile stress to the crystals resulted in a decrease in growth rate to low or

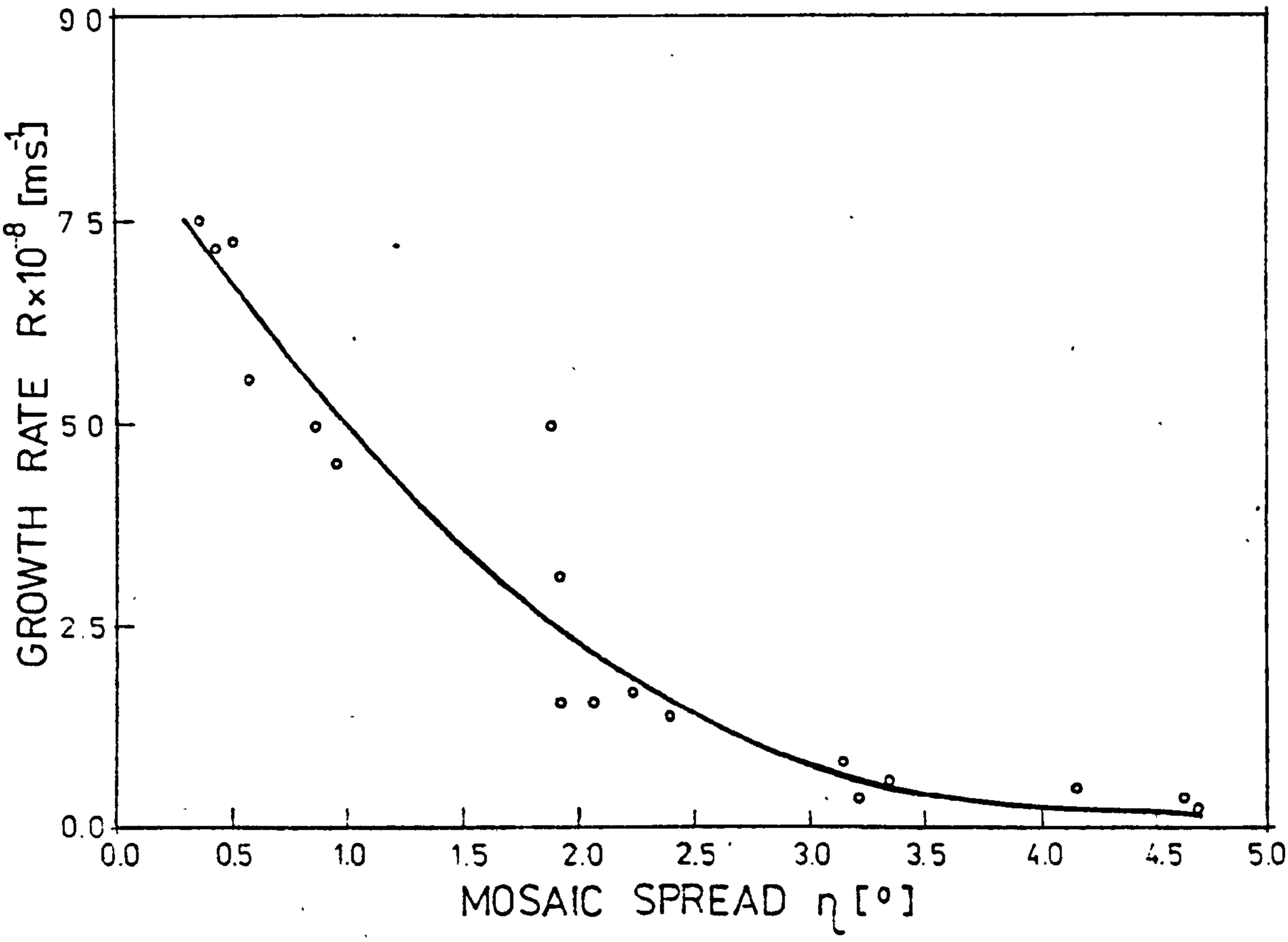

Figure 7.5. Dependence of growth rate of 18 randomly chosen crystals as a function of mosaic spread estimated from Laue diffraction patterns. The crystals are marked in fig. 7.3 by full circles.

even zero values at high overall strains. On release of this strain, the growth rates of the first two materials returned to the original value. Such a behaviour is characteristic for an elastic material which can be subjected to strain without plastic deformation. In contrast, sodium nitrate is ductile and undergoes plastic deformation when strained. In this case, time dependent reduction in growth rate occurred on straining. Release of the strain resulted in a return of growth rate to higher value than the original one due to the presence of new mechanical dislocations at the growing interface. Thus there is effectively a "competition" between growth rate reduction due to strain and growth rate enhancement due to dislocation generation.

In the present case the following sequence of events can be envisaged. In the stripping of secondary nucleus from a parent crystal by solution the nucleus either retains some elastic strain or this is developed in the early stages of refacetting. The particles then show a growth rate dispersion dependent on the degree of the included strain. This is observed in small particles within the present size range. Continued growth, which occurs more rapidly in more perfect crystals, results in the healing of this damage by the generation of dislocations which can promote crystal growth. These two processes can progress in competition until the crystal reaches a size where the residual strain at the surface

is minimal and the dislocation mechanism dominates. In such crystals (100-1000 μm size) the dislocation density is expected to be high and will vary little from crystal to crystal. Hence growth rate dispersion from this cause will be smaller and a more regular growth will be observed. This transition from growth rate dispersion at small crystal sizes has been noted in bulk crystallisation studies.

The question remains as to how tensile strain influences the growth process. We believe that this arises principally from its effect in increasing the surface free energy of the solid. This will, in turn, result in an increase in the relative solubility of different crystals and hence to a localized decrease in supersaturation and growth rate.

In conclusion, we note that the results presented in this chapter confirm the hypothesis that secondary nuclei formed by solvent-particle stripping process show a wide range of growth rate dispersion (0 - 7.81 $\times$ 10^{-8}m s^{-1}). This range is close to that observed in bulk crystallization systems. Examination of these crystals by synchrotron radiation Laue techniques shows that they contain different degrees of lattice strain and that the growth rate of the crystals is inversely proportional to this strain. We conclude that this variation in strain is the major cause of growth rate dispersion in microcrystals.

Chapter 8

CONCLUSIONS AND SUGGESTIONS FOR FURTHER WORK

From the results described in the present thesis a number of conclusions can be drawn. These conclusions and scope for further work are presented in this chapter.

The growth habit of pure sodium chlorate crystals is cubic at high cooling rates (supersaturations), while it is cuboid with relatively small {110} and {111} faces at low cooling rates. This observation is in contradiction with that reported by Kern [55], but it is in agreement with that reported by Simon [57]. Thus we may conclude that a low value of supersaturation and cooling rate is responsible for the transition from pure cubic habit to cuboid with {110} and {111} faces. The effect of supersaturation in changing the growth habit of $NaClO_3$ crystals is opposite to that observed in the case of NaCl crystal. This difference is due to a difference in the structure of the surfaces of the two compounds. The surface features observed on the as-grown surfaces of $NaClO_3$ crystals grown from pure solutions at different supersaturations suggest that {100} faces exhibiting the free development of growth layers are F faces, while {110} and {111} faces are microscopically rough. From the absence of growth spirals or hillocks typical of spiral growth mechanism on the {100} faces and the observation

of screw, edge and mixed dislocations in the crystals grown at low and high supersaturations, it is concluded that the presence of dislocations in $NaClO_3$ crystals probably does not play a significant role in their growth. The observations of the surface micromorphology of the crystals grown at supersaturations above 9×10^{-4} suggest that $NaClO_3$ crystals grow by the two-dimensional nucleation mechanism. This result is contradictory to that reported by Bennema [39] that BCF interpretation is applicable for growth in the supersaturation range 3×10^{-5} - 1.5×10^{-3}. However, his results were based on fitting experimental dependence of R on σ to different growth models alone. Such an approach may be misleading and supplementary experimental evidence can prove the actual growth mechanism.

Data on the nucleation kinetics (induction period as a function of supersaturation) of $NaClO_3$ from solutions containing sodium dithionate impurity show an increase in the surface free energy, γ, of $NaClO_3$ with impurity concentration. The values of γ obtained in this work (see figure 5.3) are comparable with the typical values reported for water soluble salts from measurements of induction periods [91].

Sodium dithionate ions have a profound effect on the morphology of $NaClO_3$ crystals. A ratio of 5000:1 of ClO_3^- to $S_2O_6^{2-}$ ions is enough to modify the cubic {100} habit to tetrahedral {111}. This ratio is much larger than the

ratio of 1000:1 reported by Buckley [21]. The observation of surface features of {100} faces also revealed the bunching of growth layers. Therefore, inhibition of these faces may be believed to take place by the adsorption of impurity ions on the surface. On the other hand, the appearance of {111} faces in the habit of the crystals grown from solutions containing the impurity is caused by the physical blocking of regular lattice sites by the impurity ions. The above mechanism of adsorption also implies that impurity ions may be incorporated into the lattice of the growing crystal, a fact substantiated by an increase in the lattice parameter of doped crystals. It should be mentioned that the above mechanism of habit modification is similar to the one proposed by Buckley [21].

Experiments on growth kinetics demonstrate that the supersaturation applied during the process of regeneration of a seed from pure solutions is a critical factor in determining the dislocation structure at the seed-crystal interface. The lower the supersaturation, the lower the strain developed at the interface and, consequently, the lower was the density of dislocations propagating into the growing crystal. These results suggest that there exists a close relationship between the degree of strain, the dislocation density and the value of the growth rate. Examination of the influence of tensile strain on the growth of large (several mm long)

crystals of sodium chlorate and recent information related to potash alum [62] and sodium nitrate [61] reveal that the growth rate of crystals decreases with an increase in the strain applied externally. Further support for the strain-dependent growth rate is given by the experimental dependence of growth rate on strain inherently present in small sodium chlorate crystals (of dimensions 50-150 μm). In the case of small crystals, the built-in strain is responsible for growth rate dispersion.

It should be noted that the conclusions on the growth morphology at different supersaturations, the mechanism of growth from pure solutions, the habit modification in the presence of sodium dithionate impurity, and the behaviour of the regenerating interface are qualitative. The conclusion of the strain-dependence of growth rate, on the other hand, is general in nature with speculative interpretation. These facts suggest a number of possible topics for further work.

In order to establish an exact relationship between growth habit and supersaturation, kinetic measurements should be made for {100}, {110} and {111} faces. Further, in order to arrive at an unambiguous conclusion about the mechanism of growth of the {100} faces of the crystals, growth kinetics and surface morphology should be studied simultaneously.

The mechanism of action of $Na_2S_2O_6 \cdot 2H_2O$ impurity on

the habit modification of $NaClO_3$ crystals needs quantitative analysis. The amount of impurity incorporated into the growing crystal should be determined for different impurity levels in the solution. The data so obtained on the incorporation of the impurity in the crystals should then be correlated with their defect structure.

Although the effect of strain applied externally on large crystals and inherently present in small crystals on growth rate has been established in the present work, its explanation is speculative so far and deserves quantitative description. Moreover, the following aspects of this phenomenon await further investigation: behaviour of strain inherent in small crystals during their subsequent growth, and effect of an impurity on the value of built-in strain and its correlation with growth rate dispersion.

REFERENCES

[1] A. A. Chernov, Ann. Rev. Mater. Sci. 3 (1973) 397.

[2] R. Becker and W. Döring, Ann. Physik 24 (1935) 719.

[3] A. E. Nielsen, Kinetics of Precipitation (Pergamon Press, Oxford, 1964) p. 15.

[4] A. E. Nielsen and O. Söhnel, J. Crystal Growth 11 (1971) 233.

[5] A. van Hook and A. J. Bruno, Disc. Faraday Soc. 5 (1949) 112.

[6] W. J. Dunning, in: Nucleation, Ed. A. C. Zettlemoyer (Marcel Dekker, New York, 1969) p. 1.

[7] J. W. Mullin and C. L. Leci, AIChE Symp. Ser. No. 121, 68 (1972) 8.

[8] G. D. Botsaris, in: Industrial Crystallization, Ed. J. W. Mullin (Plenum Press, New York, 1976) p. 3.

[9] J. Estrin, in: Preparation and Properties of Solid State Materials, vol. 2, Ed. W. R. Wilcox (Marcel Dekker, New York, 1976) p. .

[10] J. Garside, Chem. Eng. Sci. 40 (1985) 3.

[11] P. Hartman and W. G. Perdok, Acta Cryst. 8 (1955) 49.

[12] P. Hartman, in: Crystal Growth - an Introduction, Ed. P. Hartman (North-Holland, Amsterdam, 1973) p. 367.

[13] G. H. Gilmer and P. Bennema, J. Crystal Growth 13/14 (1972) 148.

[14] K. A. Jackson, in: Liquid Metals and Solidification (American Society of Metals, Cleveland, Ohio, 1958) p. 174.

[15] M. Ohara and R. C. Reid, Modeling Crystal Growth Rates from Solutions (Prentice-Hall, N.J. , 1973) p. 5.

[16] W. K. Burton, N. Cabrera and F. C. Frank, Nature 163 (1949) 398.

[17] W. K. Burton, N. Cabrera and F. C. Frank, Phil. Trans. Roy. Soc. (London) A 243 (1951) 299.

[18] W. J. P. Enckevort, Prog. Crystal Growth and Charact. 9 (1984) 1.

[19] K. Sangwal and M. Szurgot, J. Crystal Growth 80 (1987) 351.

[20] J. Garside, R. Janssen-van Rosmalen and P. Bennema, J. Crystal Growth 29 (1975) 353.

[21] H. E. Buckley, Crystal Growth (Wiley , New York, 1961) p. 339.

[22] N. Cabrera and D. A. Vermilyea, in: Growth and Perfection of Crystals, Eds R. H. Doremus, B. W. Roberts and D. Turnbull (Wiley, New York, 1958) p. 393.

[23] A. A. Chernov (Ed.), Modern Crystallography III: Crystal Growth (Springer, Berlin, 1984) Chapter 4.

[24] K. Sangwal, Etching of Crystals: Theory,

Experiment and Application (North-Holland, Amsterdam, 1987) Chapter 3.

[25] R. Boistelle, in: Interfacial Aspects of Phase Transformations, Ed. B. Mutaftshiev (Reidel, Dordrecht, 1982) p. 621.

[26] P. Bennema. J. Crystal Growth 5 (1969) 29.

[27] A. A. Chernov, Sov. Phys. Usp. 4 (1961) 116.

[28] J. W. Mullin A. Amathavivadhana and M. Chakraborty, J. Appl. Chem. 20 (1970) 153.

[29] D. P. Lal, R. E. A. Mason and R. F. Strickland-Constable, J. Crystal Growth 5 (1969) 1.

[30] R. F. Strickland-Constable, Kinetics and Mechanism of Crystallization (Academic Press, New York, 1968).

[31] G. D. Botsaris and G. Sutwala, AIChE Symp. Series 153, 72 (1976) 7.

[32] E. G. Denk and G. D. Botsaris, J. Crystal Growth 13/14 (1972) 493.

[33] W. Drost-Hansen, Ind. Eng. Chem. 61 (1969) 10.

[34] H. A. Miers, Proc. Roy. Soc. A71 (1903) 439;
Phil. Trans. Soc. 202 (1903) 459.

[35] C. W. Bunn, Disc. Faraday. Soc. 5 (1949) 132.

[36] W. F. Berg, Proc. Roy. Soc. A164 (1938) 79.

[37] M. Follenius, Bull. Soc. Franc. Miner. Cryst. 82 (1959) 343.

[38] S. P. F. Humpreys-Owen, Proc. Roy. Soc. A197

(1949) 218.

[39] P. Bennema, Phys. Stat. Sol. 17 (1966) 555;
J. Crystal Growth 1 (1967) 287.

[40] S. Hosoya, M. Kitamura and T. Miyata, Mineral. J. (Japan) 9 (1978) 73;
S. Hosoya and M. Kitamura, Mineral. J. (Japan) 9 (1978) 137, 147.

[41] H. Takeushi, K. Takashi, K. Tomita and M. Imanaka, J. Chem. Engng Japan 12 (1979) 209.

[42] V. V. Sipyagin, Soviet Phys. Cryst. 12 (1968) 590.

[43] A. A. Chernov, V. F. Parvov, S. M. Eskin and V. V. Sipyagin, Growth of Crystals 12 (1984) 103.

[44] B. Wojciechowski and J. Karniewicz, in: 1st European Conference on Crystal Growth (Zurich, 1978), Abstract C-4, p. 110.

[45] F. Mussard and S. Goldsztaub, J. Crystal Growth 13/14 (1972) 445.

[46] I. Kito and N. Kato, J. Crystal Growth 24/25 (1974) 544.

[47] M. Matsunaka, M. Kitamura and I. Sunagawa, J. Crystal Growth 48 (1980) 425.

[48] F. Bedarida, L. Zefiro and C. Pontiggia, in: Applications of Holography and Optical Data Processing, Eds A. Marom and A. A. Friesem (Pergamon Press, Oxford, 1977) p. 259.

[49] F. Bedarida, L. Zefiro and P. Boccacci, J. Crystal Growth 61 (1983) 641.

[50] G. Bliznakov and E. Kirkova, Z. Phys. Chem. 206 (1957) 271.

[51] G. Bliznakov and E. Kirkova, Kristall und Technik 4 (1969) 331.

[52] H. Buckley, Zeits. Krist. 75 (1930) 15.

[53] H. Buckley, Manchester Memoirs 83 (1938-39) 31

[54] C. Bunn, Chemical Crystallography (Claredon Press, Oxford, 1961) p. 21.

[55] R. Kern, Bull. Soc. Franc. Miner. Crist. 78 (1955) 497.

[56] Y. Aoki, Mem. Fac. Sci, Kyushu Univ., Ser. D. Geol. 24 (1979) 75.

[57] B. Simon, J. Crystal Growth 61 (1983) 167.

[58] M. Gonzales, A. de Andres and J. Balcazar, Estud. Geol. 38 (1982) 271.

[59] H. Offerman and J. Ulrich, in: Industrial Crystallization 84, Eds. S. Jancić and E. de Jong. (Elsevier, Amsterdam, 1984) p. 31.

[60] R. Ristić, J. N. Sherwood and K. Wojciechowski, J. Crystal Growth 91 (1988) 163.

[61] R. Ristić and J. N. Sherwood, to be published.

[62] H. Bhat, J. N. Sherwood and T. Shripathi, Chem. Eng. Sci. 42 (1987) 609.

[63] A. R. Lang, in: Modern Diffracting and Imaging Techniques in Material Science, Eds S. Amelinckx, R. Gevers and J. van Landyut (North-Holland, Amsterdam, 1978) p. 623.

[64] B. K. Tanner, X-ray Diffraction Topography, (Pergamon, Oxford, 1976) p. 24.

[65] W. W. Webb, in: Direct Observation of Imperfections in Crystals, Eds J. B. Newkirk and J. H. Wernick (Interscience, New York, 1962) p. 29.

[66] E. S. Maieran, Siemens-Report 4 (1969) 207e.

[67] A. Authier, in: X-ray Optics; Series: Topics in Applied Physics, vol 22, (Springer-Verlag, 1977), p. 145.

[68] D. K. Bowen, G. F. Clark, S. T. Davies, J. R. S. Nicholson, K. J. Roberts, J. N. Sherwood and B. K. Tanner, Nucl. Instrum. Methods 195 (1982) 277

[69] R. M. Hooper, B. J. McArdle, R. S. Narang and J. N. Sherwood, in: Crystal Growth, 2nd edn, Ed. B. R. Pamplin (Pergamon, 1980).

[70] M. Krasiński, T. Sokołowski and B. Wojciechowski, Cryst. Res. Technol. 17 (1982) 205.

[71] R. Wyckoff, The Structure of Crystals (Interscience Publishers, New York, 1948).

[72] S. Martinez, S. Garcia-Blanco and L. Rivoir, Acta Cryst 9 (1956) 145.

[73] R. M. Hooper, K. J. Roberts and J. N. Sherwood, J. Mater. Sci. 18 (1983) 81.

[74] A. J. Bradley and A. H. Jay, Proc. Phys. Soc. (London) 44 (1932) 563, 1932.

[75] J. Garside, R. Jansen van Rosmalen and P. Bennema,

J. Crystal Growth 29 (1975) 353.

[76] K. Sangwal, R. Rodriguez-Clemente and S. Veintemillas-Verdaguer, J. Crystal Growth 78 (1986) 144.

[77] R. Jansen-van Rosmalen, W. H. van der Linden, E. Dobbinga and D. Visser, Kristall und Technik 13 (1978) 17.

[78] G. M. Loicacono, Ferroelectrics 71 (1987) 49.

[79] P. D. B. Bujac, in : Industrial Crystallization, Ed. J. W. Mullin (Plenum Press, New York, 1976), p. 23.

[80] C. M. Van't Land and B. G. Wienk, ibid., p. 51.

[81] L. N. Natalina and E. B. Treivus, Soviet Phys. Cryst. 19 (1974) 389.

[82] R. J. Davey, R. I. Ristić and B. Zizić, J. Crystal Growth 47 (1979) 1.

[83] J. Garside, in: Industrial Crystallization 78, Eds E. J. de Jong and S. J. Jancić (Norh-Holland, Amsterdam, 1979).

[84] J. Garside and R. I. Ristić, J. Crystal Growth 61 (1983) 215.

[85] J. Garside, G. Webster, R. J. Davey and A. J. Ruddick, in: Industrial Crystallization, Eds S. Jancić and E. J. de Jong (Elsevier, Amsterdam, 1984) p. 459.

[86] S. J. Andrews, J. E. Hails, M. M. Harding and D. W. J. Cruickshank, Acta Cryst. A43 (1987) 70.

[87] W. F. Linke, Solubility of Inorganic and Metal Organic Compounds, vol 2 (Am. Chem. Soc., Washington, 1965), p. 1015.

[88] R. I. Ristić, J. N. Sherwood and T. Shripathi, to be published

[89] P. Bennema and G. H. Gilmer, in: Crystal Growth - an Introduction Ed. P. Hartman (North-Holland, Amsterdam, 1973) p. 263.

[90] P. Bennema and J. P. van der Eerden, in: Morphology of Crystals, Ed. I. Sunagawa (Terrapub, Tokyo,1987) p. 1.

[91] W. Kibalczyc and K. Wojciechowski, J. Crystal Growth 76 (1986) 379.

[92] O. Söhnel, J. Crystal Growth 57 (1982) 101.